VALVE PLATE DESIGN MODEL FOCUSING ON NOISE REDUCTION IN AXIAL PISTON MACHINES

by

Abhimanyu Baruah

A Thesis

Submitted to the Faculty of Purdue University

In Partial Fulfillment of the Requirements for the degree of

Master of Science in Mechanical Engineering

School of Mechanical Engineering

West Lafayette, Indiana

December 2018

THE PURDUE UNIVERSITY GRADUATE SCHOOL
STATEMENT OF THESIS APPROVAL

Dr. Sadegh Dabiri, Chair

Department of Agricultural and Biological Engineering

Dr. Andrea Vacca

Department of Agricultural and Biological Engineering

Dr. Farshid Sadeghi

Department of Mechanical Engineering

Approved by:

Dr. Jay P. Gore

Head of the Graduate Program

To my grandfather, my mama, who gave me big shoes to fill and to my advisor Dr. Monika Ivantysynova

ACKNOWLEDGMENTS

I am immensely grateful to my advisor Dr. Monika Ivantysynova for having faith in me and giving me this opportunity to work at one of the best fluid power labs in the world. I am grateful to her for constantly guiding me and encouraging me to become a better researcher and a better engineer. She will always be an inspiration for me.

I am also grateful to my committee chair, Dr. Sadegh Dabiri and my committee members, Dr. Andrea Vacca and Dr. Farshid Sadeghi for taking time out from their busy schedules to review my thesis document. I am grateful for their valuable time and input.

I shall be forever grateful to Paul Kalbfleisch, my mentor at Maha Fluid Power Lab for passing me his knowledge of valve plate research and optimization, and for showing me the light in the rabbit holes that I sometimes burrow myself into. I am grateful to the other members of the 'NVH team', Dan and Svenja for making work all the more enjoyable.

I am grateful to Susan, Connie and Anthony for all the different ways in which they make the lives of the graduate students at Maha hassle free and comfortable. I am also grateful to all my colleagues at Maha for nurturing an environment of excellence and free thinking.

I am grateful to my mom, dad and sister for standing by me through thick and thin. Knowing that I have your support has always inspired me to take up greater challenges in life. I am grateful to my girlfriend Gangotri for her love and adulation and inspiring me to sail the rough waters of graduate school with patience and a calm mind.

TABLE OF CONTENTS

Page

LIST OF TABLES

LIST OF FIGURES

Figure Page

Figure Page

SYMBOLS

a_k	Acceleration of the piston in the z - direction
a_u	Radial acceleration of the piston
A_{rHP}	Effective area available for flow between the high pressure port and the displacement chamber
A_{rLP}	Effective area available for flow between the low pressure port and the displacement chamber
F_{pi}	Reaction force on the swash plate due to the pressurization of the i_{th} displacement chamber
H_K	Piston stroke length
K	Bulk Modulus of the hydraulic fluid
K_{ef}	Effective bulk modulus
K_o	Constant bulk modulus at high pressures
Q_e	Effective flow
Q_{rHPi}	delivery flow from i_{th} displacement chamber
Q_{rLPi}	suction flow to i_{th} displacement chamber
Q_{HP}	Net delivery flow
Q_{LP}	Net suction flow
Q_{SKi}	Leakage through the i_{th} piston cylinder interface
Q_{SGi}	Leakage through the i_{th} slipper - swash plate interface
Q_{SBi}	Leakage through the cylinder block - valve plate interface
Q_{se}	Net external leakage
Q_{si}	Net internal leakage
Q_{sf}	Volumetric Losses due to incomplete filling
Q_{sK}	Compressibility Losses

Q_{th}	Theoretical flow
m	pressure related term in the equation of the effective bulk modulus
M_x	Swash plate moment in the x- direction
M_y	Swash plate moment in the y - direction
M_z	Swash plate moment in the z - direction
n	Rotational speed of the pump shaft (in rpm)
p	Displacement Chamber pressure
p_{LP}	pressure at the low pressure port
p_{HP}	pressure at the high pressure port
p_o	initial pressure
R_b	Pitch Radius
s_K	Movement of the piston along the z- axis
v_K	Piston velocity along the z- axis
v_u	Circumferential speed of the piston
V_i	Effective volume inside the displacement chamber
α	Volumetric content of entrained air
α_D	Orifice flow coefficient
β	Swash plate angle
γ	Cross Angle
ρ	Density of the hydraulic fluid
κ	Polytropic constant of air
ϕ	Angular position of the swash plate from the ODC
ω	Angular rotational speed of the pump shaft (rad/sec)

ABBREVIATIONS

AMGA II	Archive based Micro Genetic Algorithm II
CD	Crowding Distance
DC	Displacement Chamber
DCFV	DeCompression Filter Volume
DM	Decision Maker
FBNS	Fluid Borne Noise Sources
IDC	Inner Dead Center
LSODA	Livermore Solver for Ordinary Differential equations Approximate
NSGA	Non-dominating Sorting Genetic Algorithm
ODC	Outer Dead Center
OpCon	Operating Condition
PCFV	Pre Compression Filter Volume
RPM	Revolutions Per Minute
SBNS	Structure Borne Noise Sources

ABSTRACT

Baruah, Abhimanyu M.S.M.E, Purdue University, December 2018. Valve Plate Design Model focusing on Noise Reduction in Axial Piston Machines. Major Professor: Monika Ivantysynova.

The advantages of high efficiency, reliability, flexibility and high power to weight ratio make axial piston pumps popular for use in a wide variety of applications like construction and agricultural machinery, off road vehicles and aerospace applications. However, a major drawback which limits their extensive use in other commercial applications is noise. One of the important components in axial piston machines is the valve plate, which influences the transition of the suction and delivery flows into and out of the displacement chamber. Appropriate design of the valve plate can play a significant role in influencing the rate of compression and expansion in the displacement chamber, and hence contribute towards the abatement of noise in axial piston machines. Furthermore, the relief grooves in valve plates makes them relatively less sensitive to operating conditions for the operation of the pump. The high sensitivity of the valve plate design towards the pressure build up in the displacement chamber and towards the noise sources are big motivation factors towards rigorously exploring the design space to find suitable designs to meet the objective of noise reduction. This motivates the development of an advanced computational tool, colloquially called 'MiNoS', where a powerful optimization algorithm has been combined together with a novel parametrization scheme for valve plate design and a 1D simulation model of swash plate type axial piston machines to find optimized designs which can contribute towards noise reduction in swash plate type axial piston machines. Furthermore, incorporation of the appropriate constraint also helps in avoiding designs susceptible to the onset of cavitation in the displacement chamber. A case study performed using the developed computational tool has been shown later in this work.

1. INTRODUCTION

Positive displacement machines are found to have wide applications in agricultural and construction machinery, aerospace, mining equipment, manufacturing, robotics and automotive industry. Their advantages of a high power to weight ratio, accompanied by their reliability have made them significantly popular in these applications. All positive displacement machines work on the principle of converting the rotary motion of the input shaft into the reciprocating motion of the pistons, which delivers pressurized flow, or vice versa, depending on their function as a pump or motor. However, on the basis of their working mechanism, they have been classified as displacement machines of axial piston type, radial piston type, gear type, vane type or screw type.

Axial piston pumps have the advantages of robustness and high efficiency. Along with that, their ability to deliver high pressures, and with it high power make them very popular in industry. Another big advantage of axial piston machines is their flexibility in delivering power by varying the displacement of the unit. The flow obtained from such axial piston machines can be controlled as per the requirements, which has aided in the replacement of valve controlled designs with displacement control. Moreover, the same unit can be used as a pump as well as motor, which has ushered in the era of hydrostatic transmissions. Even though all the above mentioned advantages make axial piston machines very popular in industry, yet a major drawback in such machines is that of noise. At a time when other competitive and auxiliary technologies like combustion engines and electric motors have successfully solved or decreased noise problems, the same has become a major challenge in the fluid power industry. In spite of the myriad advantages provided by fluid power technology, the ugly head of noise problems limit its pervasion.

High pressures and high speeds in axial piston machines entail in high forces on its components, leading to higher air borne noise. The valve plate plays a critical role in this regard, as it influences the development of pressures which are ultimately responsible for such

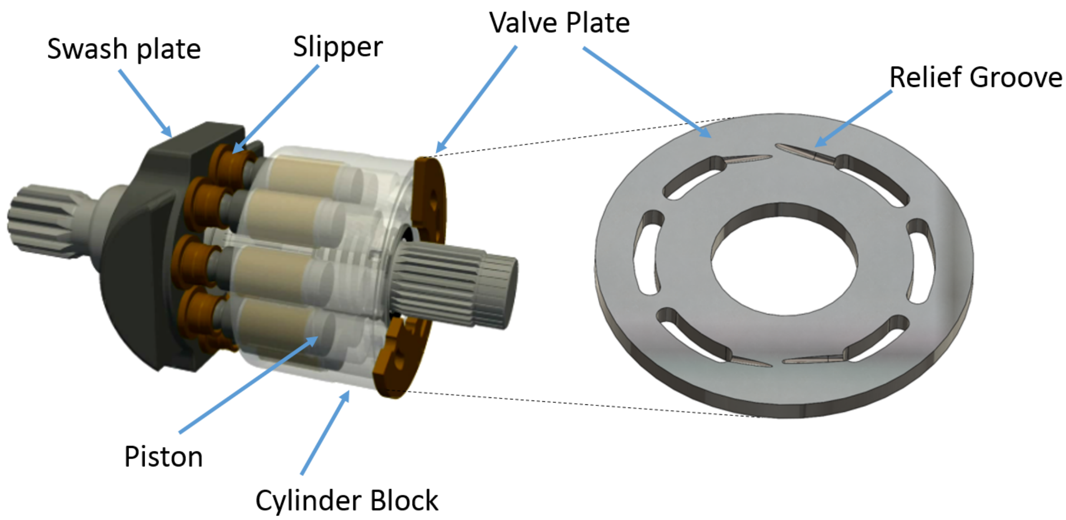

Figure 1.1. Axial Piston Pump of swash plate type and the valve plate.

resultant forces on the components. This process of valve plate design is further complicated by the operation of the pump in a wide range of operating conditions. A valve plate ideally suited to minimize noise at one operating condition may somewhat aggravate the same at a different operating condition. So, it is necessary to explore and develop a robust design methodology, which gives the optimum noise reduction over a range of operating conditions and at the same time does not compromise on efficiency too much.

The aim of this work is to design and develop a robust, efficient, and effective optimization strategy for design of the valve plate in order to reduce noise sources. In particular, the design of the relief grooves to the two kidney shaped ports is emphasized here as they make the pump relatively less sensitive to operating conditions and at the same time, is easy and simple to manufacture.

The noise emitted by a hydraulic system depends, not only on the concerned pump/motor but also on the design of the hydraulic circuit. In particular, the length of the hoses/pipes, location of the valves, etc are also responsible for the noise. However, noise arising from the vibration of the pipework originate from the flow ripples of the axial piston pump.

This work focuses only on the noise abatement of the pump/motor. Even if a pump has been optimized for noise, the hydraulic circuit may still emit noise if it is a poorly designed circuit. Analysis of a circuit for noise abatement introduces additional complexities and is difficult to optimize. Hence, we shall be focusing only on noise arising from the sources in swash plate type axial piston pumps.

Chapter 2 gives a broad overview of the state of the art and ongoing research in the field of noise reduction and also a brief study of available multi objective optimization algorithms. Chapter 3 deals with the kinematics of the swash plate type axial piston pumps with a brief description of the modeling tool used at the Maha Fluid Power Lab. Chapter 4 and 5 identify the role of valve plates as well as a little insight into the consideration of objective functions which are capable of quantifying noise sources. Along with that, the optimization methodology has also been discussed in detail. Finally, Chapter 6 presents a case study using the proposed algorithm.

2. STATE OF THE ART

2.1 State of the Art in Noise Reduction Techniques

Noise in hydraulics has been studied since the beginning of the second half of the 20th century. One of the first studies to observe noise in axial piston machines was done by Stan Skaistis at Vickers Incorporated, Detroit, Michigan (Skaistis 1962). Apart from understanding the dependency of noise on speed and pressure, this work also found that most of the noise was emitted at frequencies equal to multiples of the fundamental frequency, which is the frequency of pumping events. Most of the work done by Stan Skaistis has been accumulated in a book (Skaistis 1988), which is one of the first pioneering books on noise in hydraulic systems.

After Skaistis, further study in the domain of noise in hydraulic machinery was done by Ronald Becker at Vickers. The conclusions he derived from his experimental work have been summarised in (Becker 1970). Apart from correlating the pump harmonics to human ear response, sufficient evidence is given to correlate the rate of compression and expansion to pump loudness. This work also comments on the influence of temperature and inlet pressure on pump loudness, and in more detail, the possible sources of entrained air and its effect on pump loudness.

One of the first attempts at modeling fluid power noise was done at the Fluid Power Research Center of the Oklahoma State University. A simplistic model highlighting the relation between air borne noise and pump characteristics was developed here.

2.1.1 Fluid Borne Noise

Following the development of computational power, it was imperative to develop a tool for hydraulic pumps as well. One of the first such simulation tools was developed by Helgestad

(Helgestad, Foster & Bannister 1974), who studied the effect of ideal timing, V-shaped grooves and parallel slot restrictors on reducing pressure transients.

Around 1976, a major collaborative project was undertaken in the UK by four contractors for noise reduction in hydraulic systems. The results of this collaborative project was presented in the form of two seminars organized by the UK Institution of Mechanical Engineers (IMechE 1977) and (IMechE 1980). One of the collaborators on this project was the University of Bath, which has subsequently contributed significantly towards the domain of hydraulic system and component noise reduction. (Edge 1980), followed by (Drew, Longmore & Johnston 1998) contributed towards the development of impedence models for positive displacement machines. Further study of flow ripples and pressure pulsations here led to several publications (Edge & de Freitas 1985), (Edge & Darling 1989), (Harris, Edge & Tilley 1994), (Harrison & Edge 2000) which have thrown more light into the relation between noise and pulsating flows and pressures, and have explored innovative techniques like heavily damped check valves to reduce the same. A good summary of the origin of noise in different types of hydraulic pumps and methods to reduce them is found in (Edge 1999)

Another important research center which boasts of significant contribution to this field is Linkoping University, Sweden. Researchers here began to look into different ways of reducing flow pulsations and pressure transients. (Palmberg 1989) surmised that the rate of compression can be controlled by the design of relief grooves by appropriately limiting backflow from discharge port to the displacement chamber. A comparision of different methods of reducing flow ripples like pressure relief grooves, precompression, check valves as well as filter volumes is done in (Pettersson, Weddfelt & Palmberg 1991). Several later works have started exploring other ways of reducing noise in axial piston pumps. One such technique which has been extensively studied is the cross angle ((Johansson, Ölvander & Palmberg 2007), (Johansson 2005)). Finally, an indepth study has been described in detail in (Ericson 2012), where the author has explored cross angles, non uniform placement of pistons and also analysed the effect of entrained air on hydraulic noise. The author (ERICSON & PALMBERG 2008) also found that implementation of relief grooves reduces the sensitivity to operating conditions, air content and suction pressure.

2.1.2 Structure Borne Noise

Structure borne noise has been studied less extensively as compared to fluid borne noise. (Yamauchi & Yamamoto 1976) published one of the first works to study the effect of different parameters like rate of pressurization, speed, dead volume, relief grooves on the swash plate vibrations. A comprehensive analysis of the piston forces and moments and their contribution to noise considerations is also found in (Johansson 2005). (Palmen 2004) explored noise reduction by modifying the base plate of a swash plate type axial piston machine. (Ericson 2012) also considered the swash plate moments and piston forces as objective functions in her optimization methodology. Active control of the swash plate for noise reduction was first explored by (Kim & Ivantysynova 2017). However, this method did not help in abating noise.

2.2 State of the Art in Multi Objective Optimization

With the improvements in computing power, population based optimization methods have gained great popularity in different fields owing to their ability to explore the design space more rigorously and also for their uncanny ability to converge on globally optimum solutions. Classical optimization algorithms fall short when it comes to solving most real world problems (Kalbfleisch 2015). This has given sufficient impetus to the development of the field of metaheuristics. The term 'metaheuristics' was phrased by (Glover 1986), and combines the Greek prefix 'meta' (beyond) with 'heuristic' (a method of learning or solving problems that allows people to discover things themselves and learn from their own experiences). According to (Sörensen & Glover 2013), "a metaheuristic is a high-level problem-independent algorithmic framework that provides a set of guidelines or strategies to develop heuristic optimization algorithms". A detailed discussion on metaheuristics, its classification as well as the advantages and disadvantages are found in (Blum & Roli 2003). Among the plethora of metaheuristic algorithms, evolutionary computation has gained significant prominence in the 21st century. Evolutionary algorithms are a family of nature inspired, population based, global search and optimization algorithms. The candidate solutions to the problem are equivalent to the individuals of the population and the quality of the solutions is determined by the fitness functions.

One of the more popular types of evolutionary algorithms are the genetic algorithms. A good description of genetic algorithms and the scope of their applications can be found in (Goldberg 1989). The main aim of such population based optimization strategies is to find a set of non dominated solutions, also called the pareto front (Ehrgott 2012). The improvements in each of the individual stages of genetic algorithms and better fitness evaluation mechanisms has resulted in some efficient and effective algorithms, that can be trusted to find the global optimum. Description of some of the modern genetic algorithms relevant to the field of engineering and technology can be found in (Deb 2001).

2.3 Noise Research at MAHA Fluid Power Lab

After the development of an advanced and accurate axial piston pump simulation tool CASPAR (Wieczorek & Ivantysynova 2000), several researchers at Maha Fluid Power Lab started looking into methods for reduction of noise, not only at the component level but also at the system level. (Klop 2010) delved extensively into noise reduction in hydrostatic transmissions by developing a model to study the effect of fluid borne and structure borne noise sources on the same and validating the model with experiments performed in an anechoic chamber. Optimization of the valve plate for the reduction of noise by using computational methods was first looked into by (Seeniraj 2009). Following him, (Kim 2012) further improved Seeniraj's algorithm. After them, (Kalbfleisch 2015) further improved the process of valve plate optimization by incorporating an advanced genetic algorithm and automating the process. This work build on the dissertation work of Seeniraj, Kim and Kalbfleisch.

(Seeniraj 2009) was the first to explore the domain of valve plate design for reduction of noise sources at Maha Fluid Power Research Center. The objective functions pertaining to both fluid borne and structure borne noise sources were considered. However, the design parametrization for the valve plate that was considered was too simplistic. The work flow for Seeniraj's algorithm is given in Figure(2.1).

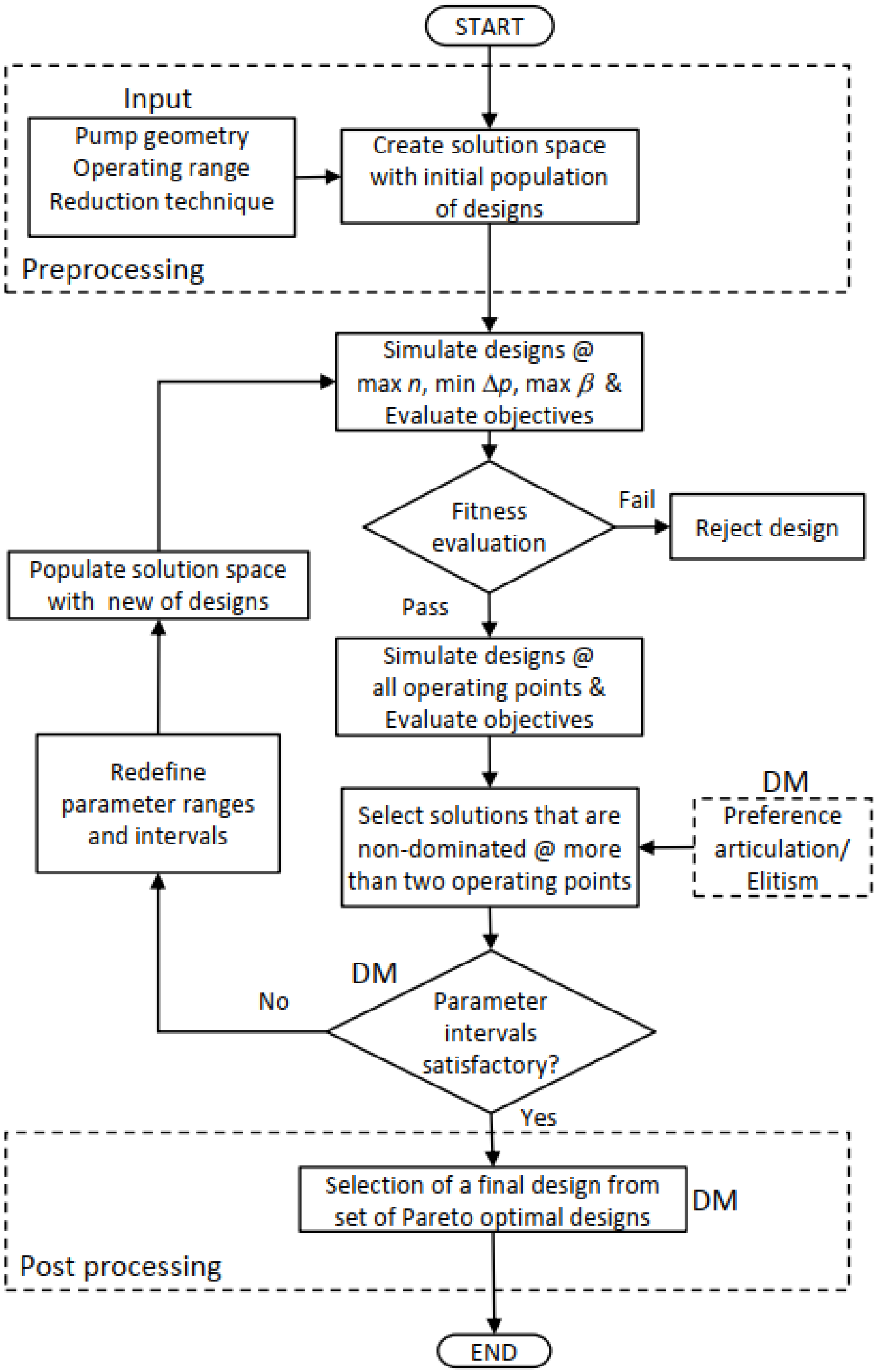

Figure 2.1. The algorithm flow chart devised by (Seeniraj 2009).

’DM’ in Figure(2.1) means ’Decision Maker’, which refers to inputs or involvement of the designer to make decisions. The presence of ’DM’ in the optimization loop implies that the optimization is not automated, and requires involvement from the designer in every loop. This leads to a major overhead of time, as the algorithm would have to wait for inputs from the designer, and would make it highly inefficient. Also, due to lack of clarity on the operating condition space, Seeniraj decided to choose the 8 extreme corner operating conditions for safety. Another major drawback was the filtering out of bad designs. The only constraint checks that were done were for overpressurization and cavitation.

Moreover, even though Seeniraj classified his algorithm as a 'Multi Objective Genetic Algorithm', there have been disagreements with future researchers on this because of the change in parameter intervals in every iteration.

(Kim 2012) improved Seenriraj's algorithm by including more constraint checks for better filtering of the designs and reducing the number of sampled operating conditions to three. However, a clear explanation for the choice of these three operating conditions was not given. The flowchart for Kim's algorithm is shown in Figure(2.2)

Even though Kim made a few improvements to Seeniraj's algorithm, the problems relating to high simulation time as well as the involvement of the 'DM' still persisted.

Apart from the overpressurization and the cavitation checks, Kim also included another constraint check for volumetric efficiency. The addition of a new constraint would help in not only more reasonable designs, but also fewer function evaluations.However, a major drawback with this constraint was the increase in computational overhead as the volumetric efficiency check would take a long time. Thus, in spite of fewer function evaluations as compared to (Seeniraj 2009), the simulation time for (Kim 2012) was greater. Also, Kim normalized the objective function values with respect to the difference between their maximum and minimum values. The parallelization of this code meant that different sets of designs were evaluated in different machines, and hence different sets had different maximum and minimum values of the objective values, and hence the designs obtained from different machines were not comparable.

After Kim, significant advances to the valve plate optimization software were done by (Kalbfleisch 2015). The improvements in computational power, along with the use of parallel

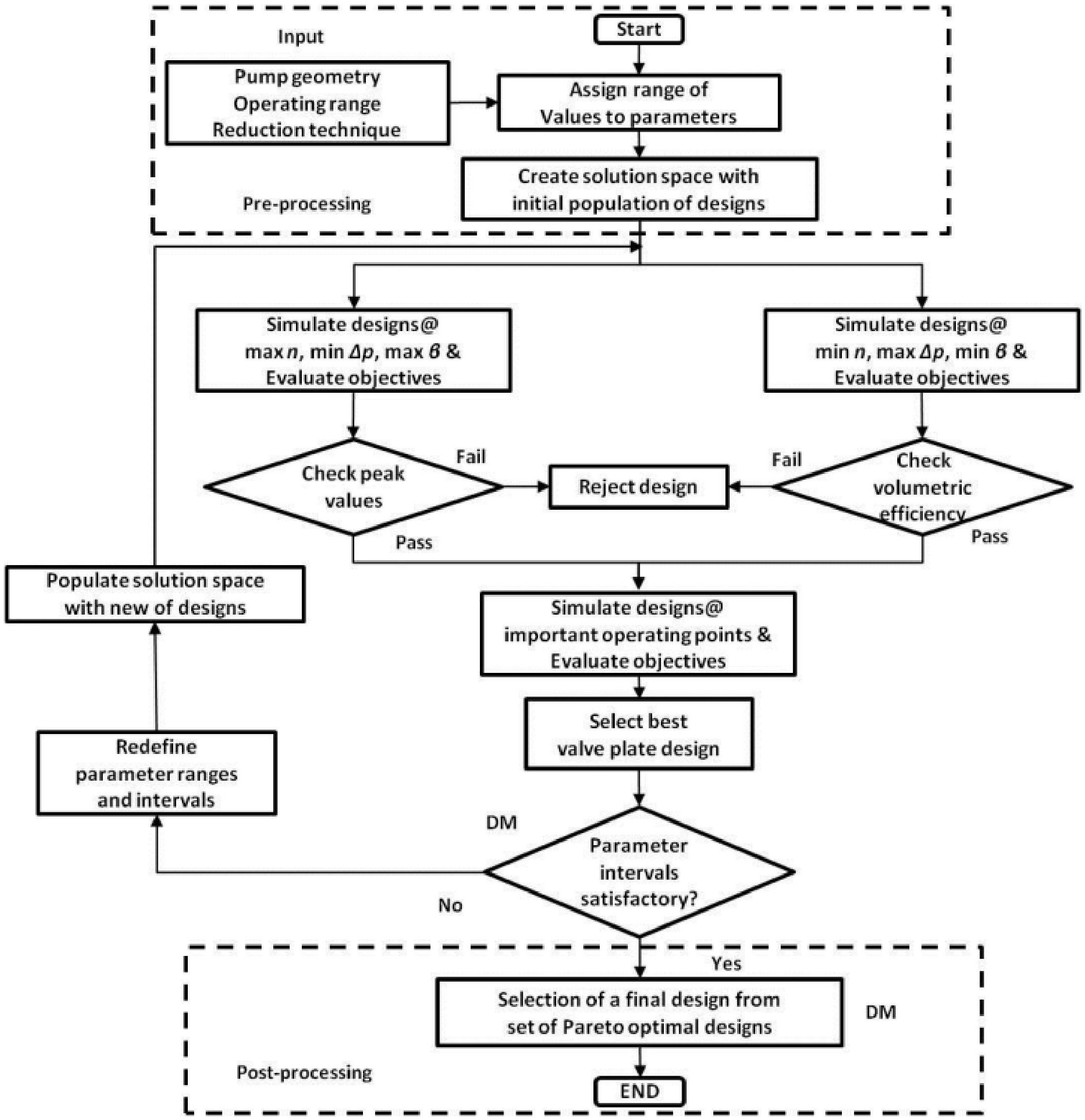

Figure 2.2. The algorithm flow chart devised by (Kim 2012).

machines helped in moving towards a population based approach for finding the optimum valve plate design. The flowchart for Kalbfleisch's algorithm is shown in Figure(2.3).

Apart from implementing a new solver LSODA (Petzold & Hindmarsh 1997), which greatly improved simulation times, Kalbfleisch automated the process of valve plate optimization by combining the in house software tool 'Pressure Module' with the genetic algorithm NSGA II (Deb, Pratab, Agarwal & Meyarivan 2002)). This did away with the

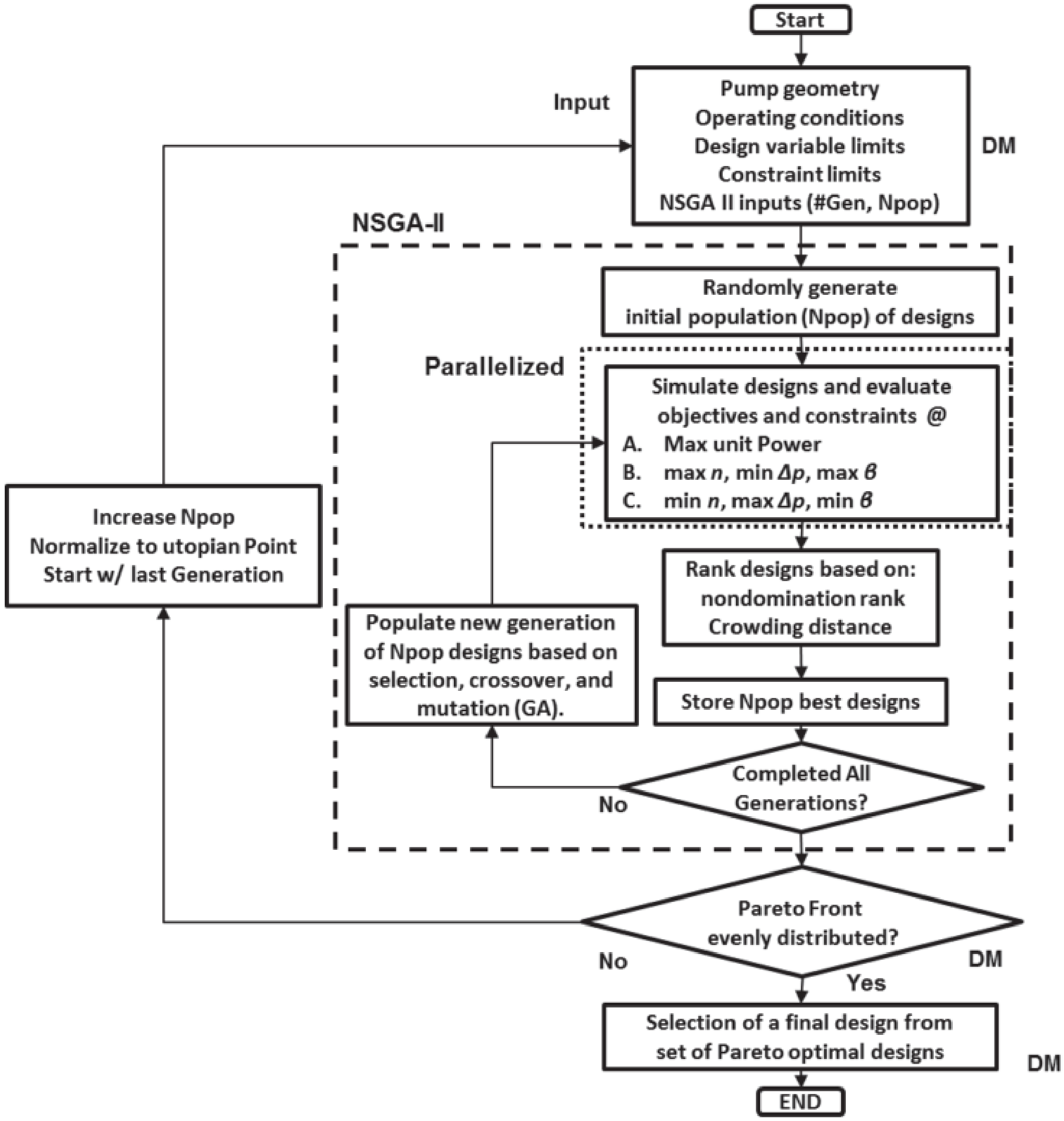

Figure 2.3. The algorithm flow chart devised by (Kalbfleisch 2015).

involvement of the 'DM' in the optimization loop. Another major advantage of this optimization methodology was that it eliminated the use of the controversial weights, which were assigned to the objective functions and did not have any specific mathematical basis for the same. The incorporation of the algorithm NSGAII with the Pressure Module resulted in a set of non dominated designs called the Pareto Front.

2.4 Aim of this work

All the works cited above have been a tremendous influence on the current work. The significant strides mades in computing power, simulation tool development for axial piston machines, development of advanced genetic algorithms and efficient post processing techniques have bolstered this work. The main aim of this work is to develop a software tool in open source programming language which takes advantage of an advanced simulation tool for swash plate type axial piston machines, coupled with parallel computation and an advanced archive based genetic algorithm to meticulously parametrize the relief groove geometry and quantify the noise sources to optimize the valve plate design for noise reduction. This software has been named ***Mi****nimization of* ***No****ise* ***S****ources* (MiNoS). The improvements to the parametrization scheme, the choice of the objective functions, the implementation and as the case study shows, the improved designs obtained are significant contributions of the current work.

3. PUMP KINEMATICS AND COMPUTATIONAL MODEL

Axial piston pumps are a set of widely used positive displacement machines, where a set of rotating pistons are used to pressurize hydraulic fluid. The two types of axial piston pumps are

- Swash plate type
- Bent axis type

Compared to bent axis designs, swash plate type axial piston pumps are simpler and have lower production costs. The also give us the advantages of robustness, high bandwidth and ease in changing the displacement of the unit (by changing the angle of the swash plate). These advantages make them very popular for most industrial applications.

3.1 Axial Piston Pump of the Swash Plate type

In axial piston pumps of the swash plate type, the pistons are supported on an inclined plate known as the swash plate, as shown in Figure(3.1).

A more detailed illustration of a swash plate type axial piston pump is shown in Figure(3.2). The spline shaft is connected to the cylinder block and thus the torque transmitted from the engine to the spline shaft causes an equivalent rotation of the block. The cylinder block rotates about the z axis with an angular speed of ω, whereas the swash plate is capable of rotation about the x axis. The swash plate angle β is measured with respect to the y axis (Figure (3.1(b))).

With the shaft rotation, the movement of the piston along the z direction is given by Equation (3.1).

$$s_K = -z \tag{3.1}$$

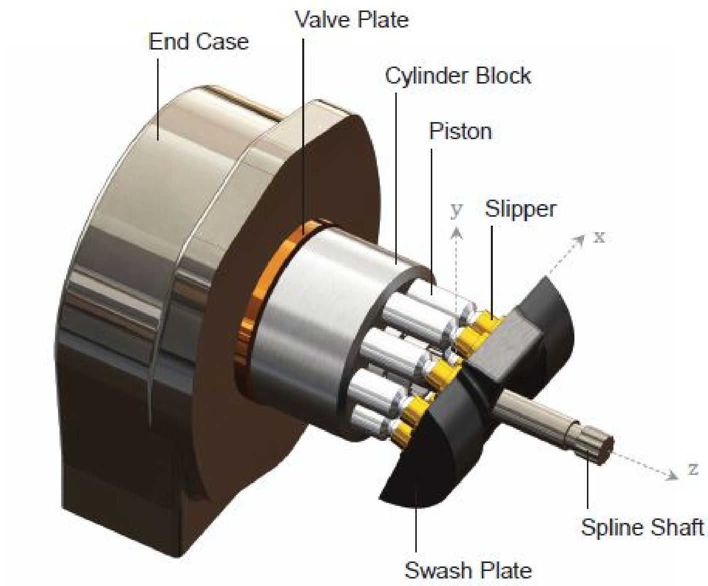

(a) Isometric View

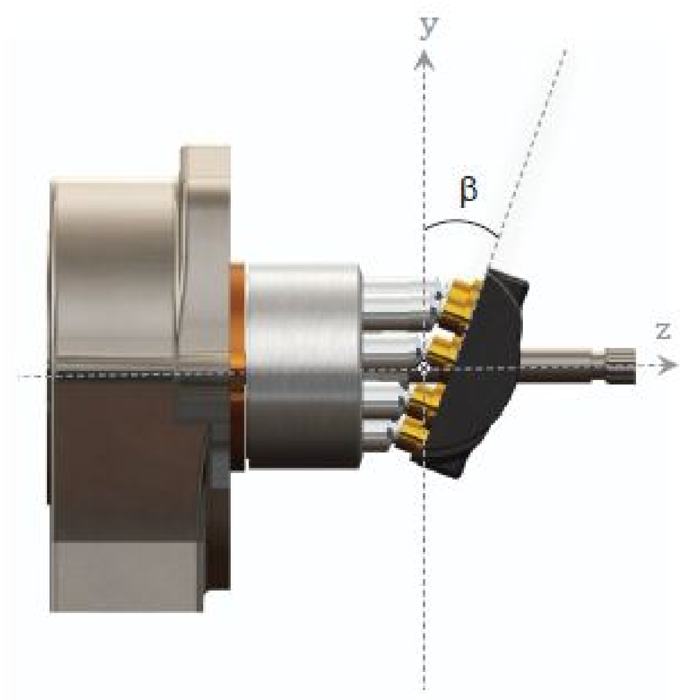

(b) Side View

Figure 3.1. Axial Piston Pump (Ernst 2015).

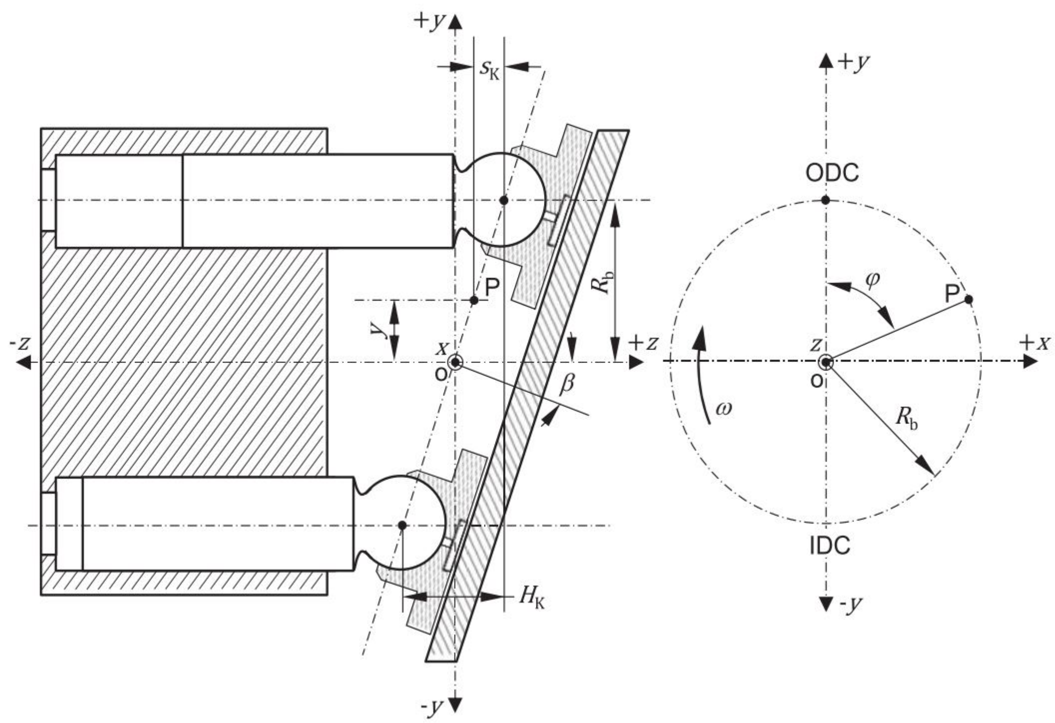

Figure 3.2. Detailed Schematic of Axial Piston Pump (Ivantysyn & Ivantysynova 2003).

The axis of each piston rotates along a hypothetical circle called the pitch circle and the radius of this circle, called the pitch radius (R_b) can be seen in Figure (3.2). From Figure(3.2),in terms of the pitch radius (R_b), the angular position of the piston (ϕ) and the swash plate angle (β) we get the equations shown.

$$z = b.\tan\beta \tag{3.2}$$

$$b = R_b - y \tag{3.3}$$

$$y = R_b.\cos\phi \tag{3.4}$$

From the above equations, the displacement of the piston can be written as shown below

$$s_K = -R_b.\tan\beta.(1 - \cos\phi) \tag{3.5}$$

From Equation (3.5) shown above, it can be seen that for a constant β, the maximum and the minimum values of the pump displacement (s_K) occur when ϕ is equal to 180° and 0° respectively. These piston positions are known as Inner Dead Center (IDC) and Outer Dead Center (ODC) respectively.

Similarly, the stroke length can be derived as

$$H_K = 2R_b.\tan\beta \tag{3.6}$$

The velocity, in terms of the pump displacement can be written as

$$v_K = \frac{ds_K}{dt} = \frac{ds_K}{d\phi}.\frac{d\phi}{dt} = \frac{ds_K}{d\phi}.\omega \tag{3.7}$$

Again, from Equation (3.5), for a constant β, the relative velocity of the piston along the z-axis is

$$\frac{ds_K}{dt} = -R_b.\tan\beta.\sin\phi \tag{3.8}$$

$$v_K = -\omega.R_b.\tan\beta.\sin\phi \tag{3.9}$$

From Equation (3.6) and Equation (3.9), v_K can be written as

$$v_K = -\frac{1}{2}.\omega.H_K.\sin\phi \tag{3.10}$$

Thus, the acceleration of the piston, in terms of v_K is obtained as

$$a_K = \frac{dv_K}{dt} = \frac{dv_K}{d\phi}.\frac{d\phi}{dt} = \frac{dv_K}{dt}.\omega \tag{3.11}$$

From equation(3.9) and (3.11), we have

$$a_K = -\omega^2.R_b.\tan\beta.\cos\phi \tag{3.12}$$

Finally, in terms of the stroke length H_K, the acceleration of the piston can be expressed as

$$a_K = -\frac{1}{2}.\omega^2.H_K.\sin\phi \tag{3.13}$$

Due to the cylinder block rotation, the circumferential speed of the piston is given as

$$v_u = R_b.\omega \tag{3.14}$$

and hence the radial acceleration of the piston is given as

$$a_u = R_b.\omega^2 \tag{3.15}$$

The coriolis acceleration is ignored for our model, as the vector of the angular velocity (ω) and the vector of the piston velocity (v_K) run parallel.

3.2 Pressure Buildup Equation

During the working cycle of the axial piston pump, pressure develops inside the displacement chamber as per the Equation (3.16) shown below. The control volume of the displacement chamber for pressure build up is shown in Figure (3.3)

$$\frac{dp}{dt} = \frac{K}{V_i}(Q_{ri} - Q_{SKi} - Q_{SBi} - Q_{SGi} - \frac{dV_i}{dt}) \tag{3.16}$$

For those interested in the derivation of this equation, I refer them to (Ivantysyn & Ivantysynova 2003).

In Equation (3.16), K refers to the bulk modulus of the hydraulic fluid, V_i is the effective volume inside the displacement chamber for that particular piston position. Q_{ri} is the net flow into the displacement chamber, given by Equation (3.17) below.

$$Q_{ri} = Q_{rHPi} + Q_{rLPi} \tag{3.17}$$

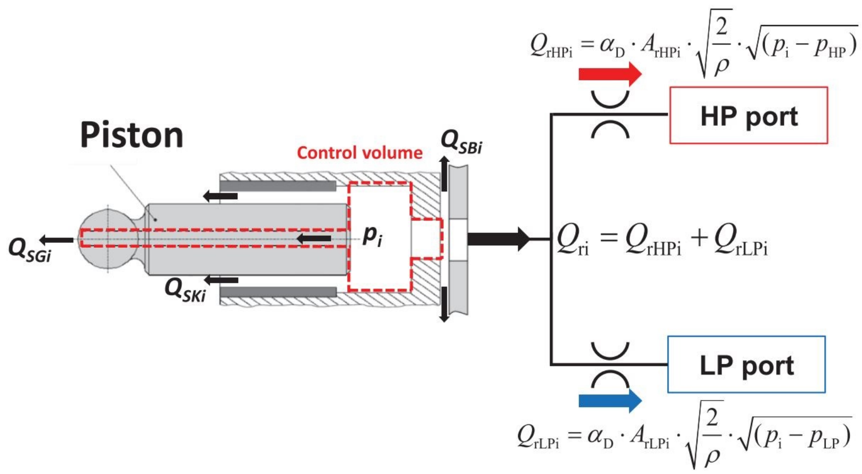

Figure 3.3. Displacement chamber control volume (Kim et al. 2014).

In Equation (3.17) above, Q_{rHPi} is the flow to the high pressure port from the displacement chamber, and Q_{rLPi} is the flow from the low pressure port to the displacement chamber. Q_{SKi} is the leakage through each piston- cylinder interface. Q_{SBi} is the leakage through the cylinder block- valve plate interface, and Q_{SGi} represents the leakage through the slipper-swash plate interface. Because of the negligible effect of the valve plate design on the external leakage and for simplification purposes, these three external leakages (Q_{SKi}, Q_{SBi} and Q_{SGi}) are ignored in our simulation model.

$\frac{dV_i}{dt}$ is the rate of change of the displacement chamber volume as the piston reciprocates. Ignoring the piston- cylinder gap, if A_K is the cross sectional area of the piston, then $\frac{dV_i}{dt}$ can be written as

$$\frac{dV_i}{dt} = v_K.A_K \tag{3.18}$$

Using Equations (3.9) and (3.18), we obtain

$$\frac{dV_i}{dt} = -\omega.R_b.A_K.\tan\beta.\sin\phi \tag{3.19}$$

$\frac{dV_i}{dt}$ can also be written in terms of the stroke length as

$$\frac{dV_i}{dt} = -\frac{1}{2}.\omega.A_K.H_K.\sin\phi \tag{3.20}$$

3.3 Flow Calculations

In Equation (3.17), Q_{rHPi} and Q_{rLPi} represent the flows to and from the high and the low pressure ports from and to each displacement chamber respectively. These flows can be represented by the orifice equations shown below

$$Q_{rHPi} = \alpha_D.A_{rHPi}.\sqrt{\frac{2|p_i - p_{HP}|}{\rho}}sgn(p_i - p_{HP}) \tag{3.21}$$

$$Q_{rLPi} = \alpha_D.A_{rLPi}.\sqrt{\frac{2|p_i - p_{LP}|}{\rho}}sgn(p_i - p_{LP}) \tag{3.22}$$

In Equation (3.21) and Equation (3.22), α_D represents the orifice constant and its value is taken as 0.6, p_i represents the displacement chamber pressure, p_{HP} and p_{LP} represent the pressures in the High Pressure (HP) port and the Low pressure (LP) port, ρ represents the hydraulic fluid density, A_{rHPi} and A_{rLPi} represent the effective areas available for flow in the orifice equations, between the displacement chamber and the HP port, and the displacement chamber and the LP port. These areas are effectively obtained from the valve plate.

3.4 Valve Plate and the Area File

The valve plate is modeled as an orifice plate between the displacement chamber and high/low pressure ports as shown in (Figure (3.4)). Figure(3.4(b)) shows an example position of a piston displacement chamber in reference to the valve plate.

As a displacement chamber rotates from $\phi = 0°$ to $\phi = 360°$, the effective area available for flow is calculated. This is done with the help of an in house CFD tool, AVAS (Ivantysynova, Huang & Christiansen 2004). In AVAS, the rotation of the displacement chamber, in fixed steps, with respect to the pressure ports is considered (Figure (3.5(a))), and for each such position, the streamline of the flow between the displacement chamber volume and the port volume is solved (Figure (3.5(b))). The minimum area perpendicular to this streamline is calculated and is stored in a text file, which we call the area file.

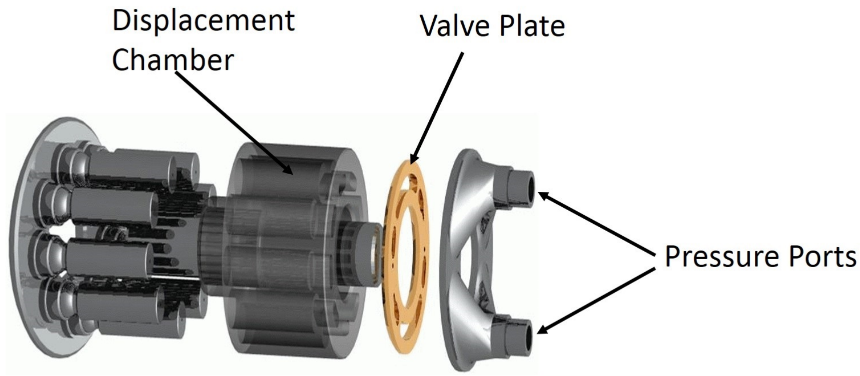

(a) Axial piston pump: exploded view.

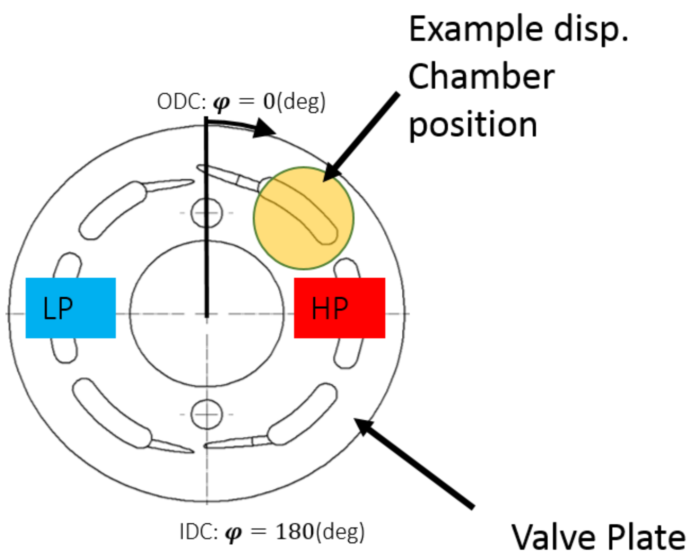

(b) Valve plate and an example position of the displacement chamber in reference to the valve plate.

Figure 3.4. The valve plate providing the area for fluid flow between the ports and the displacement chamber.

This area file, represents the terms A_{rHPi} and A_{rLPi} in Equations (3.21) and (3.22) respectively. The first order system of ODEs obtained by combining Equations (3.16), (3.17), (3.21), (3.22) and the equations for the port pressures is solved iteratively and for each angle step, the corresponding areas (A_{rHPi} and A_{rLPi} are chosen by the program from the area file).

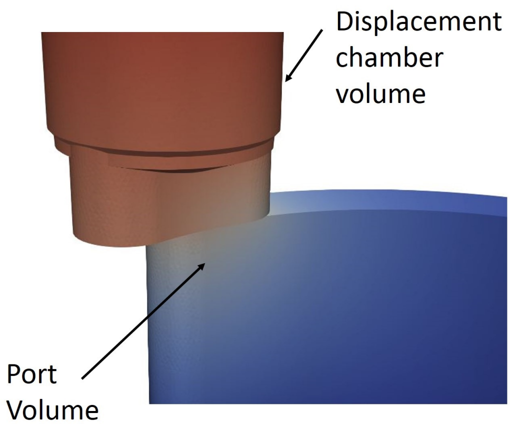

(a) DC volume and valve plate volume.

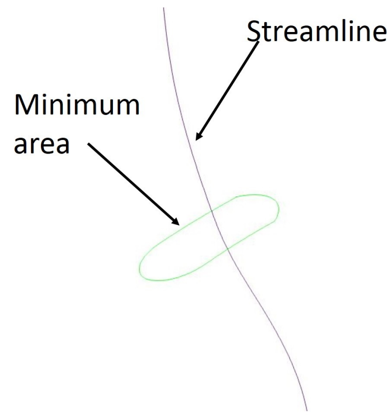

(b) Streamline and the minimum cross section perpendicular to it.

Figure 3.5. Finding the minimum cross sectional area in AVAS.

An example area file is shown in Figure (3.6) below. When the area is sufficiently large, the flow is high and hence slight changes in the areas do not affect the pressure in the displacement chamber much. The critical regions are the regions around the ODC and the IDC (where the areas are small), examples of which are shown in Figure (3.7) below. In these regions, the flows are smaller on account of smaller areas, and hence the displacement chamber pressure is more sensitive to the areas. The design of the area file around the ODC and the IDC becomes a crucial factor for controlling the pressurization and depressurization inside the displacement chamber.

Another important thing to note is that even though, for majority of the rotation, the displacement chamber is exposed to only one port (either the high pressure or the low pressure port), however at regions close to the ODC and/or IDC, the displacement chamber can be open to both the high pressure and the low pressure ports, as can be seen from the example area files in Figure(3.7). This is known as crossporting.

Thus, the design of the valve plate around the ODC and the IDC has significant influence on the pressurization of the displacement chamber, and is one of the reasons behind the greater emphasis given on the same in this work.

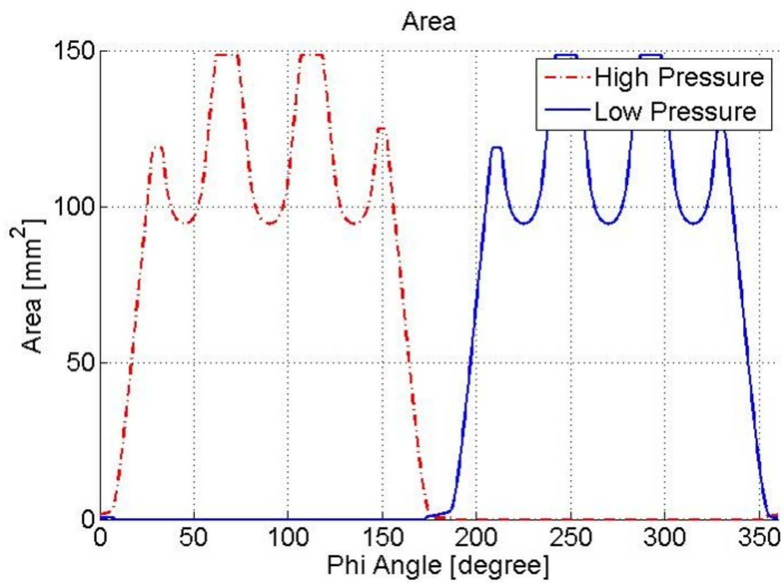

Figure 3.6. Example area file.

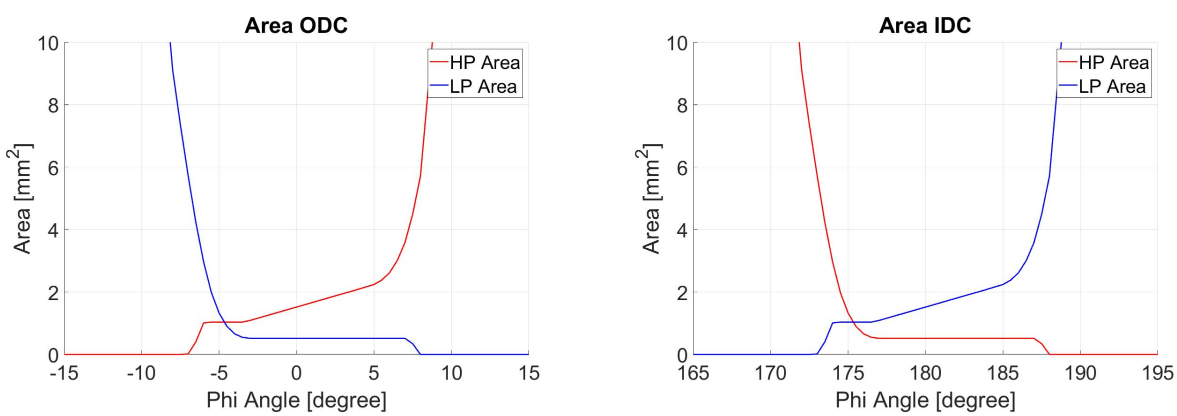

(a) ODC Area.

(b) IDC Area.

Figure 3.7. The area file around the ODC and the IDC.

3.5 Leakage* (Q_s*)

The relation between the theoretical flow rate (Q_{th}) and the the actual flow rate(Q_e) of a pump is given by (Ivantysyn & Ivantysynova 2003)

$$Q_e = Q_{th} - Q_s \tag{3.23}$$

Q_s is the flow rate loss of an axial piston pump, given by

$$Q_s = Q_{Se} + Q_{Si} + Q_{Sf} + Q_{Sk} \tag{3.24}$$

In Equation (3.24), Q_{Se} represents the external loss, i.e, the loss through the piston-cylinder, cylinder block- valve plate and the slipper- swash plate interfaces. These interfaces are extremely difficult to simulate, and the valve plate design does not have a significant influence on them. As a result, these external losses have been ignored. For details regarding the modeling of external leakage, the readers are referred to the dissertations of (Schenk 2014), (Zecchi 2013) and (Pelosi 2012).

Q_{Si} represents the internal losses, the majority of which is accounted for by crossporting. Crossporting is the phenomenon that arises when the valve plate design allows for the displacement chamber to be connected to both the high and low pressure ports simultaneously. This typically occurs near the ODC and the IDC, with the valve plate design allowing the displacement chamber to be open to both the ports simultaneously. This leads to the pressure in the displacement chamber being somewhere between that of the two ports. As a result, there will be crossport flow in the opposite direction. This flow in the opposite direction reduces the instantaneous flow, and with it the volumetric efficiency.

Q_{sf} are the losses due to incomplete filling of the displacement chamber.These losses can be avoided with proper pump design and have been neglected.

Compressibility losses (Q_{sk}) arise on account of the compressible nature of the hydraulic oil. For a constant mass of oil, the increase in pressure inside the displacement chamber decreases the volumetric flow rate of the oil, and this compressibility loss is accounted for by this term Q_{sk}.

Using the assumptions of neglecting the external losses and the filling losses, a variant of the flow loss term Q_s^* is introduced, which is given by equation(3.25) below.

$$Q_s{*} = Q_{Si} + Q_{Sk} \tag{3.25}$$

3.6 Swash Plate Moments

The pistons are supported on the swash plate, and the displacement of the pump can be changed by changing the swash plate angle (β) as can be seen from Figure(3.2). The pressure force in each displacement chamber entails in a reactant force on the swash plate, and the sum of the reactant forces from all the pistons results in a net moment on the swash plate, as can be demonstrated from Figure(3.8)

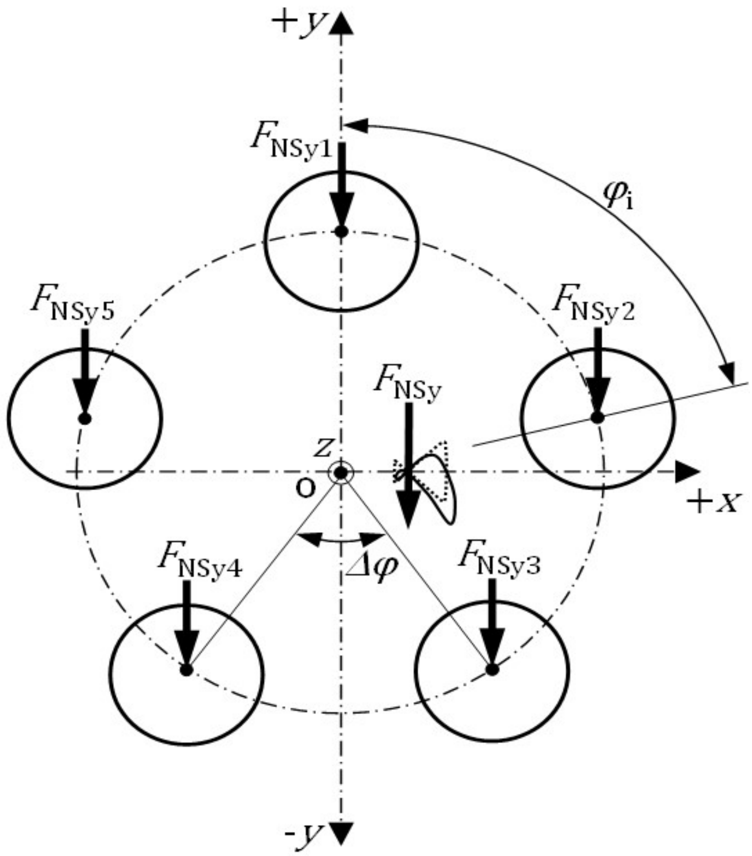

Figure 3.8. Resultant force on swash plate (Ivantysyn & Ivantysynova 2003).

Interestingly, it is seen that as the pump rotates on the shaft, the point of application of the force changes and follows the dotted line shown in Figure(3.8). This results in a non constant or fluctuating swash plate moments, in the $x-$, $y-$ and $z-$ directions.

The equations for the swash plate moments along the $x-$, $y-$ and $z-$ directions are given by

$$M_x = \frac{R_b}{\cos^2\beta}\sum_{i=1}^{z} F_{pi}\cos\phi_i \tag{3.26}$$

$$M_y = R_b\sum_{i=1}^{z} F_{pi}\sin\phi_i \tag{3.27}$$

$$M_z = -R_b\tan\beta\sum_{i=1}^{z} F_{pi}\sin\phi_i \tag{3.28}$$

F_{pi} is the reaction force on the swash plate due to the i^{th} displacement chamber and z is the number of pistons.

3.7 Validation of Pressure Module

A 1D simulation model of the swash plate type axial piston pump has been developed at Maha Fluid Power Research Center which is colloquially referred to as Pressure Module. This simulation tool solves the pressure build up equation (Equation (3.16)) to find the instantaneous displacement chamber pressure. The model has been verified with experimental data for several operating conditions. One such validation, for the operating condition of 3000 rpm speed, 100% displacement and 250 bar high pressure port is shown in Figure(3.9). Figure(3.9) establishes the accuracy of Pressure Module and validates the software tool (Kalbfleisch 2015)

3.8 Modes of Operation

With the current advances made in the field of displacement control, variable displacement pumps, exhibiting four quadrant operation have become tremendously popular. The four quadrants, exhibiting two modes for pumping and two modes for motoring are shown

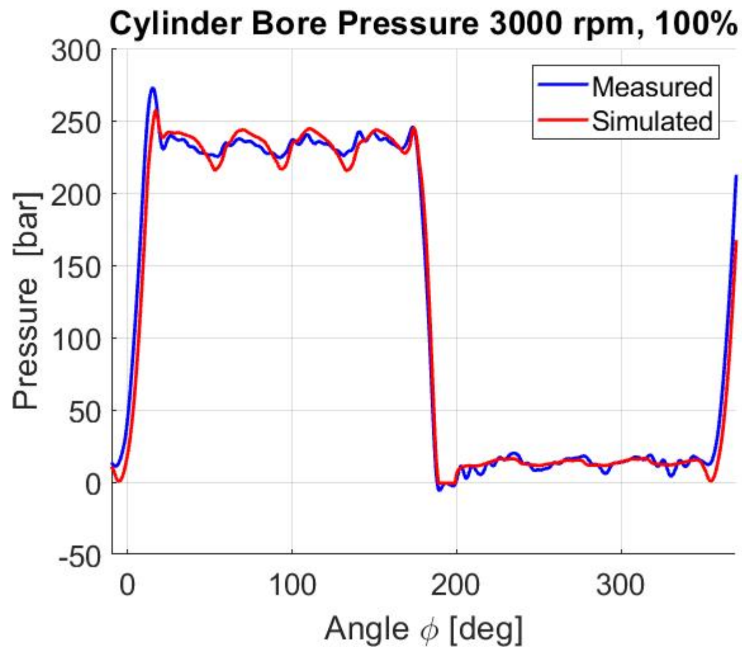

Figure 3.9. Validation of the simulation tool Pressure Module.

in Figure(3.10) below. The modes 3 and 4, having swash plate angle (β) negative are said to be overcenter. With the capability of Pressure Module to simulate modes 1 and 2, one of the aims of this work was to extend the Pressure Module to include modes 3 and 4 (overcenter pumping and motoring) as well. As will be shown in this section, this can be done by simple manipulation of the area file.

Figure(3.10) shows one valve plate whose absolute position remains the same (the relief groove numberings (1,2,3,4) of the valve plate remain the same for all the four modes), whereas the position of the high and low pressure ports, and the ODC and IDC are adjusted to represent the appropriate mode. The relative positions of the ODC and IDC are inverted when the swash plate is taken overcenter. AVAS generates the area file corresponding to Mode 1. On closer look into the valve plate for modes 1 and 3 (Figure(3.11)) with parallel positions of the ODC and the IDC and of the two ports, it can be seen that, the relative positions of valve plate quadrants 2 and 4 interchange, and 1 and 3 interchange. Following this methodology, the area file obtained for mode 1 can be manipulated for overcenter pumping (mode 3).

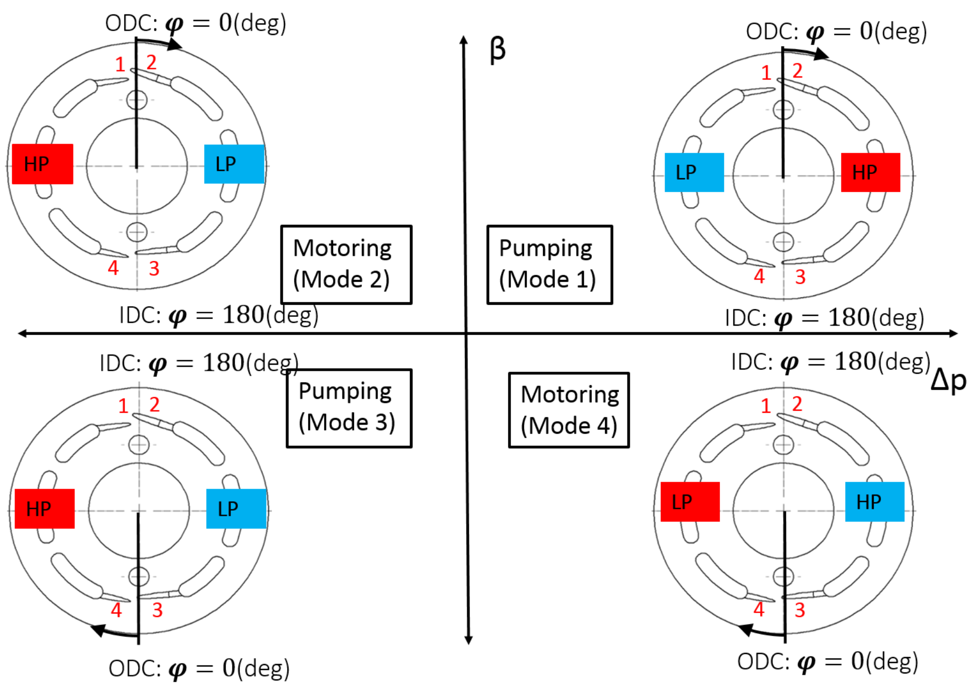

Figure 3.10. Modes of operation.

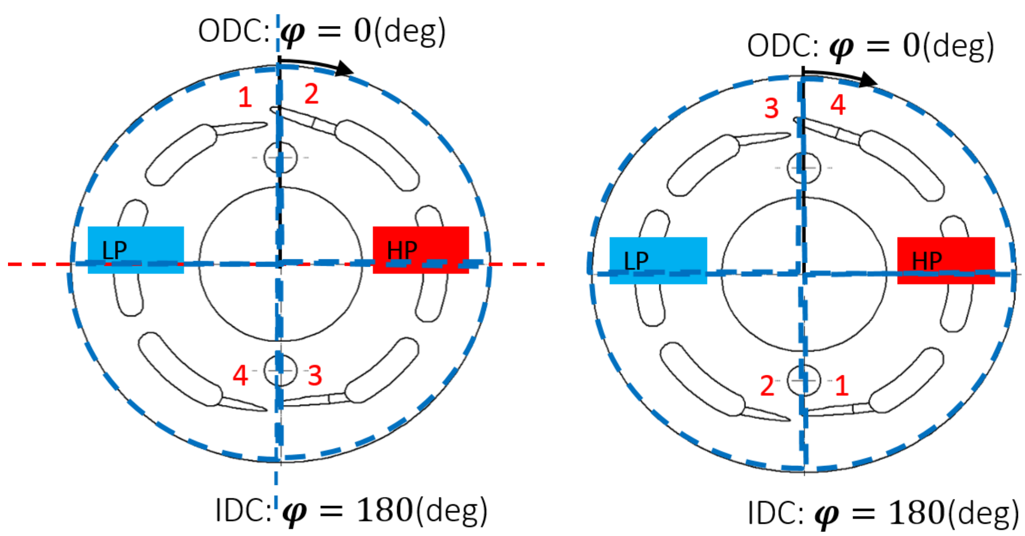

(a) Mode 1

(b) Mode 3

Figure 3.11. Pumping (mode 1) and Overcenter Pumping (mode 3).

3.9 Entrained Air

One of the most important characteristics of hydraulic oil is the bulk modulus, which inherently represents the stiffness of the hydraulic oil as a function of pressure and temperature.The bulk modulus greatly influences the build up of pressure in the displacement chamber. The bulk modulus of the hydraulic oil, however, tends to be highly affected by the presence of entrained air, which then affects the pressure build up in the displacement chamber and then finally ends up influencing the fluid borne and structure borne noise sources. As stated in (Schrank, Stammen & Murrenhoff 2014), the bulk modulus of hydraulic oil is affected by pressure, temperature as well as the presence of entrained air.

Air, in hydraulic fluids can exist in three forms: dissolved air, entrained air and/or foaming. The presence of dissolved air does not affect the fluid properties or the system behaviour (Schrank & Stammen 2014), and the amount of air that can dissolve in the fluid increases with pressure, as given by Henry- Dalton's law. Foaming generally occurs when there is more than 30% air in the oil, by volume which makes it a relatively rare phenomenon. Among all the three forms, entrained air has the highest potential to cause damage as it can increase foam potential, oxidation, pump cavitation, varnishing and sometimes even overheating.

The real challenge and unpredictability arises when the air in the fluid in present either as entrained air or as foam. In (Totten, Sun & Bishop 1997), some of the possible sources of air ingression in a hydraulic system have been discussed which can be summarized as:

- Release of dissolved air due to decrease in pressure
- Contamination of the fluid
- Presence of vacuum, such as leaks during pump suction
- Improper design of the reservoir
- Improper valve plate design (if the valve plate is designed with a large decompression zone)

Apart from reduction in the fluid bulk modulus, the presence of entrained air has been found to impact the volumetric and hydromechanical efficiencies, leading to the onset of cavitation and worsen noise problems. In (Taylor & Michael 2018), it has been experimentally verified that the presence of entrained air decrease the volumetric efficiency of different grades of ISO VG46 oil. While the presence of entrained air increase the hydromechanical efficiency, this increase is found to be smaller, as compared to the decrease in volumetric efficiency. Furthermore, another important conclusion from this was that entrained air was responsible for significant increase in measured ISO 5326 loudness of axial piston pumps.

A well designed system can have volumetric content of air as low as 0.5% upto 10% (ERICSON & PALMBERG 2008). Owing to the significant influence imparted by the presence of entrained air in noise as well as efficiencies, it was reasonable to include a model for the same in our computational model.

The entrained air model that is being looked into and incorporated in this work is the IFAS model, developed by Murrenhoff (Murrenhoff 2011). This model is much more reasonable and accurate as compared to the preexisting air model present in the simulation tool, 'Pressure Module'. The previous model simply multiplies the original bulk modulus by the difference of unity and the estimated volume fraction of air in the fluid. Compared to this model, the IFAS model is much more accurate. Two important reasons for choosing this particular model are:

1. The IFAS model has been validated through experiments (Kim & Murrenhoff 2012)

2. The IFAS model does not add too much overhead time to our simulation model.

The equation for the IFAS model is:

$$K_{ef} = \frac{(1-\alpha)(1+\frac{m.(p-p_0)}{K_0})^{\frac{-1}{m}} + \alpha.(\frac{p_0}{p})^{\frac{1}{\kappa}}}{\frac{1}{K_0}.(1-\alpha).(1+\frac{m.(p-p_0)}{K_0})^{-\frac{m+1}{m}} + \frac{\alpha}{\kappa.p_0}.(\frac{p_0}{p})^{\frac{\kappa+1}{\kappa}}} \tag{3.29}$$

In Equation 3.29, K_{ef} is the effective bulk modulus, K_0 is a constant term equal to the bulk modulus at high pressures, α is the volumetric content of the entrained air at initial pressure p_0, p is the pressure, κ is the polytropic constant of air, m represents the pressure related term in the bulk modulus of oil. For no entrained air ($\alpha = 0$), Equation(3.29) simplifies to

$$K_{ef} = K_0 + m(p - p_0) \tag{3.30}$$

With the assumption that the bulk modulus varies linearly with pressure, m is the proportionality constant.

The IFAS model has been validated through experiments for different levels of entrained air (Kim & Murrenhoff 2012). The same model has been validated through three different experimental methods for different levels of entrained air, and the results obtained for all three of them are significantly satisfying (Figure(3.12)).

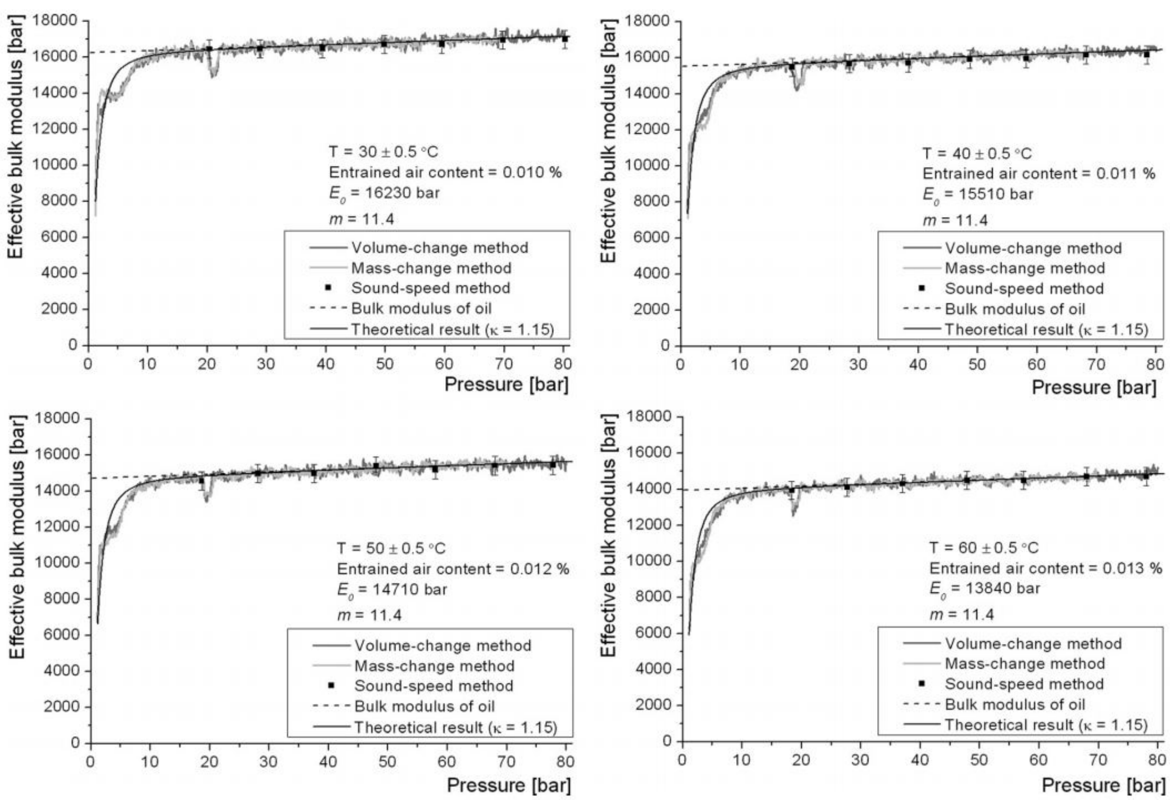

Figure 3.12. Experimental Validation of the IFAS Entrained Air model (Kim & Murrenhoff 2012).

Additionally, a significant correlation between the simulation as well as experimental results was also obtained for pressures below 1 bar, as can be seen from Figure(3.13(b)). This gives sufficient impetus to implement the model in Pressure Module.

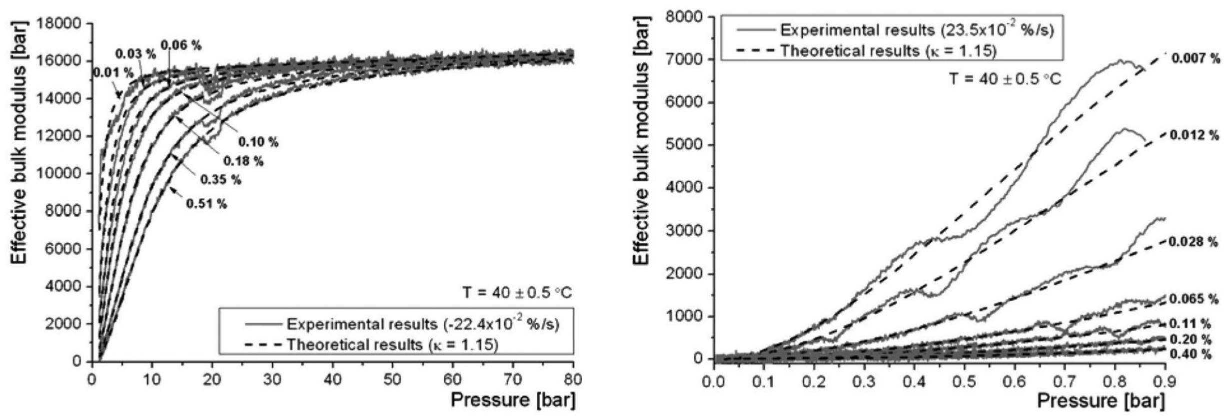

(a) High pressure validation

(b) Low pressure validation

Figure 3.13. Experimental validation of the IFAS Entrained Air Model for low and high pressures (Kim & Murrenhoff 2012).

3.9.1 Simulations of the IFAS Model

With the incorporation of the IFAS Entrained Air Model in Pressure Module, the effect of different levels of entrained air was analysed on the displacement chamber pressure, as well as the port pressures and swash plate moments.

The presence of entrained air increases the compressibility of the hydraulic fluid. This leads to a decrease in the effective fluid bulk modulus, leading to a slower pressurization rate initially, followed by a rapid increase. This can be seen from Figure (3.15) and Figure (3.14), where the rate of compression evidently seems to be affected as the entrained air levels increase. However, the effect on the rate of expansion seems to be less. This effect on the change in the rate of compression and expansion because of the change in the bulk modulus of the hydraulic fluid also results in sharp spikes in the piston flow around the ODC and the IDC (Figure (3.16)).

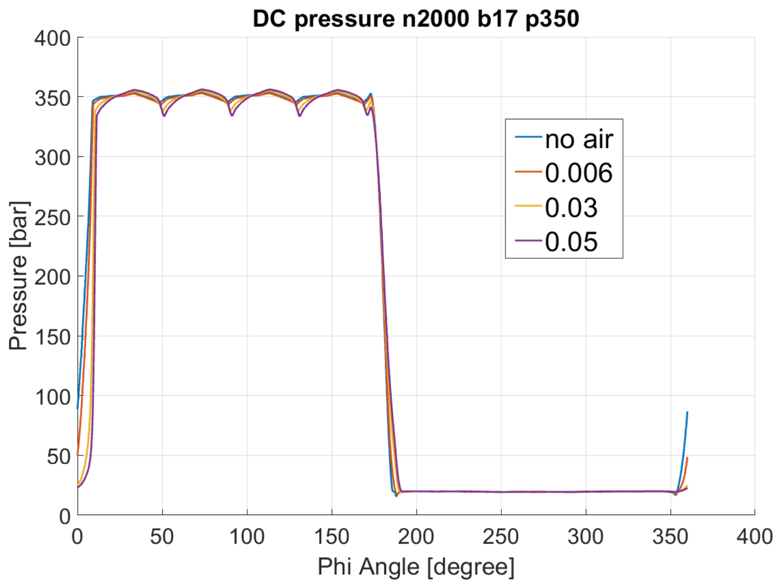

Figure 3.14. Impact of entrained air on the displacement chamber pressure.

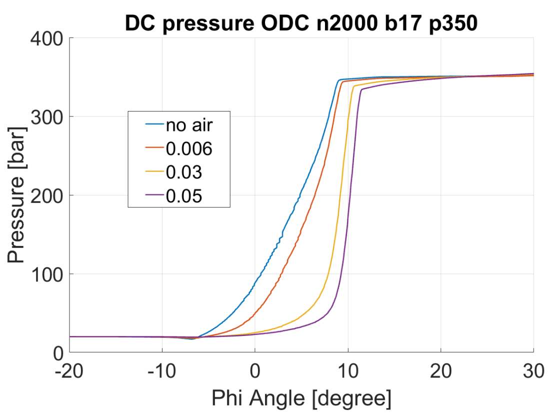

(a) Effect of entrained air on DC compression

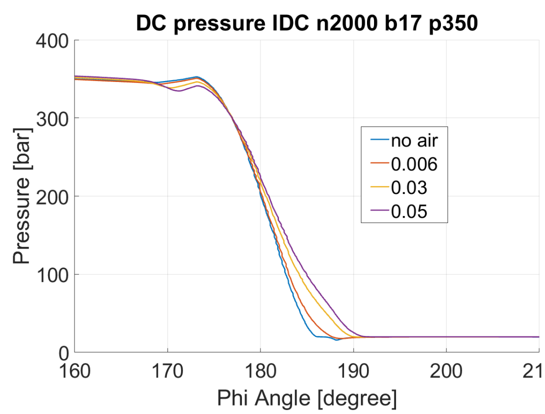

(b) Effect of entrained air on DC expansion

Figure 3.15. Effect of the presence of entrained air on compression and expansion inside the displacement chamber

Even though the effect on the rate of compression and the rate of expansion is marginal, yet the same is found to have a tremendous influence on the swash plate moments in the x- and the y- directions. As the level of entrained air increases, the swash plate moment ripples also increase, which can then lead to greater structure borne noise (Figure(3.17)).

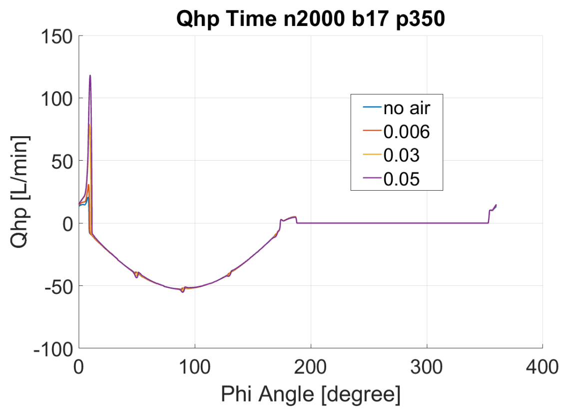

(a) Effect of entrained air on the delivery flow.

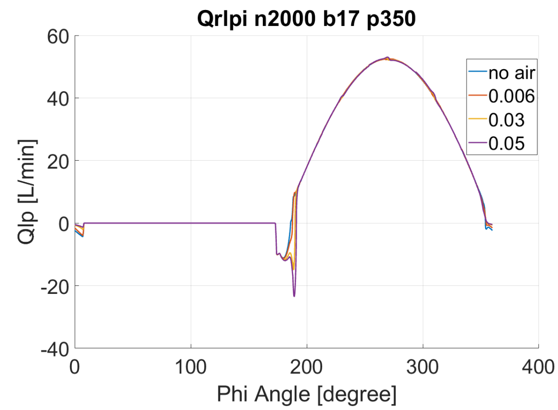

(b) Effect of entrained air on the suction flow.

Figure 3.16. Effect of the presence of entrained air on the delivery and suction flows.

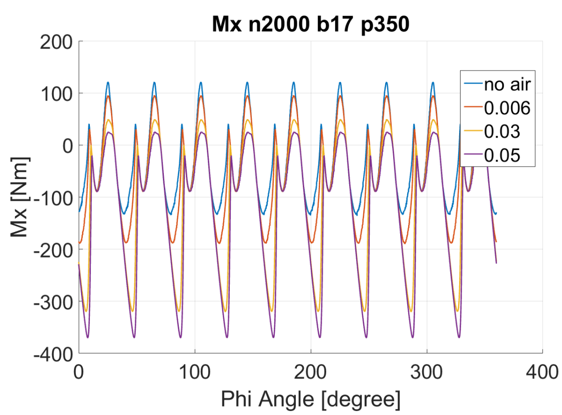

(a) Effect of entrained air on the swash plate moment M_x.

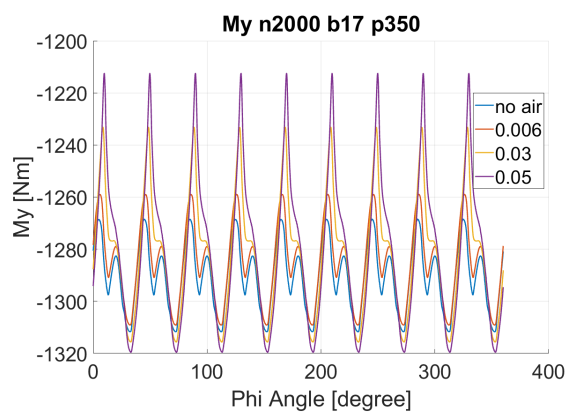

(b) Effect of entrained air on the swash plate moment M_y.

Figure 3.17. Effect of the presence of entrained air on the swash plate moments in the x- and y- directions.

Finally, on observing the port pressures as well, it can be seen that the amplitudes of the high pressure port pressure ripples increase with an increase in the level of entrained air, thus signifying an increase in fluid borne noise sources.

In summary, it can be seen from these simulation results that the presence of entrained air has the capability to exacerbate both fluid borne and structure borne noise sources.

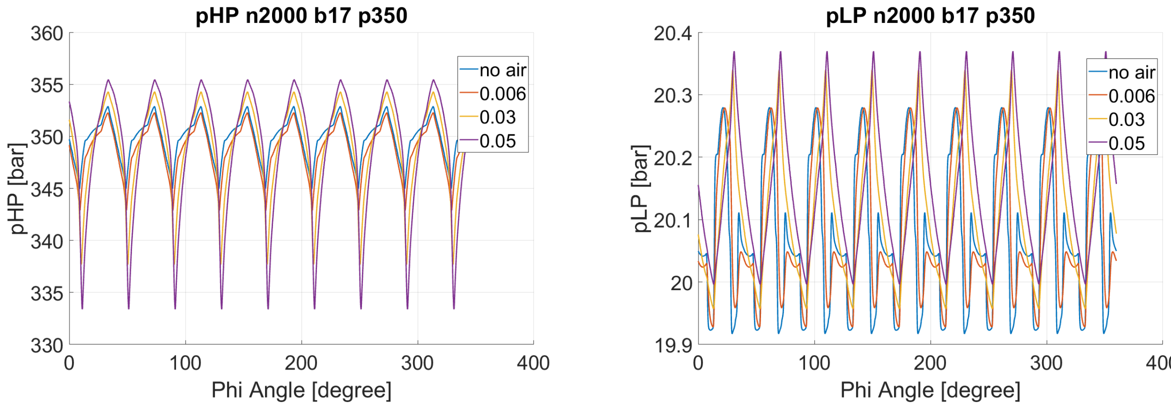

(a) Effect of entrained air on high pressure port.

(b) Effect of entrained air on low pressure port.

Figure 3.18. Effect of the presence of entrained air on the pressures of the delivery port and the suction port.

Keeping the same in mind, the verified IFAS Entrained Air model has been incorporated in the Pressure Module.

4. NOISE SOURCES IN AXIAL PISTON MACHINES AND REDUCTION TECHNIQUES

As it has been mentioned previously, one of the major challenges of axial piston machines is the high noise, and in order to address this problem it is important to understand the sources of noise. Traditionally, noise in hydraulic machines are classified into two types- fluid borne noise sources (FBNS) and structure borne noise sources (SBNS). In spite of this classification, both these sources are interrelated. In this chapter, the origin of both these noise sources is discussed and the role of valve plate design in influencing them has been taken up in detail as well. Along with it, some of the innovations in pump design from noise reduction considerations have been discussed as well.

4.1 Noise Sources

In the domain of hydraulics, air borne noise has frequently been classified as 'fluid borne noise' and 'structure borne noise'. In spite of their interrelation, most research works treat them and their contribution towards air borne noise as separate entities.

4.1.1 Fluid Borne Noise Sources (FBNS)

The net flow from a displacement chamber fluctuates in nature because of pump kinematics, fluid compressibility effects and internal leakage. The pump kinematic effects arise because of the presence of a fixed number of pistons, and several studies have shown that the amplitude of the flow ripples is greater for an even number of pistons than for an odd number of pistons. Analytical calculations of the theoretical flow rate has shown that the amplitude of the flow ripple is greater for higher rotational speeds and for the same rotational speed, it is greater for an even number of pistons than for an odd number of pistons (Ivantysyn

& Ivantysynova 2003). Figure (4.1) shows the simulated results using 'Pressure Module' for an identical pump with even and odd number of pistons, from which the higher flow ripples are fairly obvious in the case of even number of pistons. This is the main reason why most pumps are designed with an odd number of pistons.

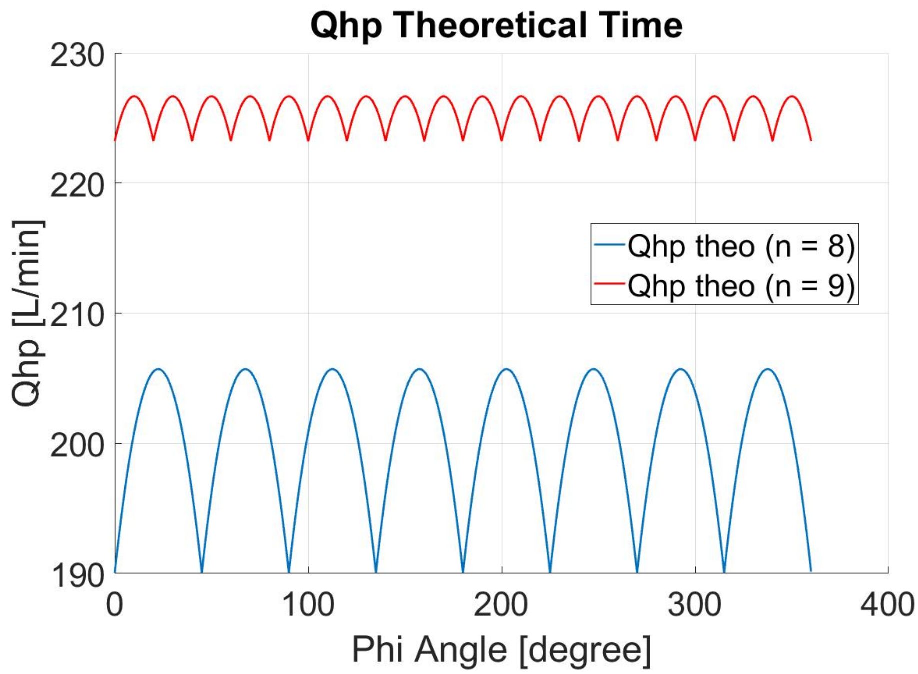

Figure 4.1. Theoretical flow for a pump with odd and even number of pistons.

From Figure (4.2) however, it can be seen that for the actual flow, the contribution of the kinematic flow towards the actual flow ripples is very less as compared to other reasons like compressibility and reverse flow which have been discussed next.

Another big contributing factor towards pump flow fluctuations is the presence of compressibility effects. After the piston reaches the outer dead center (ODC), and starts compressing the fluid in the displacement chamber as it opens to the delivery port, the flow rate of the fluid in the chamber decreases due to its compressibility. This decrease in flow rate due to the pressure increase leads to compressibility loss in the flow, and leads ultimately to more fluctuations in the net flow.

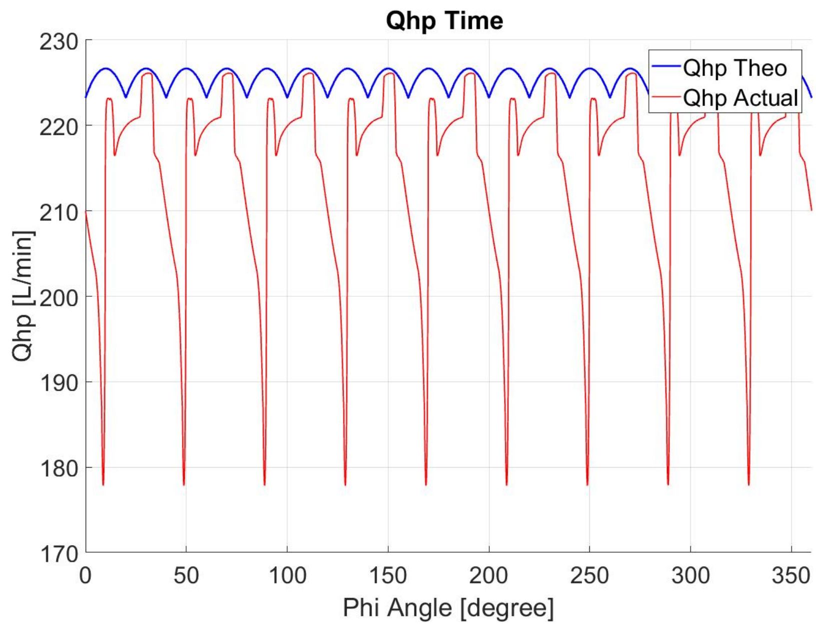

Figure 4.2. Actual flow from a pump. including compressibility losses and back flow.

Another important reason behind the occurrence of fluctuations in the net actual flow is due to reverse flow near the ODC and the inner dead center (IDC). At the ODC, as the displacement chamber closes to the low pressure suction port, the pressure inside the chamber increases. However, if the displacement chamber opens to the high pressure delivery port before the DC pressure equalizes the delivery port pressure, there is a reverse flow from the high pressure delivery port to the displacement chamber until their pressures equalize. Likewise, at the inner dead center (IDC), if the displacement chamber opens to the low pressure suction port before the pressure in the displacement chamber drops down to the suction port pressure, there will be a reverse flow from the high pressure displacement chamber to the low pressure port until their pressures equalize. These reverse flows around the ODC and the IDC are responsible for additional fluctuations to the net flow, as well as lower the volumetric efficiency of the pump.

If the displacement chamber is open to both delivery and suction ports simultaneously (at the ODC and/or IDC), the corresponding reverse flow is known as crossport flow, since the fluid flows from one port to the displacement chamber, to the other port. Even though crossport flow increases flow ripples and decreases volumetric efficiency, it will be seen later in this chapter that the same can be compromised, since it gives us greater control over the rate of pressurization in the displacement chamber.

The coupling of the net pump flow and the displacement chamber pressure by the pressure build up system of ODEs (Equation (3.16)) leads to the flow fluctuations transforming to pressure fluctuations. A remarkable explanation of this unsteady periodic flow leading to airborne noise (ABN) can be found in (Edge 1999). These pressure fluctuations travel through the attached pipework at the local acoustic velocity, and at points where there is a change of cross section, or pipe junctions and components, a part of the wave reflects back to the pump, where additional reflection takes place. These waves interact to create complex standing waves in the fluid in the pipeline. These pressure fluctuations finally lead to fluctuating forces on the pipeline and framework, leading to component vibration and air borne noise. A schematic showing this process of the generation of air borne noise from flow fluctuations is shown in Fig(4.3).

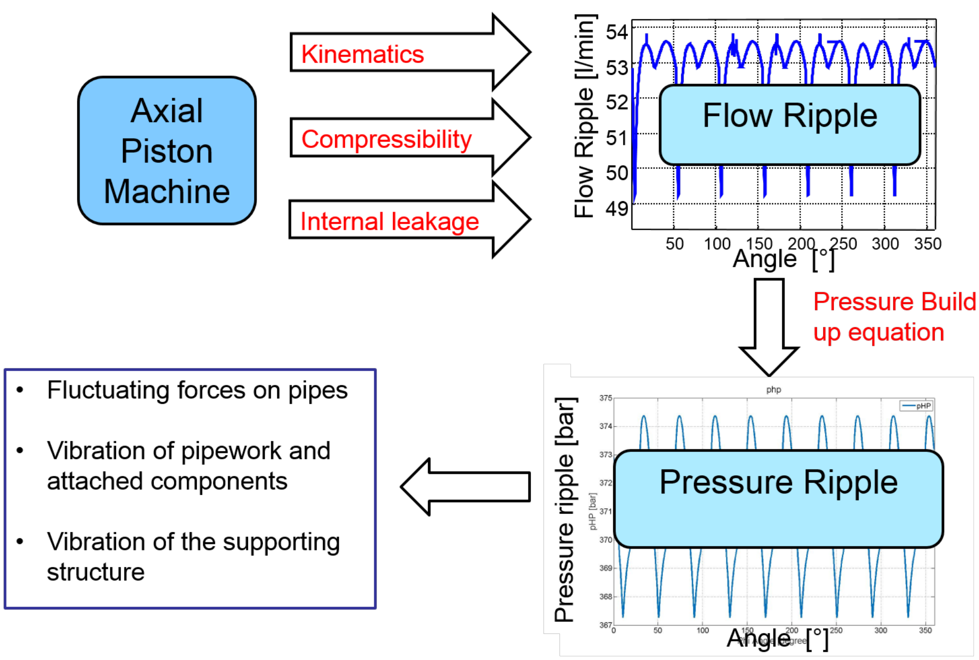

Figure 4.3. Generation of component vibration from fluctuating flows.

4.1.2 Structure Borne Noise Sources (SBNS)

The fluctuating pressures in the displacement chamber result in a net fluctuating moment on the swash plate, given by Equations(3.26), (3.27) and (3.27). Figure(4.4) shows example plots of the swash plate moments in the M_x, M_y and M_z direction.

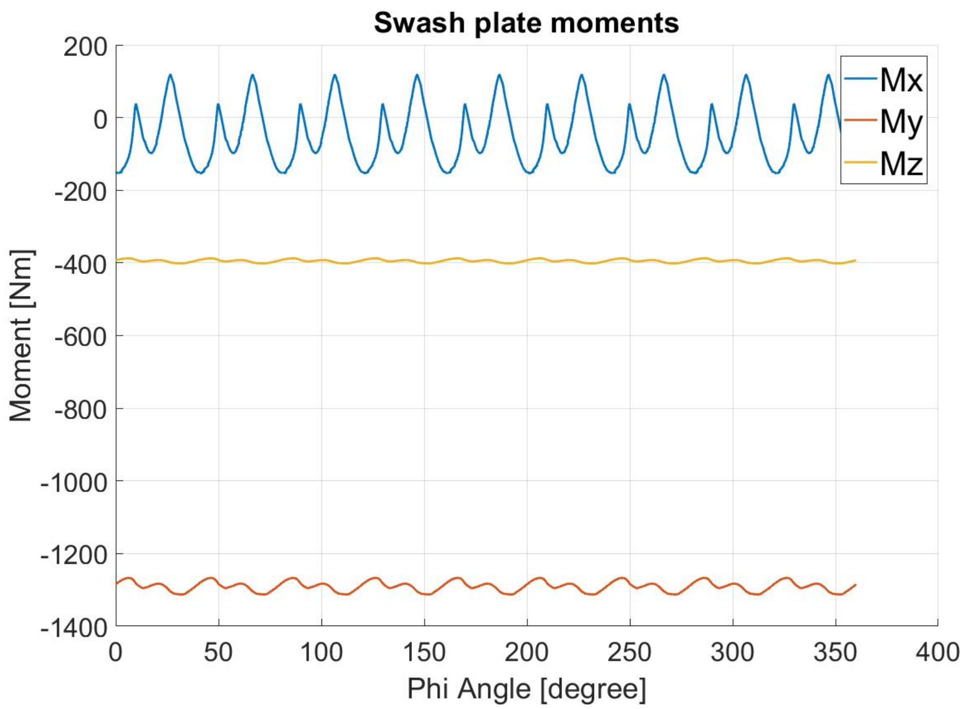

Figure 4.4. Swash Plate Moments in the x-. y- and z- directions.

This fluctuating periodic moment on the swash plate is responsible for vibrations of the swash plate, which is reacted by the case and lead to case vibrations and additional air borne noise. A schematic showing the generation of structure borne noise from displacement chamber pressure is shown in Figure(4.5) below.

For the same pump, comparing ΔM_x, ΔM_y and ΔM_z for the same operating condition, it can be seen that the ripples for M_x are much larger as compared to that of M_y and M_z. Thus, it is usually assumed that M_x contributes more towards structure borne noise than M_y or M_z.

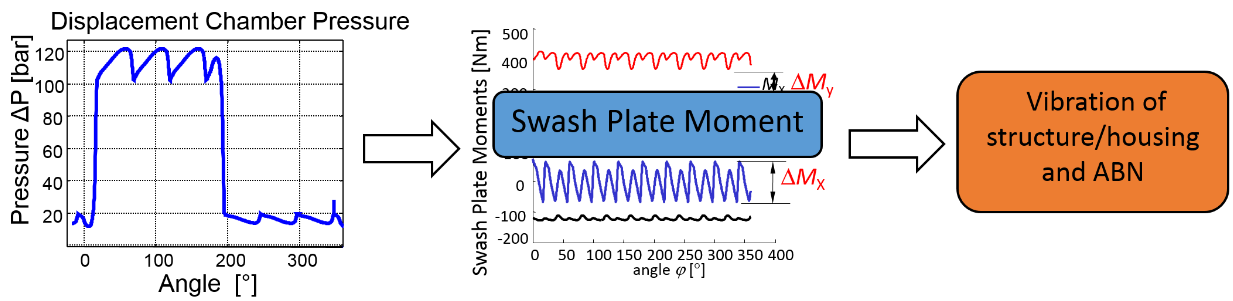

Figure 4.5. Generation of component vibration from swash plate moments.

4.1.3 Noise due to Cavitation

Cavitation is the phenomenon of the rapid collapse of air bubbles in a fluid. It typically occurs in regions where the static pressure becomes lower than the vapour pressure of the liquid. In hydraulic pumps, sometimes the pressure at the suction may become too low. The pressure inside the displacement chamber may also become too low if there is delay in opening to the ports at the IDC. As the static pressure reduces, the dissolved air comes out as air bubbles as the pressure falls below the vapour pressure. After this, as the bubbles flow into a high pressure region, or as the pressure in the displacement chamber increases, these bubbles rapidly collapse, creating shock waves and microjets. These microjets are responsible for erosion of the pump, and create unwanted noise. Therefore, during pump operation, it is essential to avoid cavitation, particularly around the suction and inside the displacement chamber at IDC.

4.2 Displacement Chamber Pressurization Rate

The ODE pressure build up equation (Equation (3.16)) gives us directly the rate of pressurization inside the displacement chamber. The effect of displacement chamber pressurization on the swash plate moments and noise has been studied in several previous works (Becker 1970), (Yamauchi & Yamamoto 1976). The critical regions are around the ODC and the IDC, when the chamber switches from one port to the other. The rate of compression and expansion at the ODC and IDC exert significant influence in the displacement chamber pressure as well as noise. In particular, lower rates of compression and expansion help in reducing pressure pulsations (Helgestad et al. 1974), (Kim, Kim, Jung, Oh & Jung 2004).

(Ivantysynova, Seeniraj & Huang 2005) found that a higher compression rate leads to greater forces on the swash plate, and with it greater structure borne noise. However, the relation is much more complicated than a direct correlation as the timing of the compression also plays an equally significant role.

The detrimental effect of a high rate of compression on the pump loudness was experimentally analysed by (Becker 1970). A more rapid rise or fall in displacement chamber pressure causes sudden loading of the mechanical parts of the pump. This aggravates noise problems (Helgestad et al. 1974). It is desirable that pressurization and depressurization should be as slow as possible in order to load and unload the piston smoothly. (Ericson, Ölvander & Palmberg 2008).

The net force on the swash plate fluctuates between a maximum and a minimum as pistons enter and leave the high pressure port. The frequency content of this fluctuation depends on the rate of pressurization of each displacement chamber. Therefore, a smaller rate of compression will result in a better control over the swash plate moments, and with it, eliminating the annoying high frequency vibrations and noise.

For reasons similar to above, a high rate of expansion in the displacement chamber is also undesirable as it may aggravate noise problems by inducing sudden loading and unloading of the mechanical components, increase pressure ripples and can increase the swash plate moment peak-to-peak amplitudes as well.

In summary, control over the rate of pressurization and depressurization in the displacement chamber gives us good control over the noise sources.

4.3 Role of Valve Plate

One of the easiest and most effective ways to influence the displacement chamber pressure is by manipulating the area in the valve plate. The compression and expansion of the hydraulic fluid in the displacement chamber is heavily influenced by the portplate timing. The ODC and the IDC, where a displacement chamber transitions from the low pressure port to the high pressure port, and vice versa respectively, are two critical regions which significantly affect the pressurization in each displacement chamber.

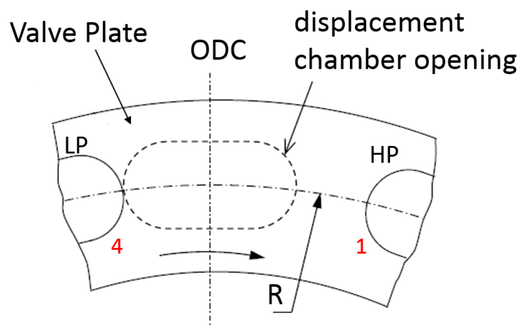

(a) Port areas and displacement chamber opening at ODC.

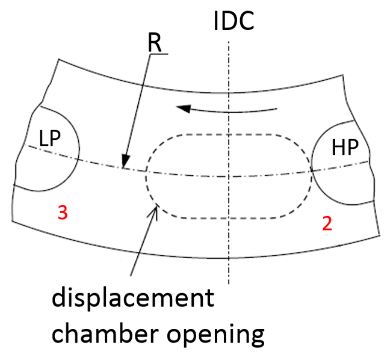

(b) Port areas and displacement chamber opening at IDC.

Figure 4.6. The opening of the displacement chamber to the suction port and the delivery port for an example port plate.

Traditionally, valve plates were designed keeping one particular operating condition in mind. At the ODC, when the displacement chamber closes off to the suction port (Figure(4.6(a))), the pressure in the chamber starts increasing as the piston starts moving from ODC and IDC, and it opens to the delivery port when the displacement chamber pressure and delivery port pressure are equal. A similar situation occurs at the IDC as well (Figure(4.6(b))). At the IDC, after the displacement chamber closes to the delivery port, the pressure in the displacement chamber starts decreasing as the piston starts moving from the IDC to the ODC, and the valve plate is designed to open the displacement chamber to the suction port when the two pressures are equal at that particular operating condition. This is known as 'ideal timing'.

A major limitation of this design technique is that it works only for one operating condition, and other operating conditions may result in overpressurization, cavitation, low efficiencies and higher noise.

For example, in figure(4.6(a)), if the kidney port closes too soon, the displacement chamber may go to lower pressures. Or if the closing of port 4 is delayed, it may cause reverse flow. Likewise, if the displacement chamber opens to the delivery port too soon, reverse flow may be seen, whereas if it opens late, it may cause overpressurization in the displacement chamber.

A similar situation is seen at the IDC as well (Figure(4.6(b))). If the kidney port closes too soon, it may cause overpressurization whereas a delayed closing may cause reverse flow. Similarly, if the kidney port opens to the suction port at the IDC too soon, a reverse flow may be seen, whereas delayed opening can cause cavitation.

Relief grooves attached to the kidney ports at ODC and IDC provide an easy and effective way of controlling the pressurization of the displacement chamber, by controlling the flow in and out of the displacement chamber. Appropriate design of relief grooves help in reducing the rate of compression and expansion in the displacement chamber. Design the relief grooves at the ODC and the IDC independently gives us sufficient freedom to reduce both the rate of compression as well as the rate of expansion simultaneously. This, in turn, helps in avoiding overpressurization peaks and underpressurization leading to cavitation, but comes at a cost to the volumetric efficiency of the pump.The presence of relief grooves, which allow small areas for flow transfer between the displacement chamber and the ports before the chamber opens to the kidney shaped port also cause reverse flow (or cross port flow if the displacement chamber is open to both the suction and delivery ports simultaneously). Yet, the fact that these relief grooves help in abating the possible fluid borne and structure borne noise sources makes reverse flow and crossport flow a necessary evil. The relief grooves extend the period over which reverse flow occurs and hence reduce the magnitude of high frequency flow ripples (Harrison & Edge 2000). The effect of relief grooves is also dependent on the suction and delivery pressures, as well as the rotational speed and pump displacement. Hence, the design and optimization of relief grooves is usually done for a range of operating conditions.

Figure(4.7) shows a portion of an example valve plate with a linear relief groove on the high pressure port side at the ODC. Even though this figure shows a linear groove, it is to be emphasized that in this work, we do not restrict to linear grooves only.

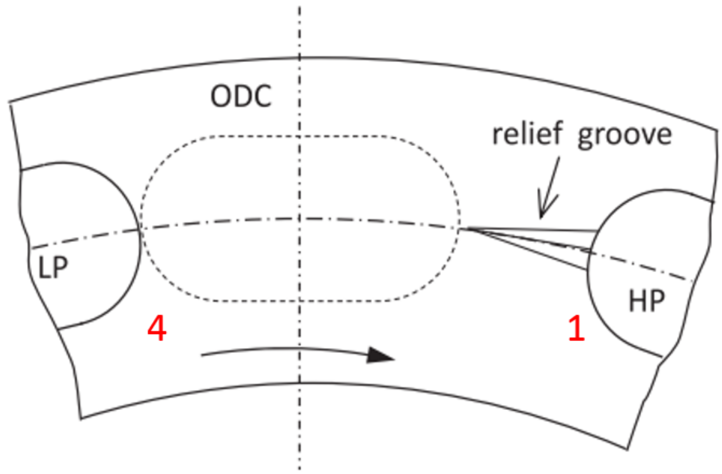

Figure 4.7. The displacement chamber opening to a port plate with a linear relief groove at ODC.

4.4 Other noise reduction techniques

In addition to the design of relief grooves, several other designers have explored other novel methods of noise abatement as well. A discussion on the same can be found in (Harrison & Edge 2000) and (Seeniraj 2009).

4.4.1 Precompression and Decompression Filter Volumes

(Pettersson et al. 1991) were the first to come up with the novel concept of precompression filter volumes (PCFV), which is a small volume connected through a narrow opening to the valve plate (Figure (4.8)). PCFV helps in pressurizing the displacement chamber to the delivery port pressure before it opens to the same.

The PCFV helps in noise reduction over a range of operating conditions. However, (Ivantysynova et al. 2005) found that, with the use of PCFV, even though the pressure ripples and flow ripples get abated, yet the high pressurization rate ($\frac{dp}{dt}$) lead to greater swash plate moment ripples which are the main source of structure borne noise. The principle of decompression filter volumes (DCFV) is similer to PCFV, with the difference being that

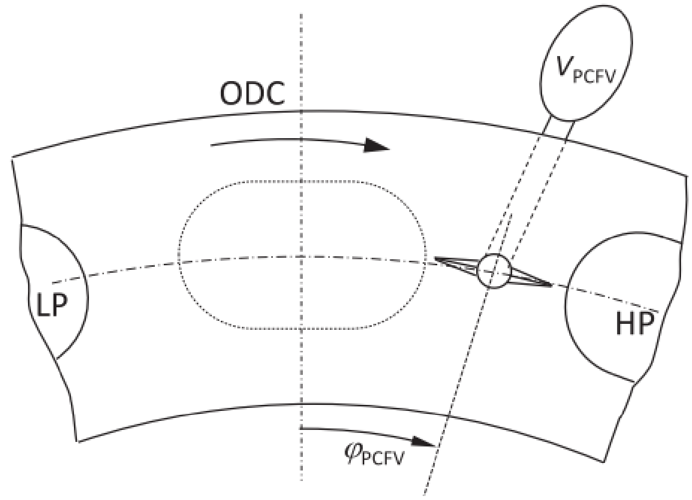

Figure 4.8. Pre Compression Filter Volume (Kalbfleisch 2015).

DCFV helps in reducing the displacement chamber pressure to the suction port pressure before it opens to the same. DCFVs suffer from the same drawback of high swash plate moment due to high rate of expansion.

4.4.2 Check Valves and Heavily Damped Check valves

(Helgestad, Foster & Bannister 1973) introduced check valves to avoid reverse flow. These check valves open the displacement chamber to the delivery port only when the displacement chamber pressure equalizes the delivery port pressure. However, this method is limited by the check vale dynamics and the undamped oscillations of the poppet create additional noise.

To remove this additional noise from the undamped oscillations of the poppet in the check valve, (Harrison & Edge 2000) came up with a heavily damped check valve (HDCV). This technique was found to reduce delivery flow ripples. But the implementation is expensive and also it has not been tested for higher speeds.

4.4.3 Cross Angle

Cross angle (γ), for an axial piston pump, is an inclination for the swash plate, perpendicular to the traditional direction of swash plate inclination (β). The introduction of the cross angle changes the position of the ODC and the IDC. (Johansson et al. 2007) has experimentally verified the reduction of flow ripples by using cross angles. Cross angle also makes the flow transients less sensitive to operating conditions. However, implementation of the same is expensive and needs redesigning of the pump. This is one of the main reasons why this technique is not yet popular in industry.

4.4.4 Active Cancellation Devices

Several researchers have also explored active cancellation devices, for reduction of flow ripples and moment ripples. (Kim & Ivantysynova 2017) used least mean squared filters for active vibration control of the swash plate. Satisfactory noise reduction was not found in this work. The use of such active noise reductions techniques is also infeasible from an economic point of view as they require installation of expensive sensors and actuators.

Even though several new technologies have been patented for noise reduction in axial piston machines, yet they are severely limited at high speeds because of the rapid opening and closing of the displacement chamber to the pressure ports. Moreover, high costs and lack of reliability has further hindered their popularity. Along with the low sensitivity to operating conditions, low cost of implementation and reliability makes relief grooves very popular with manufacturers for reduction of flow ripples and swash plate moments. Replacing the traditional trial and error method with a systematic optimization procedure for groove design is another step forward in cheap and effective reduction of noise sources in axial piston machines.

5. OPTIMIZATION METHODOLOGY

The tremendous influence that the valve plate design has on the pressurization of the displacement chamber, and with it on the effective sources of noise makes it an ideal candidate for optimization. Proper design of the valve plate will help us in abating the noise sources through appropriate control of the displacement chamber pressure. Current advances in computational power and optimization techniques has the potential to do away with the age old trial and error methods for valve plate design. This chapter describes such an optimization methodology adopted for valve plate design. The 1D simulation model for axial piston pumps has been combined with a population based genetic algorithm (AMGA2) to create the software tool 'MiNoS' for the objective of relief groove optimization for noise reduction. The optimization inputs are set by a parametrization of the area file. The objective functions are determined on the basis of the structure borne and fluid borne noise sources. Finally, to reject unfeasible designs, a set of constraints have been implemented.

5.1 Problem Statement

Optimization is the process of finding the maximum or minimum of any given function or functions, by systematically exploring a given set of inputs which may or may not be subjected to constraints. As evident from their names, a single objective optimization has a single objective function whereas a multi-objective optimization problem has more than one objective functions.

Each of the objective functions can be represented as a relation of one or more input variables, which are chosen from a sample space decided by the constraints. The objective is to find the combination of the input variables for which the maximum or the minimum of the objective function or functions is obtained.

Mathematically, an example of a multi-objective minimization problem is

$$Minimize f_1, f_2, f_3, ...f_n \tag{5.1}$$

such that f_1, f_2, f_3, ...f_n are functions of $\bar{x}$

where $\overline{x} = (x_1, x_2, x_3, ...x_k)$ subjected to the constraints

$$p(\overline{x}) <= C_1 \tag{5.2}$$

and

$$q(\bar{x}) = C_2 \tag{5.3}$$

Traditionally, these multi objective optimization problems were solved by classical methods, by converting them to a single objective by assigning appropriate weights to the objective functions. However, this method is not just cumbersome, but also inadequate as additional information about the weighing factors for each objective function is needed. Since the 1990s, population based genetic algorithms have received great popularity for solving such multi-objective optimization problems. Even though the problem statement remains the same, the major difference from classical algorithms is in the method of solving, as evolutionary algorithms adopt a more heuristic approach to solving the multi-objective optimization problem.

5.2 Objective Functions

The main goal of this work is the identification and minimization of specific hydraulic parameters which can be considered good representation of fluid borne and structure borne noise sources. The origin of noise in axial piston machines, classified in literature as fluid borne and structure borne noise sources has been explained in Chapter(4). In this section, we aim at elucidating the specific objective functions which are considered for the valve plate optimization in this work, and which can be considered as good representatives of fluid borne and structure borne noise sources.

5.2.1 Normalized Rate of Compression and Expansion

The role played by the rate of compression and expansion in the discharge flow ripples and swash plate moments is of tremendous importance. A description of the significance of the expansion and compression rate is already provided in Section 4.2. A high rate of $\frac{dp}{dt}$ at the ODC and the IDC results in pressure peaks and aggravated noise problems. Besides, there have also been evidences of greater swash plate moment ripples for higher compression rates, which is undesirable.

However, the rate of compression or expansion is speed dependent as well. For the same pressure gradient, a higher speed will entail in higher $\frac{dp}{dt}$. Hence, for speed independence, the pressurization rate is normalized with speed as shown in equation(5.4).

$$\frac{dp}{d\phi} = \frac{1}{\omega}.\frac{dp}{dt} \tag{5.4}$$

An example graph of the $\frac{dp}{d\phi}$ values, plotted against the piston rotation angle ϕ is shown in Figure(5.1). From this figure, it can be seen that the maximum value of $\frac{dp}{d\phi}$ occurs at the ODC ($\phi \approx 0°$), whereas the lowest value of $\frac{dp}{d\phi}$ occurs at the IDC ($\phi \approx 180°$).

Again from the perspective of human hearing, humans are more sensitive to higher frequencies than lower frequencies. The term $\frac{dp}{d\phi}$ can also be interpreted as a frequency weighing of the displacement chamber pressure.

For a fixed speed of rotation (ω_c), the Laplace transform of the normalized pressure rate is given in Equation (5.5)

$$\mathcal{L}\Big(\frac{dp}{d\phi}\Big) = \mathcal{L}\Big(\frac{1}{\omega_c}.\frac{dp}{dt}\Big) = \frac{1}{\omega_c}\mathcal{L}\Big(\frac{dp}{dt}\Big) = \frac{1}{\omega_c}.sP(s) \tag{5.5}$$

where $P(s)$ is the Laplace transform of the displacement chamber pressure (p). Substituting $s = j\omega$ in Equation(5.5) gives the Fourier transform for analysis in the frequency domain,

$$\mathcal{L}\Big(\frac{dp}{d\phi}\Big)|_{s=j\omega} = \frac{1}{\omega_c}.j\omega.P(j\omega) \tag{5.6}$$

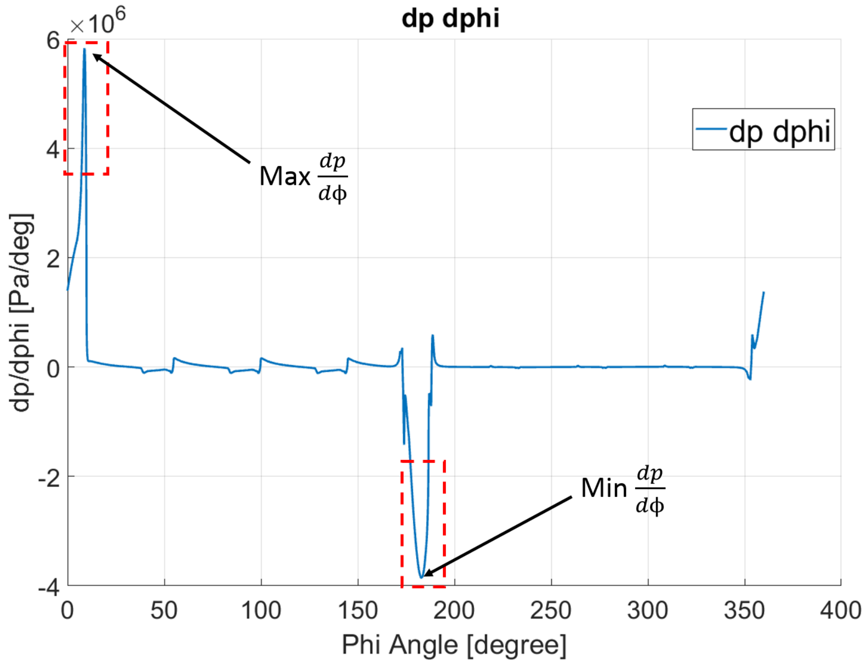

Figure 5.1. Maximum and minimum of $\frac{dp}{d\phi}$.

Thus, from Equation(5.6), it can be seen that $\frac{dp}{d\phi}$ is equivalent to a frequency weighted pressure term, and minimizing this will minimize the high frequency components.

Therefore, in order to fulfill our requirement of low compression and expansion rates, the maximum and minimum values of $\frac{dp}{d\phi}$ are taken as objective functions.

5.2.2 Amplitude of swash plate moment ripples

The rippling moments on the swash plate are understood to be the best form of structure borne noise quantification. The amplitudes of the moments in the y- and z- direction (M_y and M_z) are typically found to be lower than the moment M_x (an example is shown in Figure(5.2)). Hence, with the assumption that M_x contributes more towards the noise, we shall be considering the peak-to-peak amplitude of only M_x (ΔM_x) as an objective function.

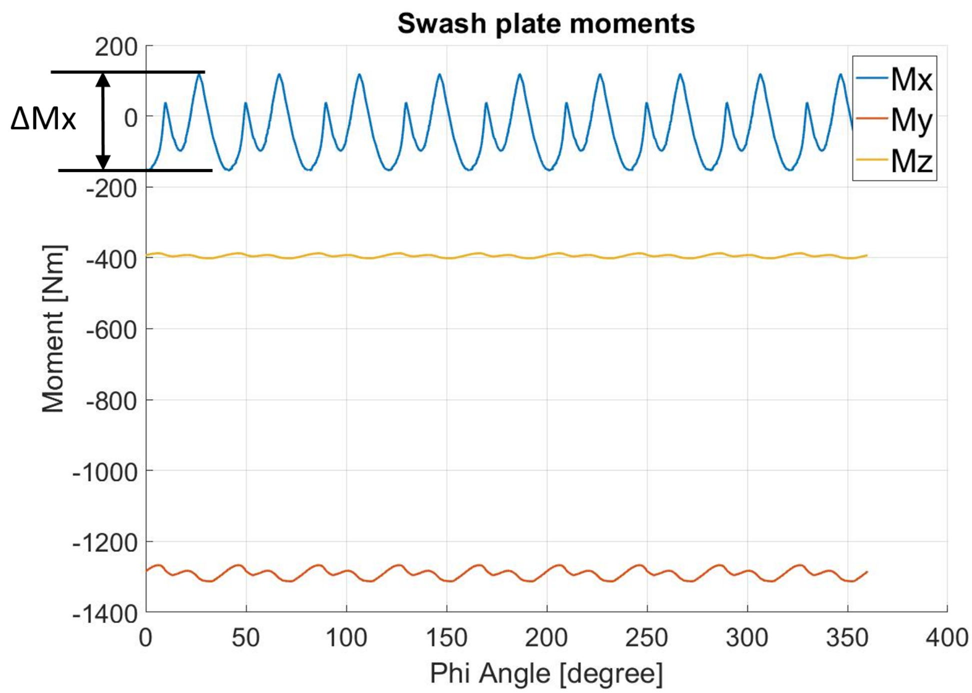

Figure 5.2. The amplitude of swash plate moment (ΔM_x).

5.2.3 Delivery port flow ripples

Fluid borne noise arises from the ripples of the delivery flow and the suction flow. These high flow ripples give rise to greater pressure transients in the pipework, leading to component vibrations and hence noise. Thus, for quieter operation, it is necessary to reduce the flow ripples as much as possible. Keeping this in mind, the peak-to-peak amplitude of the net discharge flow (ΔQ_{HP}) is considered as another objective function. We ignore the ripples of the suction flow in order to keep the number of objective functions minimal and also because the delivery flow ripple is routinely found to be greater than the suction flow ripple.

5.2.4 Leakage* %

While designing any pump, efficiency is also of paramount importance. As the algorithm searches for designs on the pareto front, it may stumble upon designs which have very high leakage % but considerably low values for the other objective functions.Thus, to keep leakage

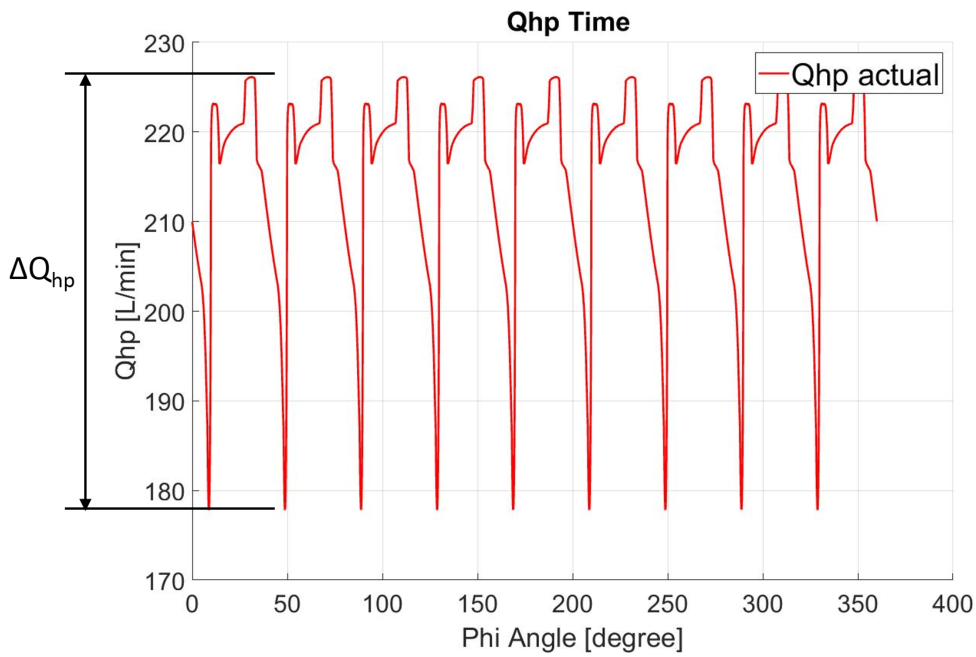

Figure 5.3. The amplitude of the delivery flow ripple (ΔQ_{hp}).

as low as possible, the fraction of the leakage flow to the high pressure flow , written here as Leakage* % is considered as an objective function.

5.2.5 Normalized Rate of swash plate moment $M_x(\frac{dM_x}{d\phi})$

The swash plate moment ripples are found to be the greatest in the x-direction (M_x). The swash plate moment M_x, along with its FFT for an example pump at the operating condition of 3000 rpm speed, 100% displacement and high pressure of 350 bar is shown in Figure (5.4)

The high fluctuating swash plate moment ripples are responsible for the vibrations of the swash plate, which are reacted by the case, and cause case vibrations. Another intuitive way to limit this highly fluctuating moment is to limit the rate of change of the moment ($\frac{dM_x}{dt}$).

From Figure (5.4(b)) and knowledge of the operating condition, it can be seen that the M_x is periodic with a frequency equal to the fundamental frequency of the pump, i.e the

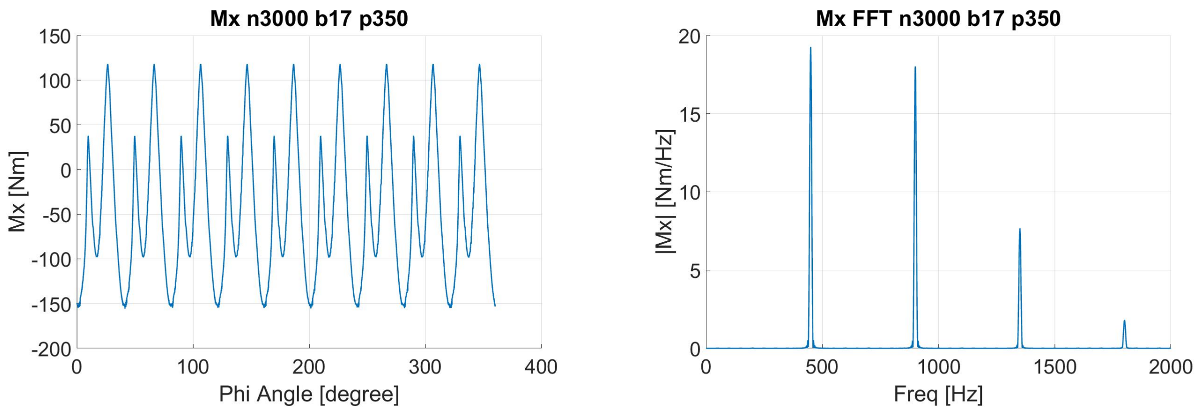

(a) Swash plate moment M_x. (b) FFT of swash plate moment M_x.

Figure 5.4. Example swash plate moment M_x and its FFT.

frequency corresponding to the product of the number of pistons and the rotational speed of the pump.

Hence, for speed independency, the rate of swash plate moment has been normalized as shown in equation (5.7).

$$\frac{dM_x}{d\phi} = \frac{1}{\omega_c}.\frac{dM_x}{dt} \tag{5.7}$$

With due consideration to the sensitivity of the human ear to high frequency, $\frac{dM_x}{d\phi}$ can also be transformed as an appropriate frequency weighted swash plate moment (M_x) in the s domain. In the s-domain, $\frac{dM_x}{d\phi}$, can be transformed as

$$\mathcal{L}\Big(\frac{dM_x}{d\phi}\Big) = \mathcal{L}\Big(\frac{1}{\omega_c}.\frac{dM_x}{dt}\Big) = \frac{1}{\omega_c}\mathcal{L}\Big(\frac{dM_x}{dt}\Big) = \frac{1}{\omega_c}.sM_x(s) \tag{5.8}$$

where ω_c is the rotational speed of the pump, and $M_x(s)$ is the Laplace transform of the time dependent swash plate moment M_x. Substituting $s = j\omega$ to obtain the Fourier transform,

$$\mathcal{L}\Big(\frac{dM_x}{d\phi}\Big)|_{s=j\omega} = \frac{1}{\omega_c}.j\omega.M_x(j\omega) \tag{5.9}$$

Minimization of $\frac{dM_x}{d\phi}$ helps in reducing the higher frequency content of M_x. An example graph of $\frac{dM_x}{d\phi}$ is shown in Figure(5.5). The objective function chosen is the difference between the maximum and the minimum values of $\frac{dM_x}{d\phi}$ ($\Delta\frac{dM_x}{d\phi}$).

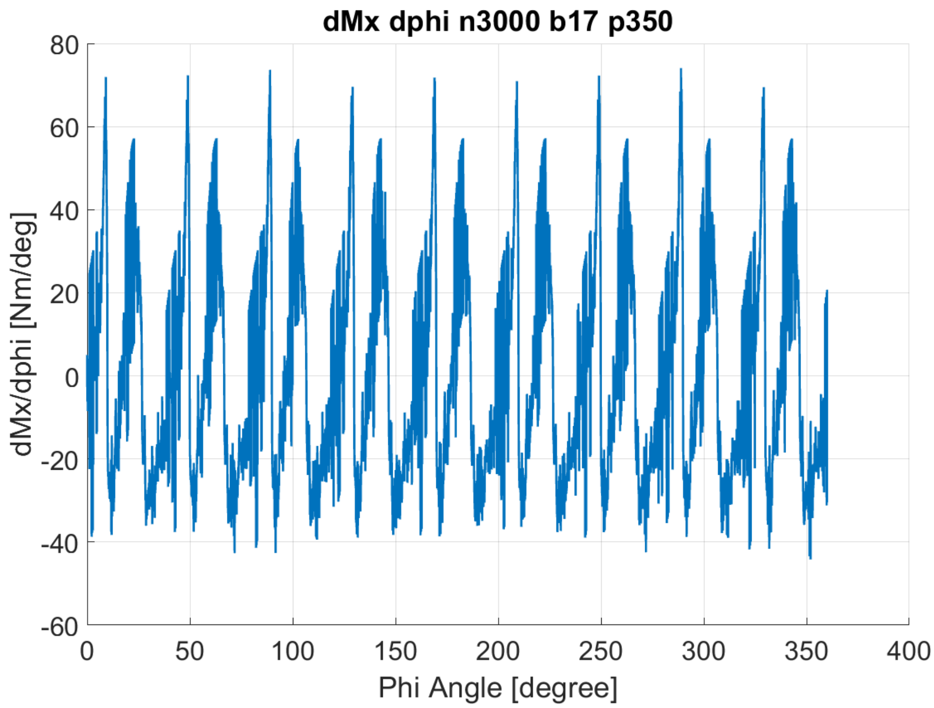

Figure 5.5. An example graph of $\frac{dM_x}{d\phi}$.

5.3 Optimization Constraints

While searching for the pareto front designs, the optimization algorithm may stumble upon designs which may mathematically be optimal, but may not be possible to implement realistically. To force the algorithm to reject such designs, constraints are implemented. All designs which fail any of these constraints are known as unfeasible designs. Only the feasible designs are considered for the successive generation of the optimization.

5.3.1 Peak Pressure Constraint

Overpressurization in the displacement chamber can momentarily lead to DC pressures higher than the set pressures(Figure(5.6)). In order to reject designs with excessively large pressure peaks, a constraint has been implemented to reject all the designs where the peak pressure goes beyond a certain upper limit of the set high pressure (Equation (5.10)).

$$p_{max} \leq L_1 \tag{5.10}$$

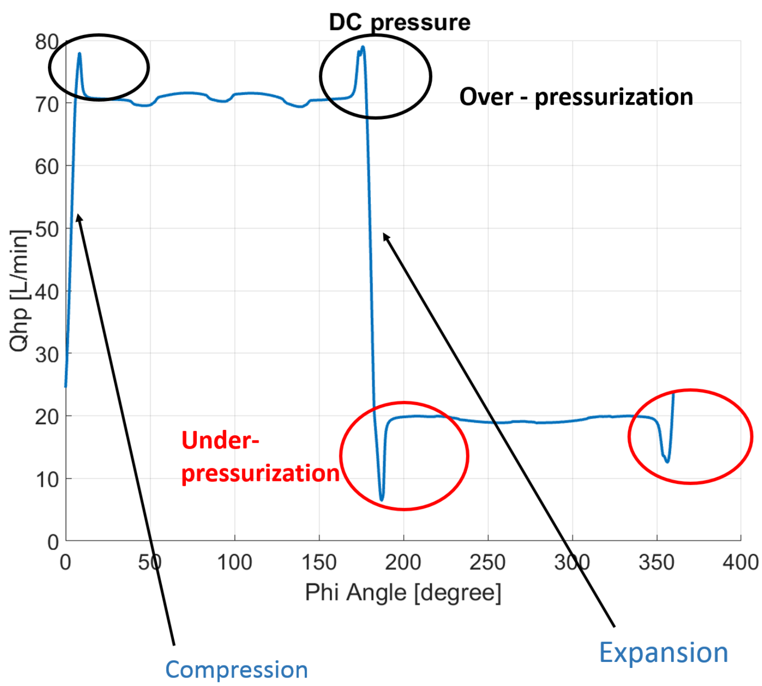

Figure 5.6. Overpressurization and underpessurization in the displacement chamber.

Similar to overpressurization, if the pressure in the displacement chamber falls too low, it would cause cavitation (Figure(5.6)), leading to shockwaves from bubble collapse. This can lead to erosion on the pump surface and louder noise levels. Hence, another constraint has been implemented to reject all the designs where the pressure in the displacement chamber falls below the set lower limit (Equation (5.11)), thus avoiding underpressurization and staying away from cavitation.

$$p_{min} \geq L_2 \tag{5.11}$$

In equation(5.10) and equation(5.11), L_1 and L_2 are the assumed upper and lower limits of the displacement chamber pressure, which are determined on the basis of the specifications laid down by the pump designer

5.3.2 Leakage* % Constraint

Even though Leakage* % is included as an objective function, the same has been included as an inequality constraint as well. Unless a suitable upper limit on the leakage* % is enforced, the algorithm might even consider designs with greater than 100% leakage, which might have good values for the other objective functions.This does not make sense realistically as the leakage flow can never be greater than the theoretical delivery flow. To avoid this, it is necessary to put an upper limit on the leakage* % (Equation (5.12)).

$$Leakage^{*}\% \leq L_3 \tag{5.12}$$

5.3.3 Set pressure constraint

These constraints were implemented to ensure that there is proper build up of pressure in the displacement chamber. Very often, the algorithm will accept designs in which the pressure does not rise or fall all the way down to the set high or low pressures respectively. Even though the algorithm would identify these as good designs since the objective function values would be less, yet such designs are unfeasible since the pressures do not rise or fall to the set high/low pressures. In order to ensure that such designs get rejected, two inequality constraints have been implemented. The first inequality constraint was such that when the displacement chamber was open to the high pressure port, the average of the simulated DC pressure is within a permissible limit of the set pressure in the high pressure port. Likewise, the other inequality constraint was to ensure that when the displacement chamber was open to the low pressure port, the average of the simulated DC pressure is within a permissible limit of the set pressure in the low pressure port.

$$max_{opcons} \frac{|p_{hpmean} - p_{hpset}|}{p_{hpset}} \leq L_4 \tag{5.13}$$

$$max_{opcons} \frac{|p_{lpmean} - p_{lpset}|}{p_{lpset}} \leq L_5 \tag{5.14}$$

These two constraints ensure that the designs for which the DC pressure does not remain within the set tolerable limits of the set pressures are rejected.

5.3.4 Simulation complete constraint

The user sets a fixed number of revolutions as an input, and as the solver solves the system of ODEs, it may get stuck in an infinite loop or fail before completing the set number of revolutions. If this happens, the objective functions that will be calculated will be erroneous as the set number of revolutions were not completed. To avoid this and reject such designs for which the set number of revolutions could not be simulated, an equality constraint has been implemented. For a particular design, if the number of revolutions simulated and completed is the same as the number of revolutions set (for all the operating conditions), the design is considered to be feasible. If any design fails to complete the set number of revolutions, even for a single operating condition, the design is considered unfeasible and is rejected.

$$h = \begin{cases} 1 & \text{if (simulated revs = set revs) (for all opcons),} \\ 0 & \text{otherwise} \end{cases} \tag{5.15}$$

If $h = 0$ for any design, it is rejected.

The constant limits L_1, L_2, L_3, L_4 and L_5 in equations (5.10), (5.11), (5.12), (5.13) and (5.14) are determined on the basis of pump specifications and the optimization requirements.

5.4 Optimization Inputs

The main aim of our multi objective optimization is to find relevant valve plate designs on the pareto front. For this, it is imperative to represent the valve plate design in terms of parametrized design variables. An appropriate scheme for representing the valve plate in mathematical terms was needed, which would serve as our design variables for the optimization. In this section, an innovative, robust and exploratory parametrizaton scheme for valve plate design is discussed, which enables us to explore much of the sample space for valve plate designs.

A detailed discussion on the concept of area file, as well as the intricacies and influence of valve plate design on the displacement chamber pressure, forces and moments is presented in Section(3.4). The relief grooves, highlighted by the numbers 1,2,3 and 4 in Figure(5.7) are the critical regions, having significant influence on the pressurization and de-pressurization in the displacement chamber. The area files corresponding to the relief grooves (1,2,3 and 4) in Figure(5.7) are shown in Figure(5.8).

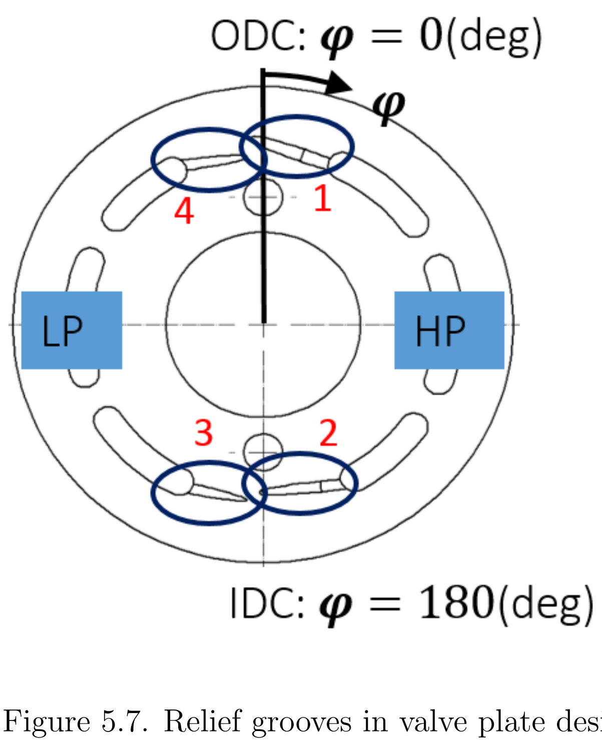

Figure 5.7. Relief grooves in valve plate design.

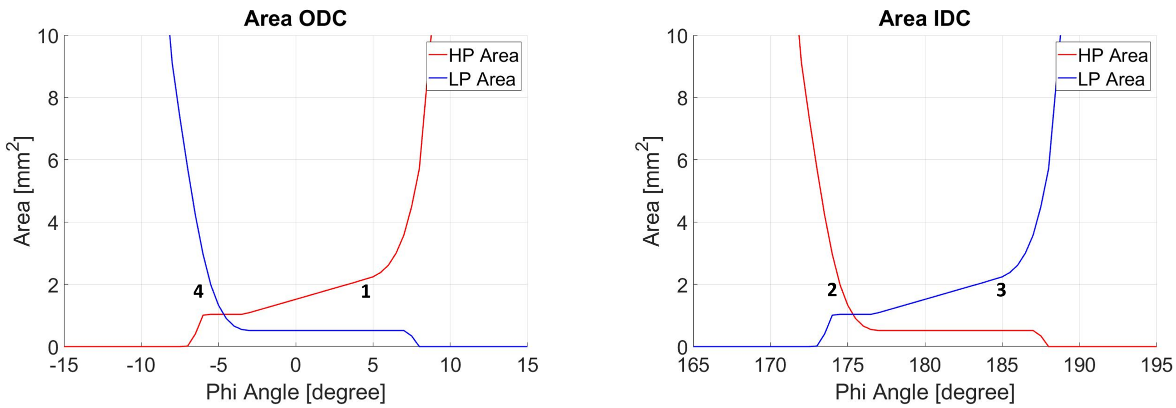

(a) ODC Area.

(b) IDC Area.

Figure 5.8. The area file around the ODC and the IDC.

Previous researchers at MAHA Fluid Power lab, working on optimization of valve plates came up with unique parametrization schemes. (Kumar Seeniraj & Ivantysynova 2011) parametrized the relief grooves in terms of the starting angle of each groove and the slope (Figure(5.9(a))). (Kalbfleisch 2015) introduced relief groove parametrization with non- linear start (Figure(5.9(b))).

The parametrization given by (Kumar Seeniraj & Ivantysynova 2011) focuses on linear grooves, mainly for simplicity, and in trend with the common valve plate designs prevalent at that time. (Kalbfleisch 2015) focuses on non- linear start grooves, mainly from a manufacturability point of view, and also with a view to explore the design space more intensely than (Kumar Seeniraj & Ivantysynova 2011). However, the focus of both works on linear grooves prevented a larger section of the design space, encompassing non linear grooves, from being explored. Moreover, with the current advances made in manufacturing, it has also become possible to realize non linear grooves.

Owing to the sensitivity of the displacement chamber pressure to the valve plate design, particularly around the relief grooves, this work focuses a lot more on exploring the design space more intensively, through a generic, flexible piece-wise linear and piece-wise spline grooves, enabling us to obtain groove designs which would have been otherwise impossible to obtain through the schemes mentioned previously.

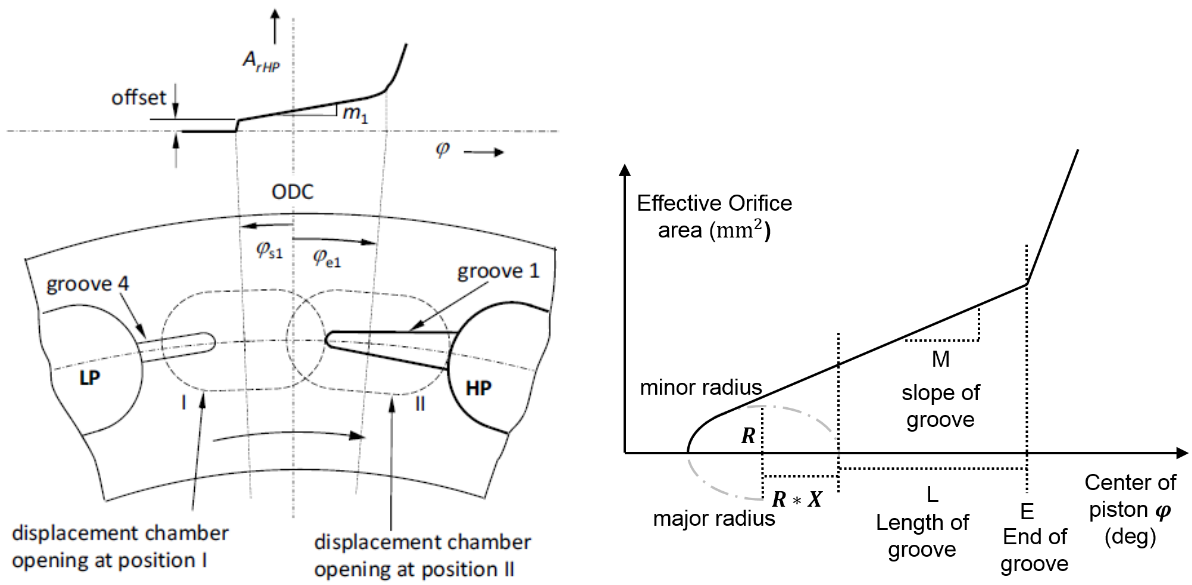

(a) Relief groove parametrization by (Kumar Seeniraj & Ivantysynova 2011).

(b) Relief groove parametrization by (Kalbfleisch 2015).

Figure 5.9. State of the art in relief groove parametrization at MAHA Fluid Power Lab.

5.4.1 Groove Numbering Convention

In order to separate the phenomena of compression and expansion, and to better understand the effect of each groove, it was suitable to address each groove independently. This resulted in a numbering scheme for the relief grooves, (Figure(5.10)). The main reason behind numbering the grooves as such was the convenience of implementing the interpolation scheme. Also, numbering each of the grooves gives greater flexibility in observing the effect of each groove.

5.4.2 Relief Groove Parametrization

Consider a generic relief groove area file as shown in Figure(5.11(a)). This groove can appropriately be represented by interpolation through N points, as shown in Figure(5.11(b)). S represents the start of the groove on the x-axis. (x_1, y_1), (x_2, y_2), (x_3, y_3).... (x_N, y_N)

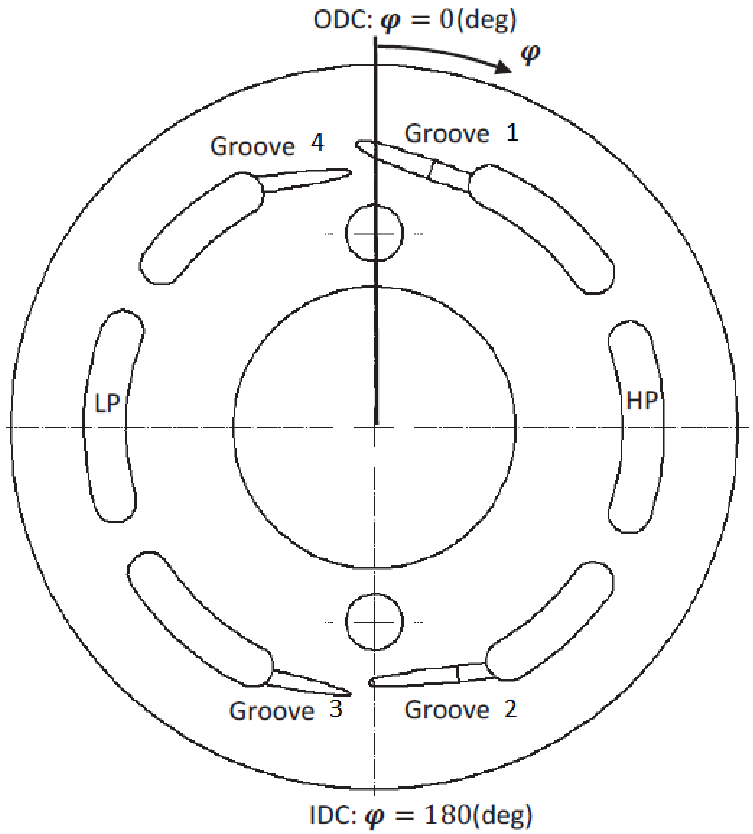

Figure 5.10. Relief groove numbering.

represent N- points on the relief groove area file. The point (x_N, y_N) represents the end of the relief groove. Following this end of the groove, the area file is assumed to increase to a maximum area value with a constant slope of the area v/s angle graph.

Every point (x_k, y_k) can be chosen to be at a distance of Δx_k along the x-axis and at a distance of Δy_k along the y-axis from the previous point. Thus, the N points can be represented by a set of N Δx's and N Δy's as can be seen from figure(5.12). Here, N is a user defined input, which equals the number of points used to represent each relief groove, including the point representing the end of the groove. Thus, for each relief groove, the variables used for representation are shown in Table(5.1).

R here is the choice of the interpolation scheme, having values from 0 - 1. If $R >= 0.5$, the N points are interpolated by a linear scheme, whereas if $R < 0.5$, the interpolation is carried

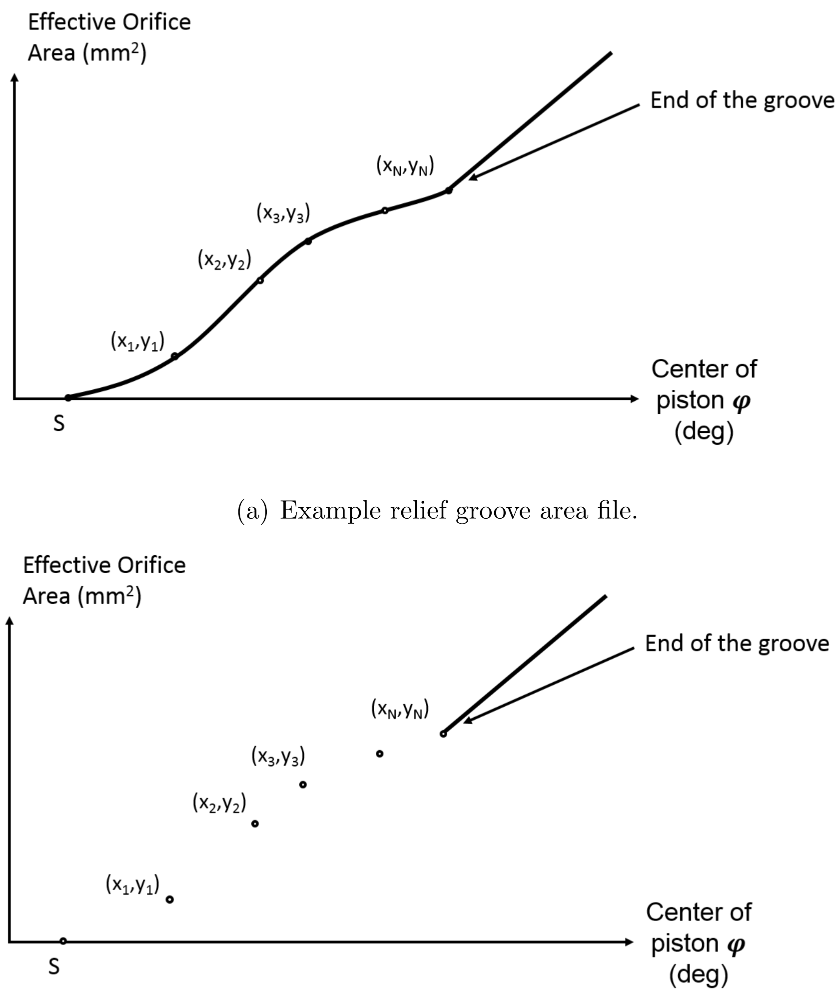

(a) Example relief groove area file.

(b) Representation with points.

Figure 5.11. Parametrization of relief groove.

out by the cubic spline scheme. Since each groove has its own option for the interpolation choice, the four grooves can be mixed and matched between piecewise linear grooves and piecewise spline grooves

The interpolation schemes have been implemented in the C++ code by using the open source GNU Scientific Library (GSL). This library provides a number of interpolation schemes which can be used without recompiling.

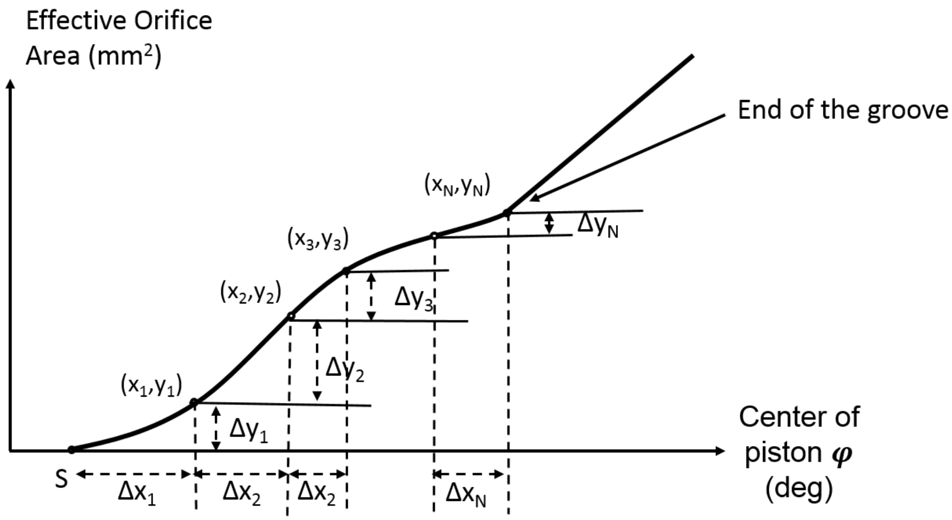

Figure 5.12. Parametric representation of relief groove.

Thus, each relief groove can be represented by a set of $(2 * N + 2)$ variables. For the four relief grooves, we have a total of $4 * (2 * N + 2)$ variables. These variables serve as our optimization inputs.

Even though the number of optimization inputs seems to be large, yet the archive based approach taken by the chosen optimization algorithm enables us to set in a high number of function evaluations which ensures that a global pareto optimal solution set is found efficiently. Also, the implementation of this interpolation scheme to obtain the area file does not add any overhead on the Pressure Module simulations, thus ensuring that the simulation time for the valve plate evaluations remain unaffected.

5.4.3 Constraint Check

As the piston moves from $\phi = 0^O$, the area available at the valve plate for flow increases. This implies that the relief groove area file has to be monotonically increasing. So, while implementing the interpolation schemes, it is necessary to check if the area files around the grooves are monotonically increasing. This is done by implementing a simple discrete gradi-

Table 5.1.
Variables for relief groove parametrization.

Variable	**Unit**
S	deg
Δx_1	deg
Δx_2	deg
Δx_3	deg
....	....
Δx_N	deg
Δy_1	mm^2
Δy_2	mm^2
Δy_3	mm^2
....	....
Δy_N	mm^2
R	[ ]

ent check at each point (Equation(5.16)), after generating the area file through interpolation. The designs that fail this constraint check are rejected.

$$\frac{\Delta(Area)}{\Delta\phi} \geq 0 \tag{5.16}$$

5.5 Optimization Algorithm

Classical optimization algorithms convert a multiple objective function problem into a single objective function, usually through a weighted sum of the different objective functions. The optimization, in such cases is run several times by assigning different weights to the respective objective functions.

Multi-objective optimization cannot be considered a simple extension of single objective optimization. An ideal multi-objective optimization algorithm gives not one, but a set of optimal solutions, each of which corresponds to a certain order of importance to the objectives. The choice of the final solution from this set is based on some trade offs or higher level information.

In contrast to classical optimization techniques where the outcome is a single optimized solution, evolutionary algorithms work with a population of solutions and are inspired by nature's evolutionary principles to obtain a pareto optimal set of solutions. Since the 90s, evolutionary algorithms have received a great deal of attention in solving multi-objective optimization problems because of their ability to converge to pareto optimal solutions in a single simulation run (Ma, Jiao, Gong & Liu 2005). Classical optimization algorithms for solving multi-objective optimization problems slowly went out of favor because of their inability to solve for concave pareto fronts, and the requirement of solving for a suitable set of weights to build the complete pareto front (Zitzler 1999).

To understand pareto optimal set, it is necessary to understand the concept of pareto domination. According to (Censor 1977), a feasible solution 'a', is said to dominate another feasible solution 'b' for an M-objective minimization problem if the following two conditions are met

$$f_i^a \leq f_i^b \quad \forall i \in \{1, M\} \tag{5.17}$$

$$f_i^a < f_i^b \quad for\, atleast\, one\, i \in \{1, M\} \tag{5.18}$$

5.5.1 Pareto Optimal Set

The concept of pareto-domination, discussed in the previous section leads us to domain of pareto optimal set (or pareto frontier). Let us consider a hypothetical problem where we are required to minimize two objective functions f_1 and f_2. Figure(5.13) shows us 8 hypothetical designs, plotted with f_1 along the x- axis and f_2 along the y-axis. Using the definition of domination given in Equations (5.17) and (5.18), we assign a domination rank to each of the designs which is equal to the number of designs which dominate it. For example, in Figure(5.13), it can be seen that design H is dominated by A, B and C. The f_1 and f_2 values of A and B are less than the same for H. Therefore, they dominate H. Comparing C and H, it can be seen that while C and H have the same f_2 values, C betters H in the value of f_1. Since H is dominated by 3 designs, it has a domination rank of 3. Table (5.2) below gives us the domination rank of all the designs, and also the list of the designs which dominate each design. The designs which have domination rank 0 are known as the non- dominated designs and the front formed by these designs is called the pareto-optimal front.

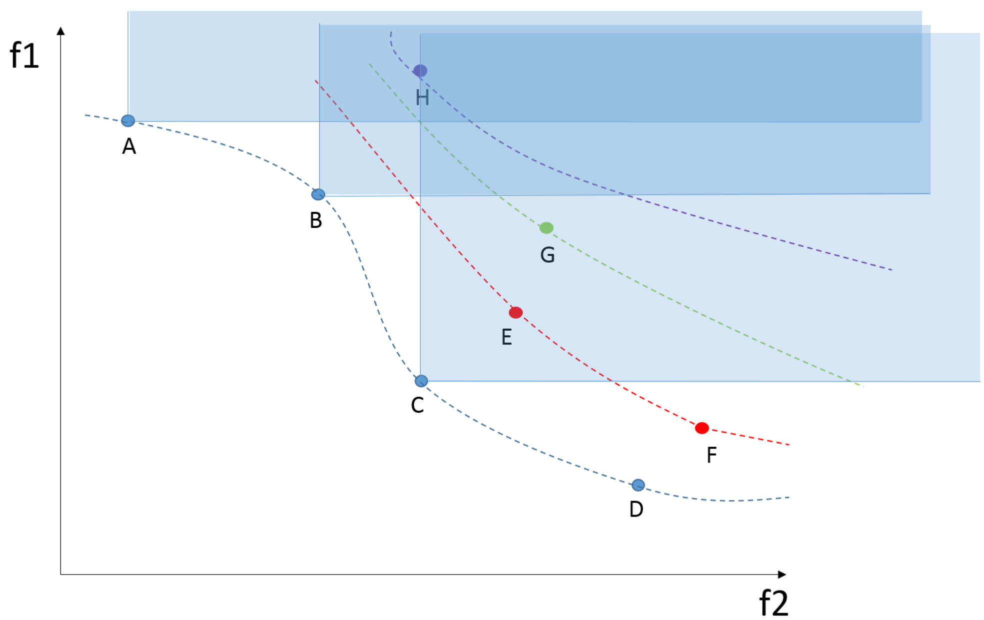

Figure 5.13. Minimization problem considered in Section (5.5.1).

5.5.2 Crowding distance metric

For any optimization algorithm, along with convergence to the pareto optimal set, it is also important to maintain a good spread of solutions. So, even though domination ranking

Table 5.2.
Domination rank of the designs for the example shown in Fig(5.13).

Design	**Dominated by**	**Domination Rank**
A	none	0
B	none	0
C	none	0
D	none	0
E	C	1
F	D	1
G	C,E	2
H	A,B,C	3

is the primary metric, as the population approaches the pareto optimal front, the crowding distance metric becomes more important to maintain good diversity in the final solution (to avoid the solutions from being too crowded in one region of the pareto front).

In our selected algorithm, the diversity of each solution is captured by using a crowding distance metric (CD) as shown in Figure(5.14).

Assuming that the solutions A, B and C have the same non-domination rank, and A and C are the nearest neighbours of B on its either side by comparing the objective functions f_1 and f_2, the crowding distance metric (CD) of B is calculated in Equation(5.19).

$$CD(B) = \sum_{i=1}^{M} l_i r_i \tag{5.19}$$

where M is the number of objective functions. Designs that have smaller CD lie in the more crowded region. Thus, if two solutions have the same non domination rank, the one with the greater CD has more chances of being selected into the population for the next generation. There is a slight modification to the formula for calculating the CD for extreme solutions which may have only left or only right neighbours. For designs having only left

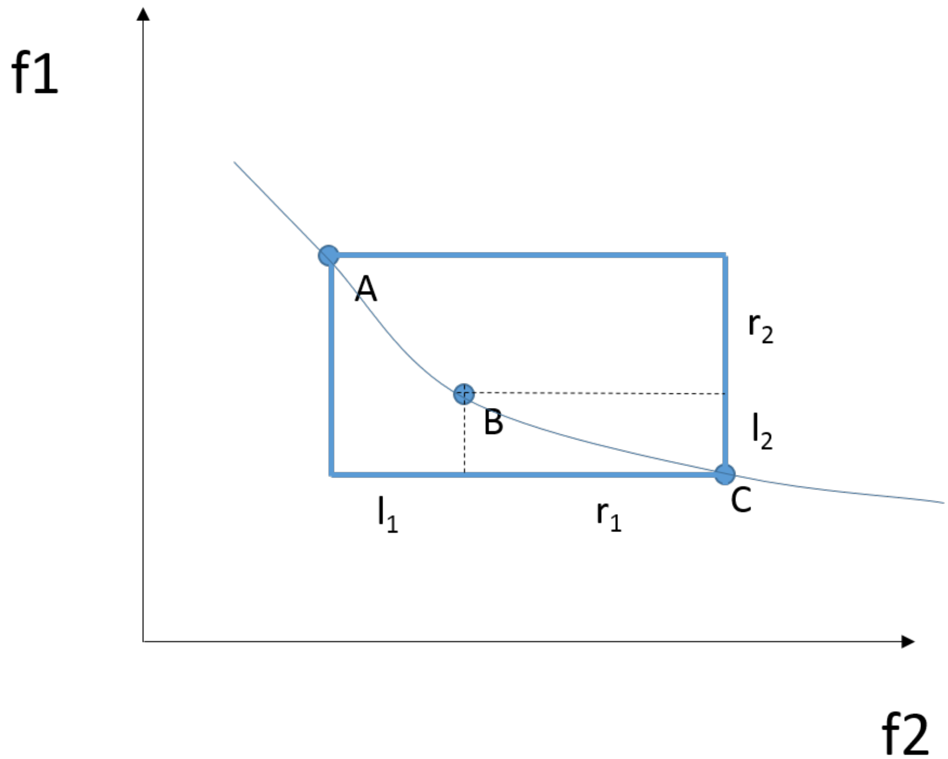

Figure 5.14. Crowding Distance Metric computation.

neighbours, the CD is calculated as the summation of l_i^2, whereas for designs having only right neighbours, CD is calculated as the summation of r_i^2.

Also, if two solutions are identical, it is recommended to remove all redundant copies of a solution for calculating the crowding distance metric (CD). Even though this adds a slight computational overhead, it is negligible as compared to the overall simulation time.

5.5.3 Algorithm Selection

Since the 1990s, a number of researchers have come up with robust genetic algorithms with a focus on finding the pareto front. A brief history of the development of such evolutionary algorithms to solve real world multi-objective optimization problems is given in Chapter

2. The algorithm that we choose is the Archive base Multi objective Genetic Algorithm II (AMGA II), developed by (Tiwari, Fadel & Deb 2011).

The main reasons behind the choice of this algorithm are

- It maintains an archive of the best solutions obtained after every generation. Using such an external archive provides useful information about the search space as well as generates a large population of pareto points at the end of the simulation.
- The archive is updated after every generation by comparing with the offspring solutions. This ensures that the best solutions stay in the archive. This phenomenon of making sure that the best solutions from one generation are carried over into the next generation without mutation is called elitism.
- Use of a micro population ensures fewer evaluations and hence improves computational time.
- Finds the global minimum/maximum even in multi-modal (a problem with one global optimum and one or more local optima) optimization problems.
- The selection of the designs is done on the basis of, not just the domination rank, but also on the basis of a diversity rank, which is used to ensure that the solutions do not remain crowded around one point in the solution space. This has been shown to improve the performance, especially in multi-modal problems.
- The implementation of a rank based mutation strategy in AMGAII helps in avoiding local extrema in multi modal problems.
- AMGA II performed significantly better than a number of other multi-objective optimization algorithms for a number of benchmark problems tested, as well as a few practical engineering problems(Tiwari et al. 2011).
- Finally, a big advantage is the availability of the AMGAII code, which has been made open source by its creators (Tiwari et al. 2011).

A flow chart of the optimization algorithm is shown in Figure(5.15) below.

The term 'evaluation' used in the flow chart refers to Pressure Module simulations. The AMGAII code has been modified and coupled with an executable file for Pressure Module, which simulates each design at the set operating conditions, and stores the objective function values in a text file. This text file containing the objective function values is then read by the optimization code and analysed to create the parent population and archive population. User inputs are required only in the stages A and B (highlighted in blue) in Figure(5.15).

The inputs to the program which need to be provided by the user are as follows:

- **Pump Geometry** : Pitch radius, number of pistons, dead volume, mass of the piston, maximum swash plate angle.
- **Oil Parameters**: properties pertaining to the type of oil used (viscosity, bulk modulus, etc).
- **Operating Conditions**: the mode of operation, the rotational speed, the swash plate angle, the pressures at the high pressure port and the low pressure port
- **Design Variable Limits** The upper and the lower limits for the relief groove design variables
- **Algorithm Inputs**: The number of evaluations, the size of the pareto optimal set, the number of objective functions and constraints
- **Other Miscellaneous Inputs** The number of revolutions, solver options, etc

After completing the specified number of function evaluations, MiNoS yields a pareto optimal design set, whose size is set in its inputs. The choice of the final design from this pareto optimal set is done by the designer, according to his requirements. This choice of the final design is subjective as the application requirements may necessitate the designer to give greater priority to some objective functions over the others. Hence, the pareto optimal set gives ample flexibility and a wide choice of designs to the designer.

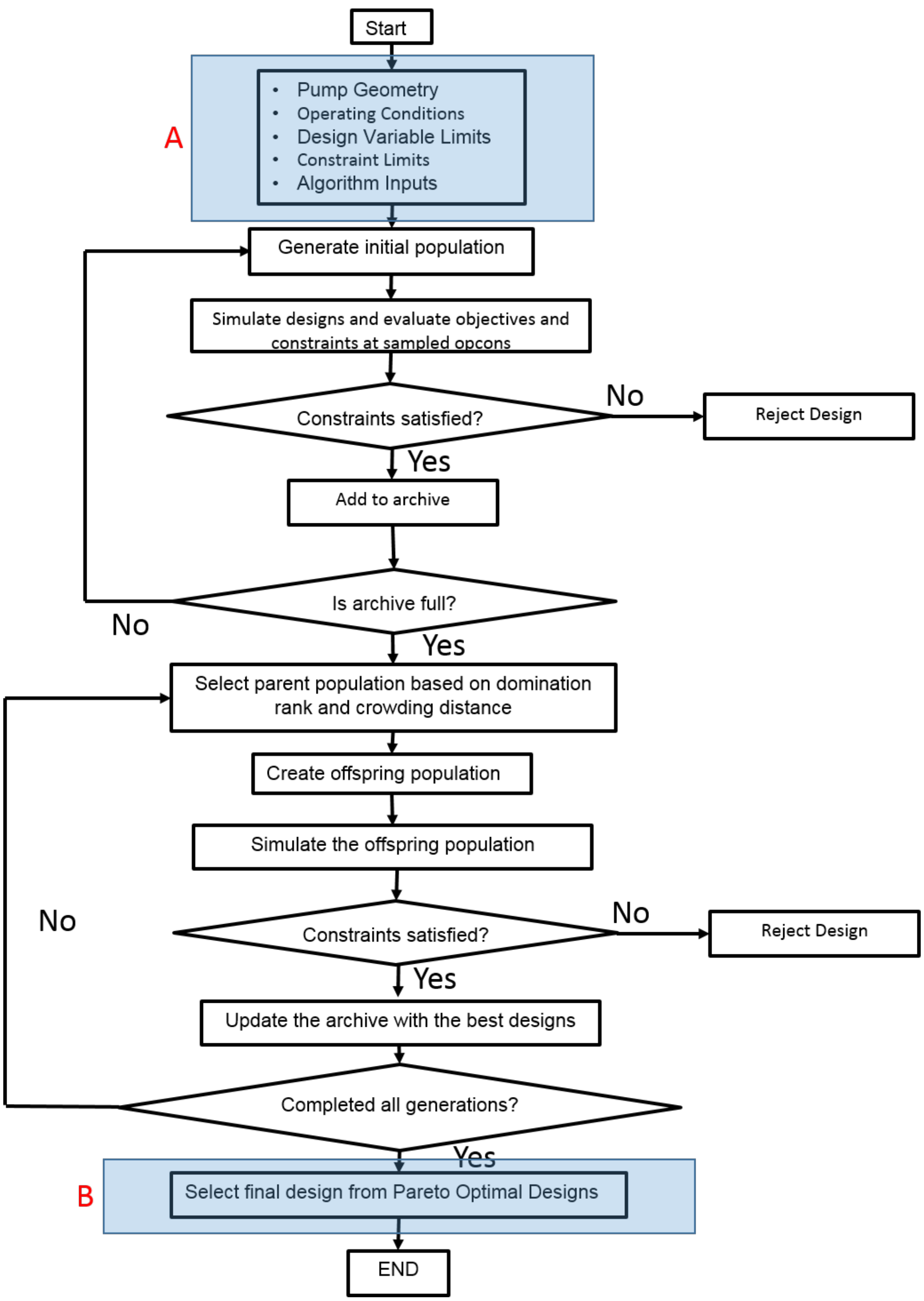

Figure 5.15. Flow chart of the relief groove optimization software tool 'MiNoS'.

6. OPERATING CONDITION SAMPLING

For each design that is being evaluated, the optimization code executes the Pressure Module and simulates that design for every operating condition that is specified. Hence, the total simulation time is in direct proportion to the number of operating conditions simulated. As a result, it is impossible to calculate the objective functions for the entire range of operation of the pump. This would not only exacerbate the simulation time, but also render the optimization algorithm near useless because of the excessive number of objective functions.

As early as 1962, (Skaistis 1962) observed that the the noise emitted by hydraulic pumps increase with an increase of fluid power. Previous work by (Klop 2010) and (Kalbfleisch 2015) have also shown that the noise generated by pump/motor is roughly proportional to the fluid power transmitted. Fluid power, on the other hand is proportional to the product of the displacement, speed and pressure differential. So, for the operating condition sampling for this work, an optimization was run with the objective functions mentioned in section (5.2) at a high power operating point. The parameter bounds for the optimization inputs are as shown in Appendix (A). Many of the pareto front valve plates were then compared with the base design to observe the variability in the maximum values of the objective functions, across a wide sample of the operating condition space.

6.1 Maximum of $\frac{dp}{d\phi}$

Figure(6.1(a)) gives us the $\frac{dp}{d\phi}$ max values for the original valve plate design for the concerned pump, whereas Figure(6.1(b)) and Figure(6.1(c)) give us the $\frac{dp}{d\phi}$ max values for two of the designs obtained from the pareto front. On comparing the three graphs, it is seen that the max $\frac{dp}{d\phi}$ for the original valve plate occurs at the corner operating point of maximum speed, maximum displacement and max pHP (high port pressure) (Opcon A). However, for designs 4 and 5, it can be seen that while the $\frac{dp}{d\phi}$ max values at this corner

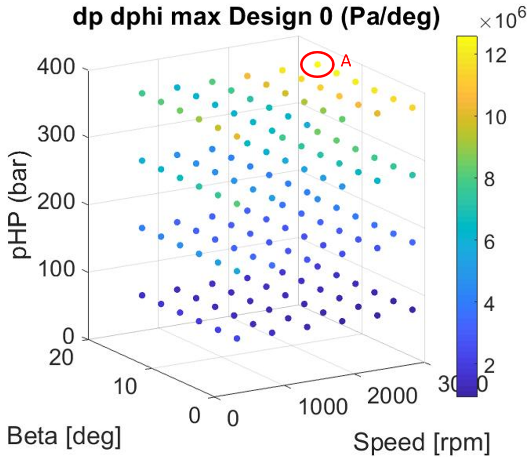

(a) Original valve plate.

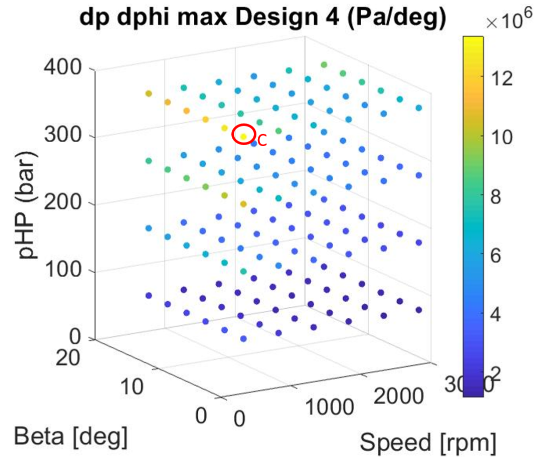

(b) Design 4.

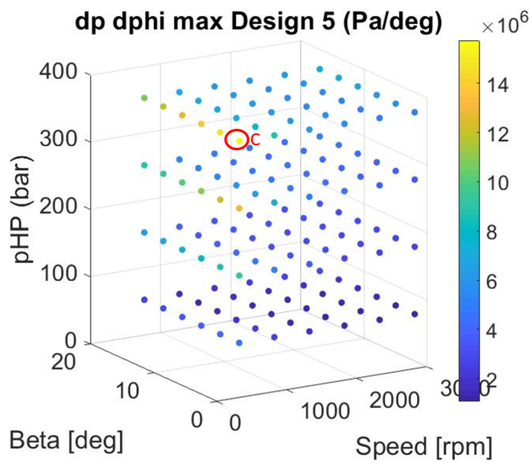

(c) Design 5.

Figure 6.1. $\frac{dp}{d\phi}$ max values for 3 valve plates across the entire operating condition sample space.

operating point is less, the maximum occurs at another corner operating point of low speed, low displacement and high pHP (Opcon C). From these observations, the $\frac{dp}{d\phi}$ max objective function is evaluated at these two corner operating points.

- Objective Function 1: $\frac{dp}{d\phi}$ **max** at high speed, high displacement, high pHP (Opcon A)

- Objective Function 2: $\frac{dp}{d\phi}$ **max** at low speed, low displacement, high pHP (Opcon C)

6.2 Minimum of $\frac{dp}{d\phi}$

The minimum value of $\frac{dp}{d\phi}$ is usually seen to occur near the IDC. For different designs obtained from the optimization, the minimum values of $\frac{dp}{d\phi}$ were compared across the operating condition space so as to find out the operating condition(s) at which the $\frac{dp}{d\phi}$ min behaviour is representative of the entire sample space.

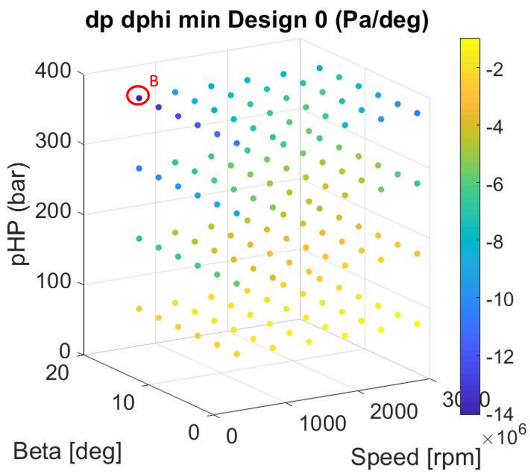

(a) Original valve plate.

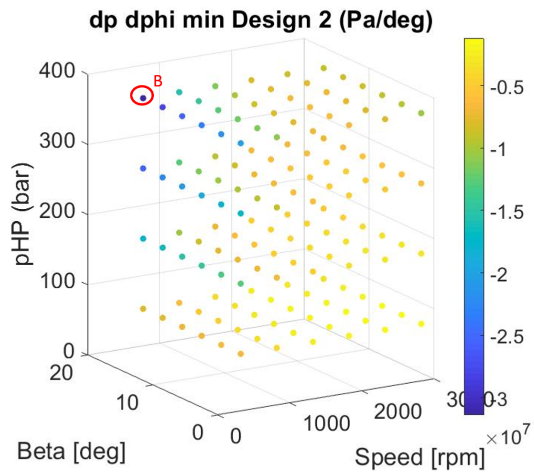

(b) Design 2.

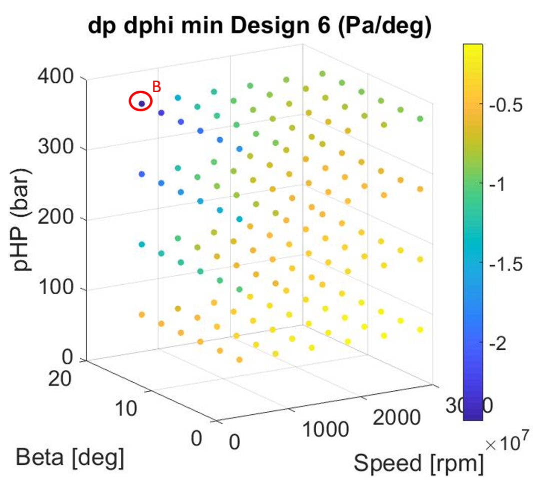

(c) Design 6.

Figure 6.2. $\frac{dp}{d\phi}$ min values for 3 valve plates across the entire operating condition sample space.

From Fig(6.2), it can be seen that for all the three designs considered, the minimum value of $\frac{dp}{d\phi}$ always occurs at the operating condition of low speed, high displacement and high pHP (Opcon B). Thus, the $\frac{dp}{d\phi}$ min at this operating condition is a good representation of the same across the entire operating condition space.

At the same time, because of the importance of the maximum power operating condition in noise considerations, the minimum value of $\frac{dp}{d\phi}$ at the high power operating condition (Opcon A) is considered as an objective function as well.

Therefore, the objective functions to reflect $\frac{dp}{d\phi}$ minimum is

- Objective Function 3: $\frac{dp}{d\phi}$ **min** at high speed, high displacement, high pHP (Opcon A)
- Objective Function 4: $\frac{dp}{d\phi}$ **min** at low speed, high displacement, high pHP (Opcon B)

6.3 Amplitude of ΔM_x

A grid study similar to the one mentioned in the previous section was done for ΔM_x as well. Figure(6.3) shows us the ΔM_x values for the original valve plate and two valve plates from the pareto front.

On observing these results, it is found that the comparative ΔM_x values across all the operating conditions for any value plate is consistently high for the operating points of high speed, high displacement, high pHP (Opcon A) and low speed, low displacement, high pHP (Opcon B). On the basis of these results, the objective functions that represent ΔM_x are

- Objective Function 5: ΔM_x at high speed, high displacement, high pHP (Opcon A)
- Objective Function 6: ΔM_x at low speed, high displacement, high pHP (Opcon B)

6.4 Amplitude of $\frac{dM_x}{d\phi}$

For the operating condition sampling of $\frac{dM_x}{d\phi}$, the amplitude values for the original valve plate and two valve plate designs obtained from the optimization were compared across the entire operating condition sampling space.

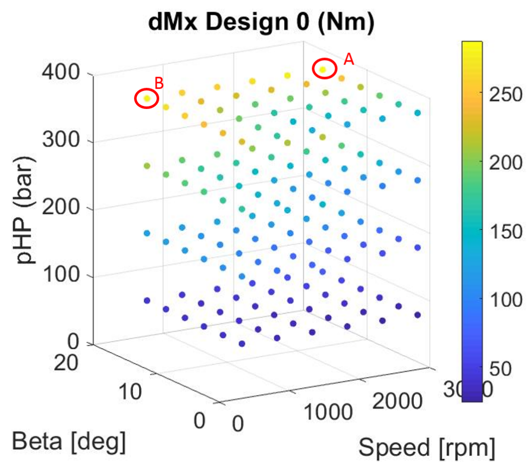

(a) Original valve plate.

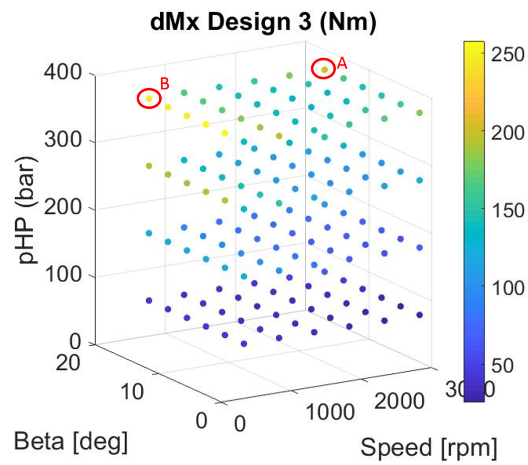

(b) Design 3.

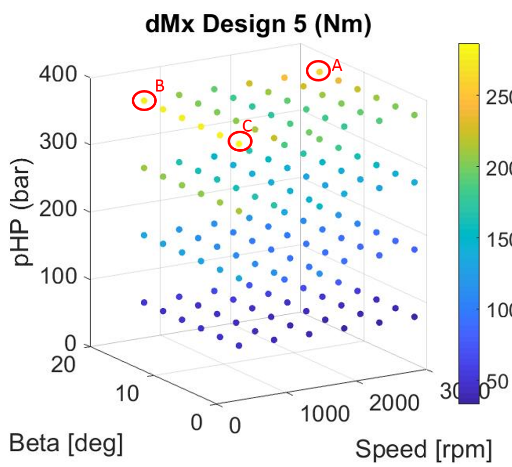

(c) Design 5.

Figure 6.3. ΔM_x values for 3 valve plates across the entire operating condition sample space.

From Fig(6.4), it can be seen that the amplitude of $\frac{dM_x}{d\phi}$ is consistently high for the operating condition of low speed, high displacement and high pHP (Opcon B). Along with this operating condition, we shall also be considering the high power operating condition (Opcon A), mainly for consistently high ΔM_x values at this operating condition.

Therefore, the objective functions for $\frac{dM_x}{d\phi}$ are:

- Objective Function 7: $\frac{dM_x}{d\phi}$ at high speed, high displacement, high pHP (Opcon A)

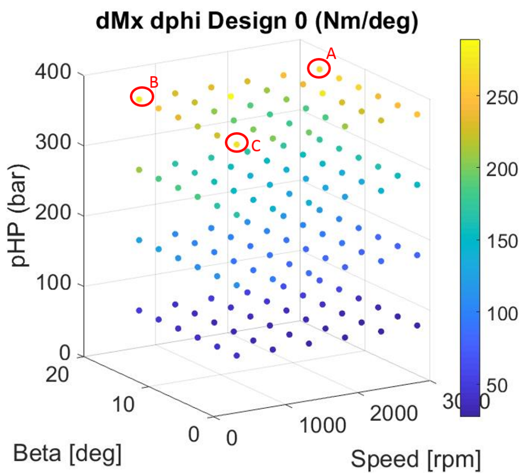

(a) Original valve plate.

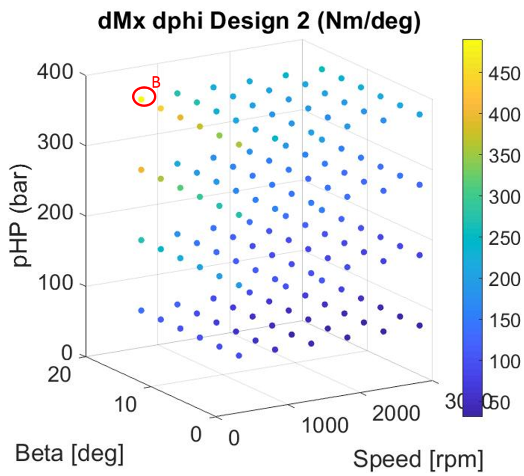

(b) Design 2.

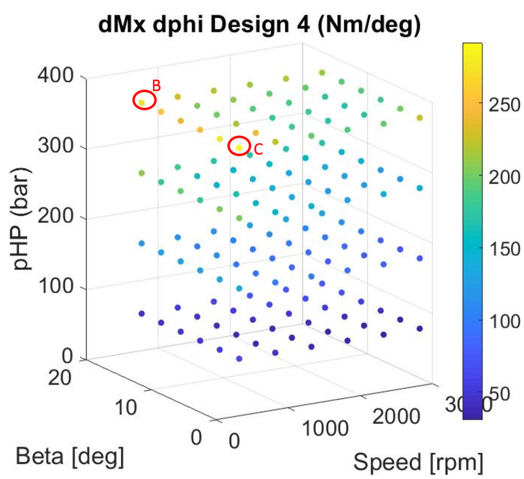

(c) Design 4.

Figure 6.4. Amplitude of $\frac{dM_x}{d\phi}$ values for 3 valve plates across the entire operating condition sample space.

- Objective Function 8: $\frac{dM_x}{d\phi}$ at low speed, high displacement, high pHP (Opcon B)

6.5 High Pressure Port Flow Ripple

To find out the operating condition at which it would best exemplify the trend of the ΔQ_{HP}, an operating condition grid study has been done across different valve plates obtained from the optimization mentioned previously.

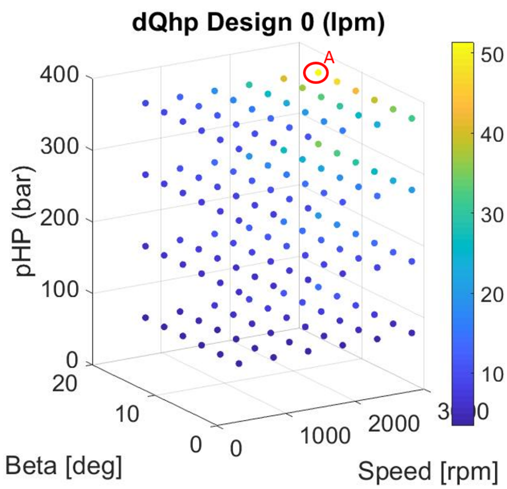

(a) Original valve plate.

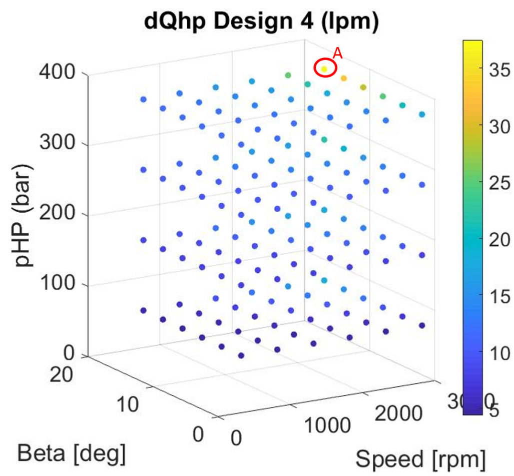

(b) Design 4.

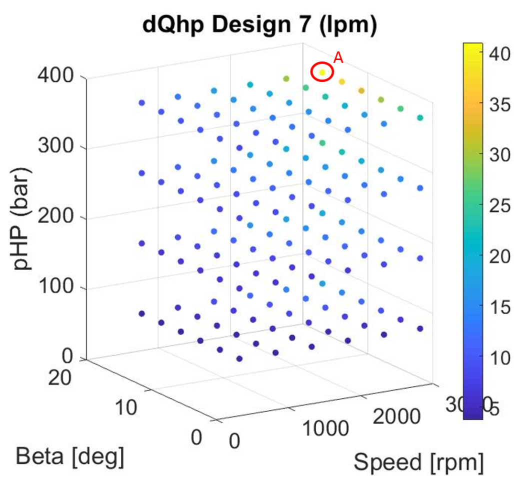

(c) Design 7.

Figure 6.5. ΔQ_{HP} for 3 valve plates across the entire operating condition sample space.

From Figure (6.5), it can be seen that for all designs, the maximum value of ΔQ_{HP} always occurs at the operating condition of maximum speed, maximum displacement and maximum pHP (Opcon A). The higher the displacement and speed, the higher is the theoretical flow. Also, the flow ripples occurring due to fluid compressibility and crossport flow is greater at higher port pressures.

Therefore, the objective function which accounts for the high pressure port flow ripple is

- Objective Function 9: ΔQ_{HP} **%** at high speed, high displacement, high pHP (Opcon A)

6.6 Leakage* %

The external volumetric losses have been ignored in our model. The modified term Q_s* has been introduced to refer to internal volumetric losses and compressibility losses only. A detailed description of the term Q_s* is to be found in Section (3.5). However, for our optimization, leakage has been normalized in reference to the theoretical net high pressure flow.

$$Leakage * \% = \frac{Q_s*}{Q_{HPtheo}} * 100\% \tag{6.1}$$

To understand the variation of this leakage* % with speed, displacement and pHP, a grid study similar to the ones shown in the previous sections was done. The leakage* % for this operating condition sampling study are shown in Figure(6.6), normalized to 1.

For all designs, the maximum leak* % values are seen at the operating condition of low speed, low displacement and high pHP (Opcon C). At this operating condition, a low theoretical flow rate, leading to a high crossport flow results in greater leakage* %. Thus, the objective function for the consideration of leakage is

- Objective Function 10: **Leakage* %** at low speed, low displacement, high pHP (Opcon C)

6.7 Cavitation and Over-pressurization Check

Cavitation check is included as one of the constraints for the optimization. The peak minimum pressure needs to be checked for cavitation so as to filter out all designs which have a high probability of cavitating the pump. This has been enforced by implementing an underpressurization check such that all designs where the pressure falls below a set lower limit are rejected.

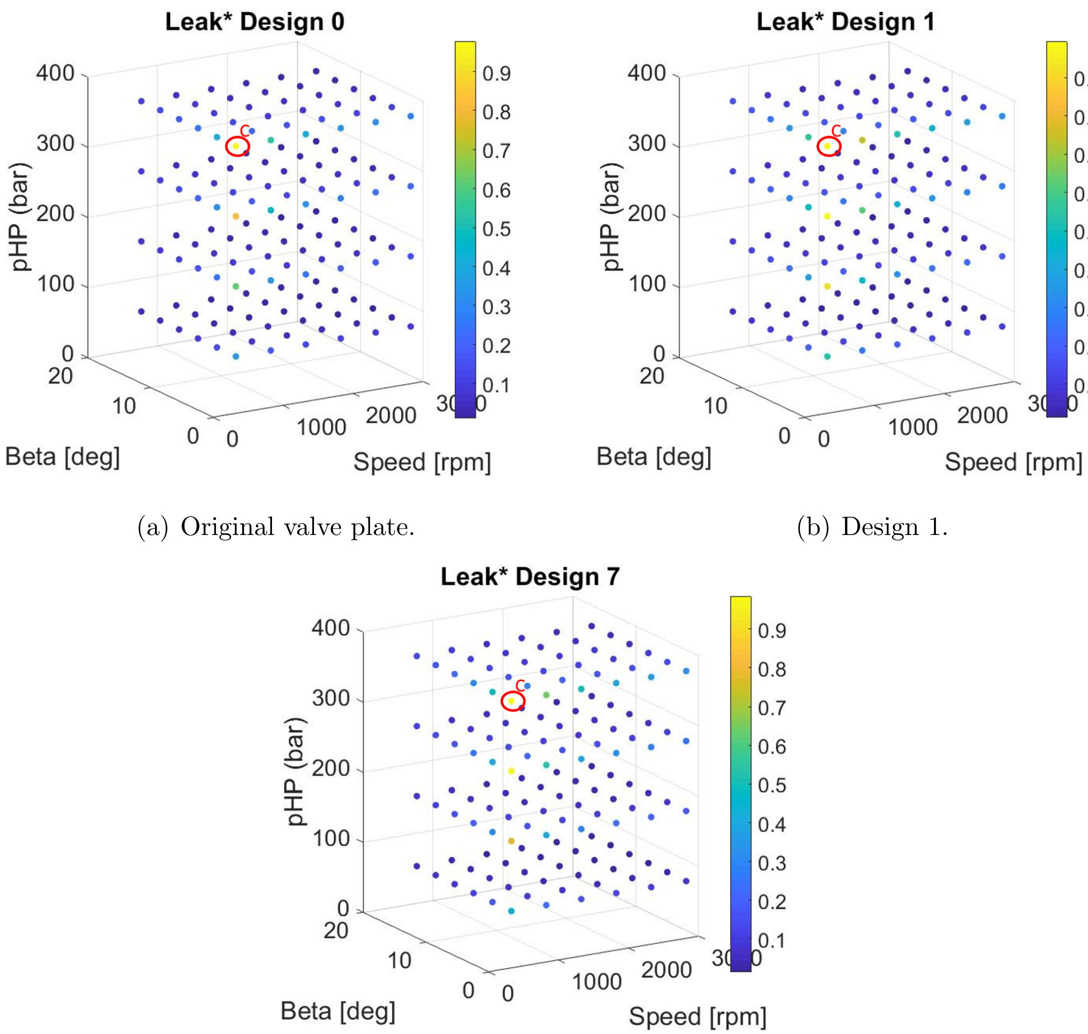

(a) Original valve plate.

(b) Design 1.

(c) Design 7.

Figure 6.6. Leakage* values for 3 valve plates across the entire operating condition sample space.

Likewise, to avoid pressure peaks, another constraint needs to be implemented to filter out designs that have very high pressure peaks.

It is impossible to do an under-pressurization and over-pressurization check for the entire operating condition sample space. The probability of under-pressurizing, and hence the pump cavitating is the highest at the operating condition of high speed, low displacement and low pHP. For the entire simulated operating condition sample space, the low pressure (pLP) is considered as 20 bar. Figure (6.7) below compares the peak minimum displacement chamber pressure for three different designs across the entire sample space.

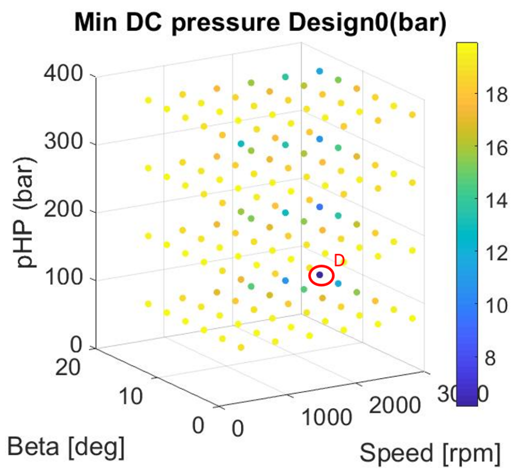

(a) Original valve plate.

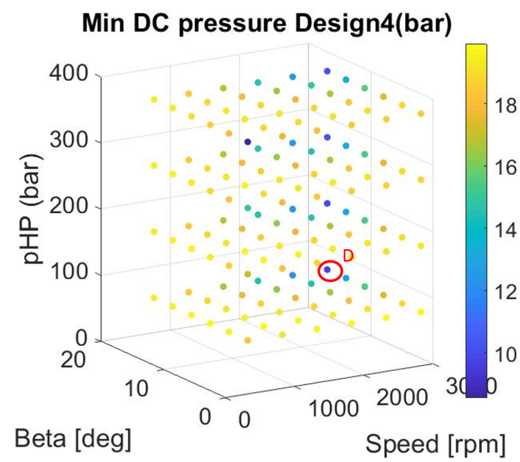

(b) Design 4.

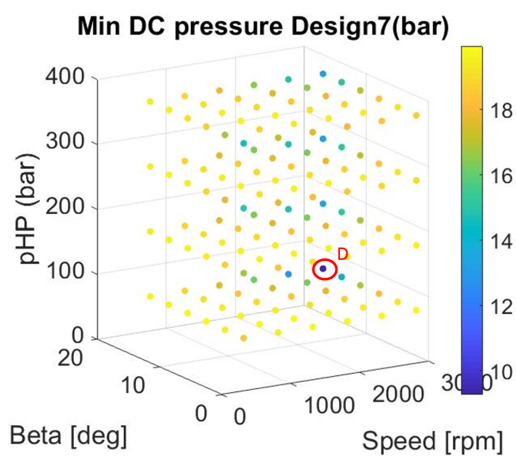

(c) Design 7.

Figure 6.7. Minimum DC pressure values for 3 valve plates across the entire operating condition sample space.

It can be seen that for all the three designs, the minimum displacement chamber pressure occurs at the operating condition of high speed, low displacement and high pHP (D).

Similarly, pressure peaks are also found to be the maximum at the same operating condition (OpCon D). For brevity, the graphs for the same are not shown here.

This gives us conclusive evidence to perform the under-pressurization (hence, avoiding cavitation as well) and over-pressurization checks at the operating condition of maximum speed, maximum displacement and lowest pHP.

7. CASE STUDY

This chapter deals with a case study comparing the performance of a few designs obtained from the optimization software tool to the performance of the base design. The geometry details of the pump is confidential and is not a part of this thesis. The parametrization scheme mentioned in Section (5.4.2) has been implemented and the parameter bounds considered for this case study have been included in Appendix A.

7.1 Case Study Inputs

For the pump considered, the maximum angle of the swash plate is 17°. In all the results presented in this chapter, the displacement of the pump is expressed in percentage of this maximum swash plate angle. Also, the nomenclature of the operating conditions follows the trend shown in the previous chapter. In relation to the pump considered and the objective functions, the operating conditions at which the objective functions are evaluated are shown in Table(7.1).

Table 7.1.
Sampled operating conditions for Case Study.

Opcon	**Speed (rpm)**	**Disp (%)**	**pHP (bar)**
A	3000	100	350
B	1000	100	350
C	1000	17.6	350
D	3000	100	70

The objective functions considered for this case study are shown in Table(7.2). Since there is no concrete information about the contribution of each objective function to audible noise, therefore all the objective functions are given equal significance. The choice of the final design from the pareto front would depend on application specific requirements and/or designer requirements. For this work, the main goal is to look for valve plate designs that dominate the original design in as many objective functions as possible, and for each objective function, the greater the decrease from the base design, the better the design is surmised to be.

Table 7.2.
Objective Functions for the case study.

Sl No	**Objective Function**
1	Leakage* % at Opcon C
2	$max\frac{dp}{d\phi}$ at Opcon A
3	$min\frac{dp}{d\phi}$ at Opcon A
4	$max\frac{dp}{d\phi}$ at Opcon C
5	$min\frac{dp}{d\phi}$ at Opcon B
6	ΔM_x at Opcon A
7	ΔM_x at Opcon B
8	$\Delta\frac{dM_x}{d\phi}$ at Opcon A
9	$\Delta\frac{dM_x}{d\phi}$ at Opcon B
10	ΔQ_{HP} at Opcon A

The constraint limits imposed during the optimization for filtering out of bad designs are shown in Table(7.3)

An important advantage of the chosen algorithm is that no tuning parameters needs to be set by the user. The algorithm dynamically tunes the optimization, on the basis of the size of the inputs, the number of objective functions and the number of constraints. The only algorithm related input that the user needs to input are the number of function evaluations and the optimum design set size. For our case study, the number of function evaluations is set as 100000 and the size of the desired optimum set is fixed at 1800. The 100000 function

Table 7.3.
Constraints for the case study.

Sl No	Constraint Type	Constraint
1	Peak Max Pressure at D	$p_{max} \leq 100bar$
2	Peak Min Pressure at D	$p_{min} \geq 10bar$
3	Leakage* % at C	Leakage* % ≤ 90
4	Set Pressure	$max_{opcons} \frac{\lvert p_{hpmean} - p_{hpset} \rvert}{p_{hpset}} \leq 10\%$
5	Set Pressure	$max_{opcons} \frac{\lvert p_{lpmean} - p_{lpset} \rvert}{p_{lpset}} \leq 20\%$
6	Finish Simulations	$h = \begin{cases} 1 & \text{if (simulated revs = set revs) (for all opcons),} \\ 0 & \text{otherwise} \end{cases}$

evaluations resulted in 184 generations, and a pareto file, consisting of 1800 designs was obtained.

7.2 Post processing

The sorting and post processing of the 1800 pareto designs was challenging because of the large number of objective functions (10) as well as no knowledge of the weights that could be assigned to each objective function. Hence, the designs were sorted on the basis of the number of objective functions where they dominate the base design. No design was found which dominated the base design in all the 10 objective functions, which indicates that the base design is also one of the designs on the pareto front. This technique of sorting designs helped us in choosing overall good designs which could dominate the base design in the maximum number of objective functions.

In Figure(7.1), we compare the objective function values for a few designs obtained from the pareto front to the base design.

From the pareto set of 1800 designs, we have selected 3 recommended designs and shall be finalizing on one on the basis of the design and performance requirements as well as weighing in the pros and cons. The base design is also compared to the designs having the best ΔM_x at the maximum power operating condition and the design with the lowest leakage.

	Leakage*	$\frac{dp}{d\varphi}$ max(A)	$\frac{dp}{d\varphi}$ min (A)	$\frac{dp}{d\varphi}$ max (C)	$\frac{dp}{d\varphi}$ min (B)	ΔM_x(A)	ΔM_x(B)	$\Delta\frac{dM_x}{d\varphi}$ (A)	$\Delta\frac{dM_x}{d\varphi}$ (B)	ΔQ_{hp}(A)
	%	bar/deg	bar/deg	bar/deg	bar/deg	Nm	Nm	Nm/deg	Nm/deg	lpm
Original Design	37.17	58.99	38.28	31.08	43.58	273.54	241.92	118.23	110.67	48.29
Best dMx(A)	82.02	30.38	29.55	42.92	77.38	197.27	215.94	75.52	95.06	28.10
Least Leakage*	22.77	38.49	61.34	50.84	68.88	338.32	350.01	117.27	137.80	33.31
Best dp dphi max(A)	65.57	22.12	39.48	56.33	49.06	223.61	215.26	98.37	105.32	25.75
Design 1	75.66	52.75	24.94	28.12	41.85	212.62	154.90	99.88	85.36	43.51
Design 2	73.87	46.08	32.97	33.09	32.55	201.47	92.56	106.07	90.18	37.22
Design 3	61.26	50.12	30.09	29.13	42.03	246.16	157.15	94.70	91.97	40.95

Figure 7.1. Raw values of the original design and a few designs taken from the pareto front.

For better understanding of the results, the percentage increase or decrease as compared to the base design values are shown in Figure (7.2). The red cells indicate an increase from the base design values, whereas the blue cells indicate a decrease from the base design values.

The comparision of the best ΔM_x and the lowest leakage designs are shown in Figure(7.3).

From this figure, it can be seen that there is a compromise between the leakage and ΔM_x. The design with the lowest amplitude of the swash plate moment at OpCon A has a leakage which is approximately 45% higher than the base design. Thus, low structure borne noise source comes at the cost of extremely high internal leakage. For the best ΔM_x design, the increase in leakage can be explained by an increase in cross porting to smoothen out the compression and expansion rates, which has an impact on the swash plate moment ripples. For the best ΔM_x design, along with the amplitude of the swash plate moment ripple, the amplitude of the ΔQ_{HP} also reduces by 37%, while the rate of compression at Opcon C, is adversely affected.

	Leakage*	$\frac{dp}{d\varphi}$ max (A)	$\frac{dp}{d\varphi}$ min (A)	$\frac{dp}{d\varphi}$ max (C)	$\frac{dp}{d\varphi}$ min (B)	ΔM_x(A)	ΔM_x(B)	$\Delta \frac{dM_x}{d\varphi}$(A)	$\Delta \frac{dM_x}{d\varphi}$(B)	ΔQ_{hp}(A)
	%	%	%	%	%	%	%	%	%	%
Original Design	0.00	0.00	0.00	0.00	0.00	0.00	0.00	0.00	0.00	0.00
Best dMx(A)	45.32	-48.51	-22.79	38.09	77.53	-53.57	-26.38	-32.88	-18.65	-36.67
Best efficiency	-10.20	-34.75	60.25	63.58	58.03	23.68	44.68	-0.82	24.51	-31.03
Best dp dphi max(A)	32.87	-62.50	3.14	81.23	12.56	-18.25	-11.02	-16.80	-4.84	-46.68
Design 1	42.96	-10.58	-34.84	-9.52	-3.97	-22.27	-35.97	-15.52	-22.87	-9.91
Design 2	41.17	-21.89	-13.88	6.46	-25.31	-26.35	-61.74	-10.29	-18.52	-22.93
Design 3	32.10	-15.04	-21.40	-6.30	-3.56	-10.01	-35.04	-19.90	-16.90	-15.20

Figure 7.2. Comparision data of the original design and a few designs taken from the pareto front.

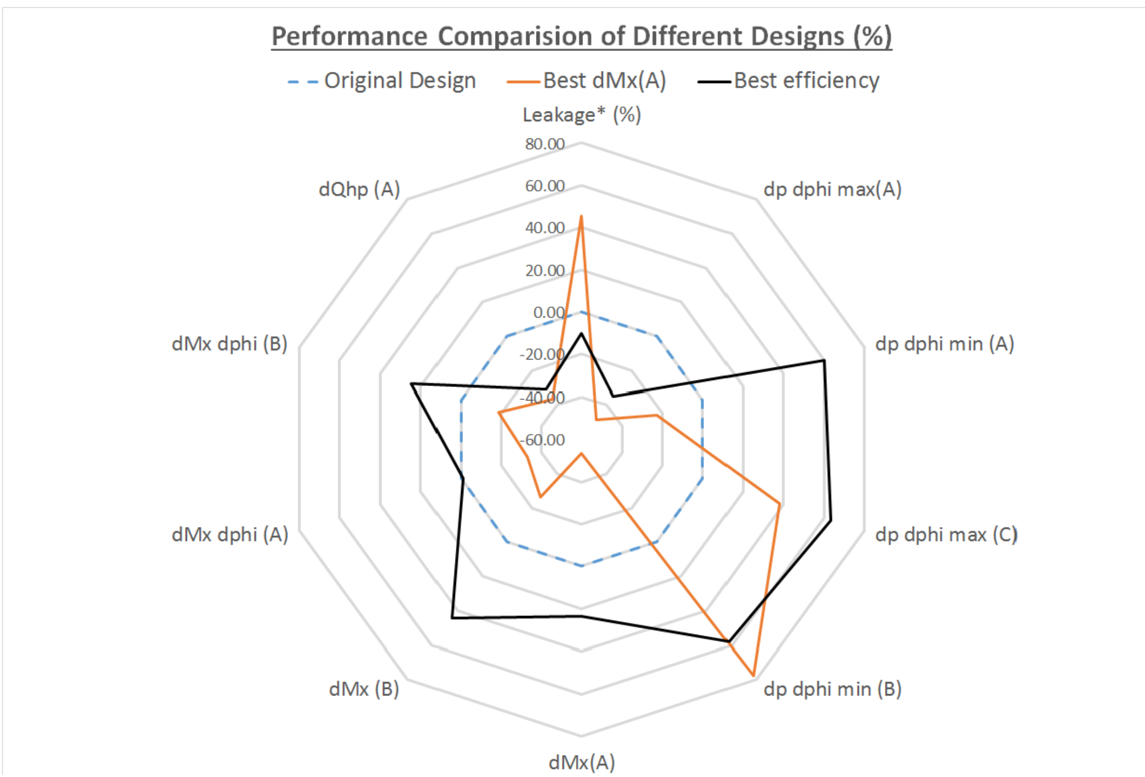

Figure 7.3. Comparision of the best ΔM_x design, lowest leakage design and the base design.

Also, another interesting thing to note is that leakage here is considered at the operating condition of minimum speed, minimum displacement and maximum pressure. This operating condition is seldom realized in the actual operation of a machine. Hence, these maximum values of leakage can be considered as exaggerated values for the actual operation of the pump. Hence, relatively low priority can be given to leakage* %.

With all the observations made above, the best ΔM_x design can be considered to be a good design which reduces the moment ripples as well as the flow ripples sufficiently.

An important correlation that can be found from the table in Figure (7.2) is that the maximum value of $\frac{dp}{d\phi}$ max at Opcon A and the value of ΔQ_{HP} at the same operating condition are directly related. So the design for the best $\frac{dp}{d\phi}$ max at Opcon A also indicates a significant reduction in ΔQ_{HP}.

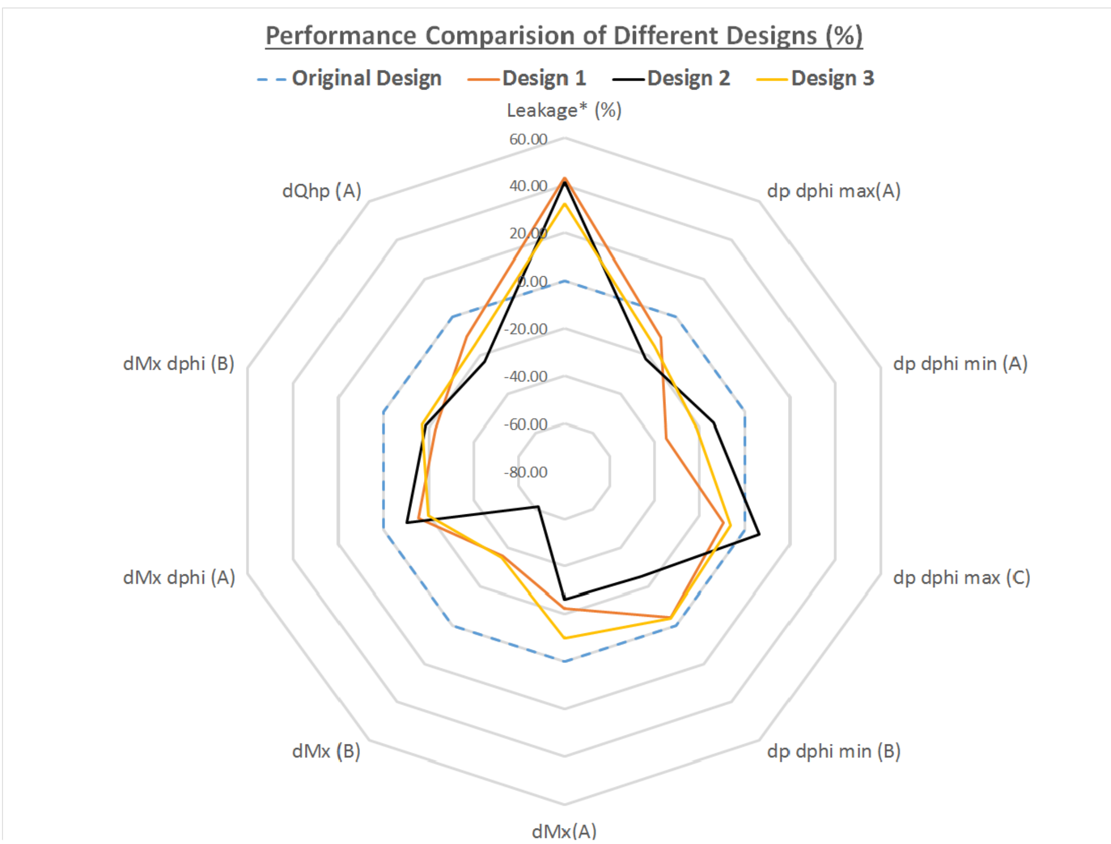

Figure 7.4. Comparision of three pareto designs and the base design.

Figure (7.4) compares three relatively satisfactory designs obtained from the pareto front to the base design. All the three designs decrease the amplitude of the swash plate moments at the operating conditions A and B, as well as the delivery flow ripple at Opcon A. Design 3 has the lowest leakage among the three, whereas Design 2 has the lowest ΔM_x at Opcons A and B, and lowest ΔQ_{HP} at Opcon A among the three designs. However, it has marginally higher values than the base design for $\frac{dp}{d\phi}$ max at Opcon C.

All the three designs significantly reduce the noise causing objective functions. However, no design could be found which gives lower values for all the 10 objective functions as compared to the base design. On comparing the three designs, it can be seen that even though Design 3 has the lower leakage among the three, yet the peak-to-peak magnitudes of ΔM_x for this design is higher at both Opcons A and C. Designs 1 and 2 have almost equivalent leakage* values. And there is a significant trade off between the two regarding the other operating conditions as well. While Design 1 dominates Design 2 in $\frac{dM_x}{d\phi}$ and the $\frac{dp}{d\phi}$ max and min values at C and A respectively, Design 2 dominates Design 1 in ΔM_x, ΔQ_{hp} and $\frac{dp}{d\phi}$ max values at Opcon A. The reduction in the noise related objective functions comes with a compromise in the efficiency as the leakage for all the three pareto front designs shown increase considerably as compared to the base design.

This drawback of higher leakage seen in the three pareto front designs can be ignored because of the rarity of this operating condition in real world applications as well as significantly lower leakage at other operating conditions.

For completion, the area files of the three recommended designs are compared against the base design in Figure (7.5), (7.6) and (7.7). From these figures, the increase in leakage can be explained by an increase in the crossport flow. The increase in crossport gives us greater control over the discharge and suction flows and with it, helps us to control the rate of compression and expansion in the displacement chamber. Furthermore, this control over the displacement chamber pressure also helps us to control the swash plate moments.

Figure(7.8) compares the leakage* % for the original design and the three optimized designs at all the four sampled operating conditions.

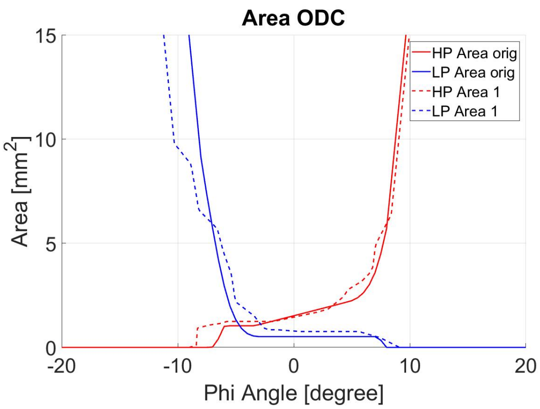

(a) Comparision of area files at ODC (Design 1).

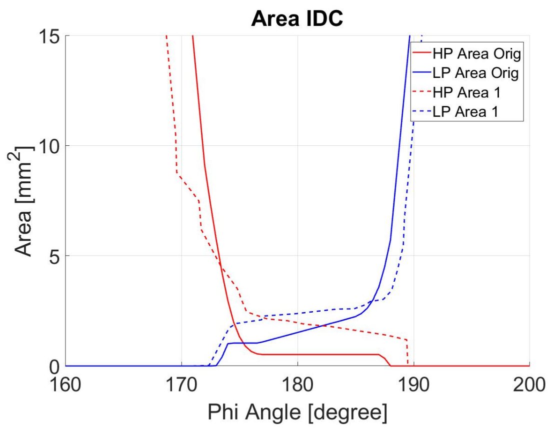

(b) Comparision of area files at IDC (Design 1).

Figure 7.5. Comparision of the area files at the ODC and the IDC between the original design and the optimized Design 1.

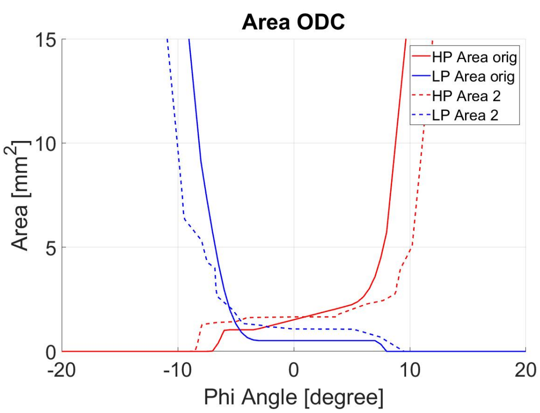

(a) Comparision of area files at ODC (Design 2).

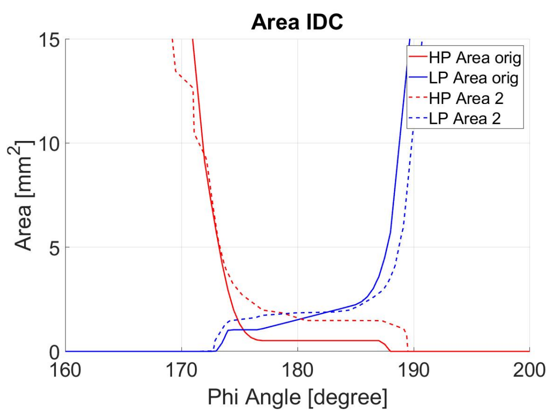

(b) Comparision of area files at IDC (Design 2).

Figure 7.6. Comparision of the area files at the ODC and the IDC between the original design and the optimized Design 2.

From Figure(7.8), it can be seen that apart from Opcon C, at all the other operating conditions, the internal leakage increases only marginally from the original design.

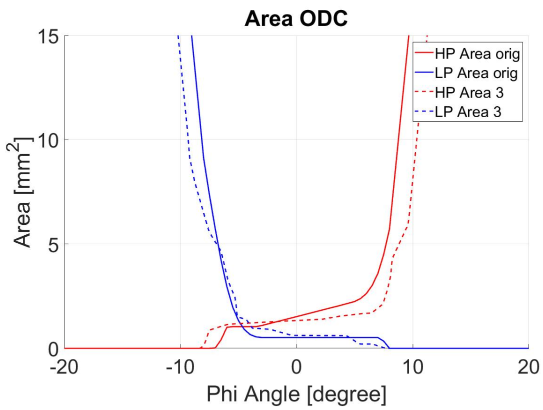

(a) Comparision of area files at ODC (Design 3).

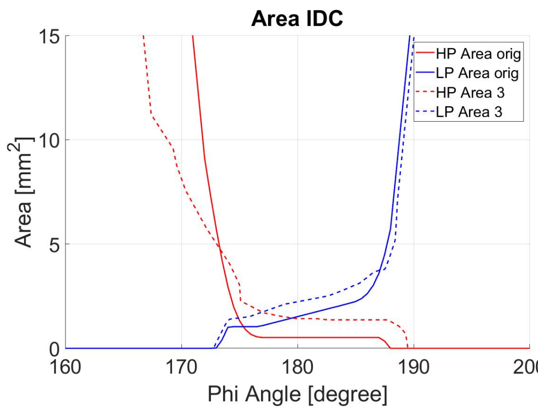

(b) Comparision of area files at IDC (Design 3).

Figure 7.7. Comparision of the area files at the ODC and the IDC between the original design and the optimized Design 3.

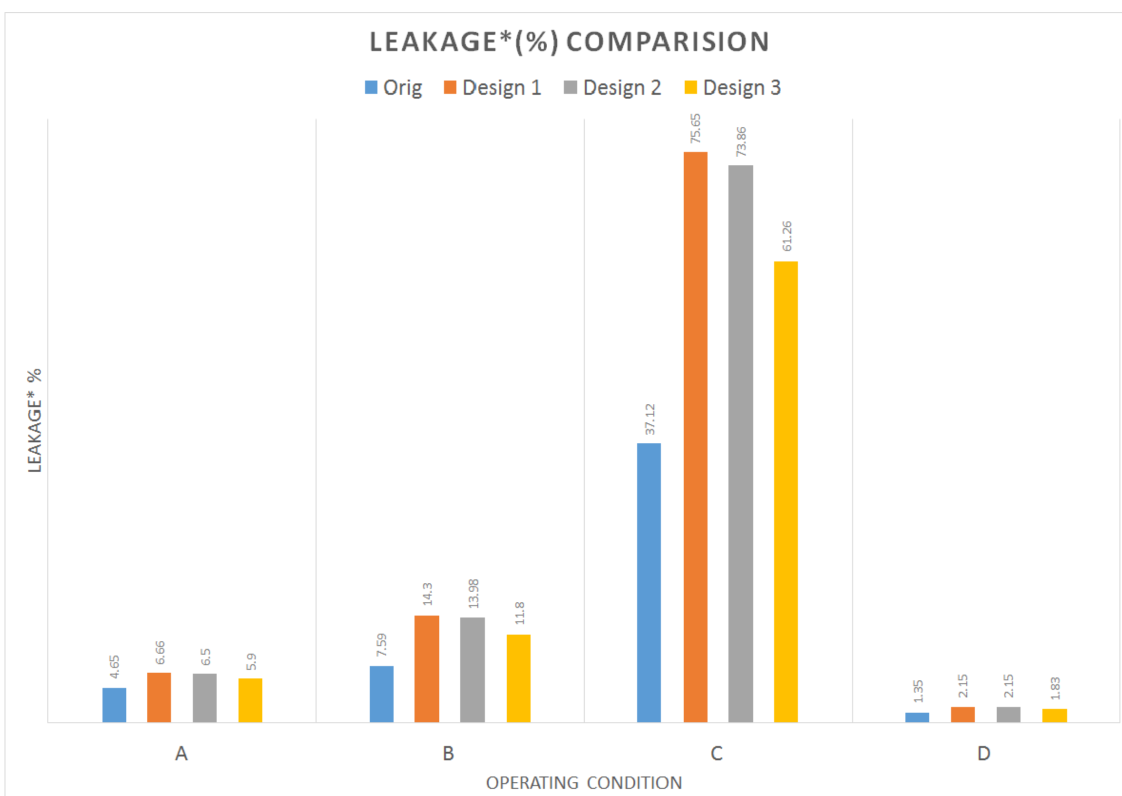

Figure 7.8. Comparision of the leakage* % for the original valve plate and the optimized valve plate for all the sampled operating conditions.

8. CONCLUSION

The crippling problem of noise in axial piston machines has baffled researchers in industry and academia alike for several years. Now that we have a better understanding of the sources of noise, yet the challenge is no less daunting because of the complexities involved in the implementation of multi-objective optimization.

This work builds on the inspiration provided by previous noise research in hydraulics to take advantage of the advances in computational power, latest multi-objective optimization algorithms and open source libraries in C++ to develop an automated software tool which focuses on the design of the valve plate to minimize all the sources of fluid borne and structure borne noise.

Some of the highlights and contributions of this work are:

1. One of the important contributions was the improvement in the swash plate type axial piston pump simulation tool Pressure Module. Apart from introducing features for the simulation of a unit in motoring and overcenter pumping, an entrained air model was implemented as well. This experimentally validated entrained air model was used to simulate a pump with various levels of entrained air. As the levels of entrained air increase, it affects the effective bulk modulus finally leading to a greater swash plate moment ripple and port pressure ripple and hence greater structure borne and fluid borne noise respectively.

2. An innovative and exploratory parametrization scheme for valve plate design was implemented which gives greater flexibility in design choice from all the previous parametrization schemes. The interpolation scheme has been successfully implemented using the open source GNU Scientific Library for C++. This implementation does not add any overhead on the Pressure Module simulations. Even though this increases the number of optimization inputs, yet the effectiveness of the scheme, improvements

in computational power, parallelization and the effectiveness of the optimization algorithm does not add a whole lot of computational overhead.

3. An archive based optimization algorithm (AMGA II) was used. The use of an external archive in this algorithm enables it to reach the global optimum in fewer function evaluations. This advantage aids the large number of optimization inputs to reach pareto optimality, without a tremendous overhead.

4. A new set of objective functions have been introduced with due consideration given to the sensitivity of the human ear to high frequencies. Keeping this in mind, a set of frequency weighted objective functions have been introduced.

5. A case study was done using the optimization tool, and the results obtained were impressive. Even though no design was found which could dominate the base design in all the 10 objective functions, yet a compromise in the leakage enabled us to obtain several designs which could dominate the base design significantly in all the objective functions which are related to noise. This compromise is acceptable because the operating condition considered for leakage is that of minimum speed, minimum displacement and maximum pressure which is seldom used in real world applications.

8.1 Future Work

Even though the final design obtained during the case study shows promising results, yet the same needs to be verified by experiments. This would require the designing the final valve plate and comparing the performance of this design to the base design.

Also, the objective functions for the optimization have been chosen keeping the pumping mode of operation in mind. It would be interesting to optimize the valve plate for the motoring mode as well, and observe the performance of the final design obtained. For motoring mode, an important change would be the sampling of the operating conditions at which the chosen objective functions make the most impact.

Thirdly, even though an entrained air model has been implemented, the optimization has been carried out by considering no entrained air in the hydraulic fluid. An interesting study is to observe the performance of the optimized valve plate to the levels of entrained air and also to search for a valve plate which is insensitive to the level of entrained air in the hydraulic fluid.

REFERENCES

REFERENCES

Becker, R. J. (1970), 'Quieting Hydraulic Systems and Components', *SAE Technical Paper* .
URL: *http://papers.sae.org/700711/*

Blum, C. & Roli, A. (2003), 'Metaheuristics in combinatorial optimization: overview and conceptual comparison', *ACM Computing Surveys* **35**(3), 189–213.

Censor, Y. (1977), 'Applied Mathematics and Optimization Pareto Optimality in Multiobjective Problems', *Applied Mathematics and Optimization* pp. 41– 59.

Deb, K. (2001), *Multi-Objective Optimization Using Evolutionary Algorithms*, John Wiley & Sons, Inc., New York, NY, USA.

Deb, K., Pratab, S., Agarwal, S. & Meyarivan, T. (2002), 'A Fast and Elitist Multiobjective Genetic Algorithm: NGSA-II', *IEEE Transactions on Evolutionary Computing* **6**(2), 182–197.

Drew, J. E., Longmore, D. K. & Johnston, D. (1998), 'Theoretical analysis of pressure and flow ripple in flexible hoses containing tuners'.
URL: *http://pii.sagepub.com/content/212/6/405.abstract*

Edge, K. (1980), 'The Theoretical Prediction of the Impedance of Positive Displacement Pumps'.

Edge, K. (1999), Designing Quieter Hydraulic Systems Some Recent Developments and Contributions, *in* 'Proceedings of the JFPS International Symposium on Fluid Power', Vol. 1999, pp. 3–27.
URL: *http://joi.jlc.jst.go.jp/JST.Journalarchive/isfp1989/1999.3?from=CrossRef*

Edge, K. A. & Darling, J. (1989), 'The Pumping Dynamics of Swash Plate Piston Pumps', *Journal of Dynamic Systems, Measurement, and Control* **111**(2), 307.

Edge, K. A. & de Freitas, F. J. (1985), 'A study of pressure fluctuations in the suction lines of positive displacement pumps', *Proceedings of the Institution of Mechanical Engineers, Part B: Journal of Engineering Manufacture* **199**(4), 211–217.

Ehrgott, M. (2012), 'Vilfredo pareto and multi-objective optimization', *Doc. Math* pp. 447–453.

Ericson, L. (2012), *On Fluid Power Pump and Motor Design : Tools for Noise Reduction.*

Ericson, L., Ölvander, J. & Palmberg, J.-O. (2008), On optimal design of hydrostatic machines, *in* 'Proceedings of the 6th International Fluid Power Conference, IFK, Vol WS', pp. 273–286.

ERICSON, L. & PALMBERG, J.-O. (2008), 'Measurement of Free Air in the Oil Close To a Hydraulic Pump', *Proceedings of the JFPS International Symposium on Fluid Power* **2008**(7-3), 647–652.
URL: *http://joi.jlc.jst.go.jp/JST.Journalarchive/isfp1989/2008.647?from=CrossRef*

Ernst, M. H. (2015), *Design solutions for piston machines with high operating pressures and water as a working fluid.*

Glover, F. (1986), 'Paths for Integer Programming', *Computers and Operations Research* **13**(5), 533–549.

Goldberg, D. (1989), 'Goldberg: Genetic algorithms in search, optimization & machine learning, addison', *Wesely Publishing Co., Inc* **1998**(3), 25.

Harris, R. M., Edge, K. A. & Tilley, D. G. (1994), 'The Suction Dynamics of Positive Displacement Axial Piston Pumps', *Journal of Dynamic Systems, Measurement, and Control* **116(2)**(June 1994), 281.
URL: *http://dynamicsystems.asmedigitalcollection.asme.org/article.aspx?articleid=1406577*

Harrison, K. A. & Edge, K. A. (2000), 'Reduction of axial piston pump pressure ripple', *Proceedings of the Institution of Mechanical Engineers, Part I: Journal of Systems and Control Engineering* **214**(1), 53–64.
URL: *http://journals.sagepub.com/doi/10.1243/0959651001540519*

Helgestad, B., Foster, K. & Bannister, F. (1973), Noise in an axial piston pump, *in* 'Seminar on Noise emitted by fluid power equipmentits causes and control', Institution of Mechanical Engineers, pp. 51–61.

Helgestad, B. O., Foster, K. & Bannister, F. K. (1974), 'Pressure Transients in an Axial Piston Hydraulic Pump', *Proceedings of the Institution of Mechanical Engineers* **188**(1), 189–199.
URL: *http://pme.sagepub.com/content/188/1/189.abstract*

IMechE (1977), 'Seminar on quiet oil hydraulic systems'.

IMechE (1980), 'Seminar on quiet oil hydraulic systems'.

Ivantysyn, J. & Ivantysynova, M. (2003), *Hydrostatic Pumps and Motors: Principles, Design, Performance, Modelling, Analysis, Control and Testing*, english edn, Akademia Books International, New Delhi, India.

Ivantysynova, M., Huang, C. & Christiansen, S.-K. (2004), 'Computer Aided Valve Plate Design - An Effective Way to Reduce Noise', *SAE Technical Paper* (724), Olems, L. (2000) Investigations of the temperatur.
URL: *http://dx.doi.org/10.4271/2004-01-2621*

Ivantysynova, M., Seeniraj, G. K. & Huang, C. (2005), 'Comparison of Different Valve Plate Designs Focusing', *The Ninth Scandinavian International Conference on Fluid Power* pp. 1–16.

Johansson, A. (2005), Design principles for noise reduction in hydraulic piston pumps : simulation, optimisation and experimental verification, PhD thesis, Linkping UniversityLinkping University, Fluid and Mechanical Engineering Systems, The Institute of Technology.

Johansson, A., Ölvander, J. & Palmberg, J. O. (2007), 'Experimental verification of cross-angle for noise reduction in hydraulic piston pumps', *Proceedings of the Institution of Mechanical Engineers. Part I: Journal of Systems and Control Engineering* **221**(3), 321–330.

Kalbfleisch, P. K. (2015), 'Computational Valve Plate Design', pp. Olems, L. (2000) Investigations of the temperatur.

Kim, D. (2012), 'Contribution to digital prototyping of axial piston pumps/motors'.
URL: *http://search.proquest.com/docview/1323762978/*

Kim, J. K., Kim, H. E., Jung, J. Y., Oh, S. H. & Jung, S. H. (2004), 'Relation between pressure variations and noise in axial type oil piston pumps', *KSME International Journal* **18**(6), 1019–1025.

Kim, S. & Murrenhoff, H. (2012), 'Measurement of Effective Bulk Modulus for Hydraulic Oil at Low Pressure', *Journal of Fluids Engineering* **134**(2), 021201.
URL: *http://fluidsengineering.asmedigitalcollection.asme.org/article.aspx?articleid=1440094*

Kim, T. & Ivantysynova, M. (2017), 'Active vibration control of swash plate-type axial piston machines with two-weight notch least mean square/filtered-x least mean square (LMS/FxLMS) filters', *Energies* **10**(5).

Kim, T., Kalbfleisch, P. & Ivantysynova, M. (2014), 'The effect of cross porting on derived displacement volume', *International Journal of Fluid Power* **15**(2), 77–85.

Klop, R. J. (2010), *A simulation-based investigation of the influence of valve plate design to reduce noise of compact power-split-drive transmissions.*

Kumar Seeniraj, G. & Ivantysynova, M. (2011), 'A multi-parameter multi-objective approach to reduce pump noise generation', *International Journal of Fluid Power* **12**(1), 7–17.

Ma, W., Jiao, L., Gong, M. & Liu, F. (2005), 'An Novel Artificial Immune Systems Multi-objective Optimization Algorithm for 0 / 1 Knapsack Problems', pp. 793–798.

Murrenhoff, H. (2011), *Grundlagen der Fluidtechnik, Teil 1: Hydraulik.*

Palmberg, J. (1989), 'Modelling of Flow Ripple from Fluid Power Piston Pumps', *2nd Bath International Power Workshop, University of Bath, UK* .

Palmen, A. (2004), 'Noise reduction of an axial piston pump by means of structural modification', *4th International Fluid Power Conference - IFK 2004* **48**(4), 121–132.

Pelosi, M. (2012), *An investigation of the fluid-structure interaction of piston/cylinder interface.*

Pettersson, M., Weddfelt, K. & Palmberg, J. (1991), 'Methods of Reducing Flow Ripple from Fluid', *SAE Technical Paper* **100**(1991), 158–167.

Petzold, L. & Hindmarsh, A. (1997), 'Lsoda; computing and mathematics research division', *Lawrence Livermore National La boratory, Livermore, CA* .

Schenk, A. (2014), *Predicting lubrication performance between the slipper and swashplate in axial piston hydraulic machines.*

Schrank, K. & Stammen, C. (2014), 'Investigation of Different Methods To Measure the Entrained Air', pp. 1–8.

Schrank, K., Stammen, C. & Murrenhoff, H. (2014), A new approach to model a multi-phase hydraulic capacity and its experimental validation, *in* '9th International Fluid Power Conference', Vol. 2.

Seeniraj, G. K. (2009), *Model based optimization of axial piston machines focusing on noise and efficiency.*

Skaistis, S. (1962), 'Sounds of Hydraulics, Pumps and Motors', *Design News* pp. 14–19.
URL: *https://www.youtube.com/watch?v=G1mOt6R3bJw*

Skaistis, S. (1988), *Noise Control for Hydraulic Machinery (Fluid Power and Control)*, first edn.

Sörensen, K. & Glover, F. W. (2013), 'Metaheuristics', *Encyclopedia of Operations Research and Management Science* **1**, 960–970.
URL: *http://www.opttek.com/sites/default/files/Metaheuristics.pdf*

Taylor, R. I. & Michael, P. (2018), 'AN INVESTIGATION OF HYDRAULIC FLUID COMPOSITION AND AERATION IN AN AXIAL PISTON PUMP', pp. 1–10.

Tiwari, S., Fadel, G. & Deb, K. (2011), 'AMGA2: Improving the performance of the archive-based micro-genetic algorithm for multi-objective optimization', *Engineering Optimization* **43**(4), 377–401.

Totten, G., Sun, Y. & Bishop, R. (1997), 'Hydraulic fluids: foaming, air entrainment and air releasea review', *SAE technical paper* (41 2), 1–13.
URL: *http://papers.sae.org/972789*

Wieczorek, U. & Ivantysynova, M. (2000), 'CASPAR - A Computer Aided Design Tool for Axial Piston Machines', *Bath Workshop on Power transmission and Motion Control PTMC* pp. 113–126.

Yamauchi, K. & Yamamoto, T. (1976), 'Noises generated by hydraulic pumps and their control method', *Mitsubishi Technical Review* .

Zecchi, M. (2013), *A novel fluid structure interaction and thermal model to predict the cylinder block / valve plate interface performance in swash plate type axial piston machines.*

Zitzler, E. (1999), 'Evolutionary algorithms for multiobjective optimization : Methods and applications', **13398**(30).

APPENDICES

A. TABLE OF CASE STUDY OPTIMIZATION INPUT LOWER AND UPPER BOUNDS

The upper and the lower bounds for the optimization inputs are shown in the tables below. Each groove is defined by 16 points (N = 16) and the total number of optimization inputs are 136.

Table A.1.: Optimization Inputs for **Groove 1** for the Case Study

Groove No.	**Input**	**Lower Limit**	**Upper Limit**
	S	-9°	6°
	R	0	1
	Δx_1	0.05°	1.50°
	Δx_2	0.05°	1.50°
	Δx_3	0.05°	1.50°
	Δx_4	0.05°	1.50°
	Δx_5	1°	3°
	Δx_6	0.05°	1.50°
	Δx_7	2°	4°
	Δx_8	2°	4°
	Δx_9	0.05°	1.50°
	Δx_{10}	0.50°	2.50°
	Δx_{11}	0.05°	1.50°
	Δx_{12}	0.05°	1.50°
	Δx_{13}	0.05°	1.50°
	Δx_{14}	0.05°	1.50°

continued on next page
Groove 1

Table A.1.: *continued*

Groove No.	**Input**	**Lower Limit**	**Upper Limit**
	Δx_{15}	$0.05°$	$1.50°$
	Δx_{16}	$0.05°$	$1.50°$
	Δy_1	$0.0\ mm^2$	$0.10\ mm^2$
	Δy_2	$0.00\ mm^2$	$0.60\ mm^2$
	Δy_3	$0.1\ mm^2$	$1.10\ mm^2$
	Δy_4	$0.00\ mm^2$	$0.20\ mm^2$
	Δy_5	$0.00\ mm^2$	$0.20\ mm^2$
	Δy_6	$0.01\ mm^2$	$0.19\ mm^2$
	Δy_7	$0.00\ mm^2$	$1.00\ mm^2$
	Δy_8	$0.00\ mm^2$	$1.00\ mm^2$
	Δy_9	$0.01\ mm^2$	$0.29\ mm^2$
	Δy_{10}	$0.00\ mm^2$	$0.70\ mm^2$
	Δy_{11}	$0.00\ mm^2$	$0.50\ mm^2$
	Δy_{12}	$0.00\ mm^2$	$0.70\ mm^2$
	Δy_{13}	$0.00\ mm^2$	$0.70\ mm^2$
	Δy_{14}	$0.10\ mm^2$	$1.10\ mm^2$
	Δy_{15}	$0.30\ mm^2$	$1.80\ mm^2$
	Δy_{16}	$0.30\ mm^2$	$1.80\ mm^2$

Table A.2.: Optimization Inputs for **Groove 2** for the Case Study

Groove No.	**Input**	**Lower Limit**	**Upper Limit**
	S	-9.5°	6.5°
	R	0	1
	Δx_1	0.05°	1.50°
	Δx_2	0.05°	1.50°
	Δx_3	1°	3°
	Δx_4	4°	6°
	Δx_5	1°	3°
	Δx_6	0.1°	2°
	Δx_7	0.05°	2°
	Δx_8	0.05°	2°
	Δx_9	0.05°	2°
	Δx_{10}	0.50°	2°
	Δx_{11}	0.05°	2°
	Δx_{12}	0.05°	2°
	Δx_{13}	0.05°	2°
	Δx_{14}	0.05°	2°
	Δx_{15}	0.05°	2°
Groove 2	Δx_{16}	0.05°	2°
	Δy_1	0.0 mm^2	0.70 mm^2
	Δy_2	0.00 mm^2	0.70 mm^2
	Δy_3	0.1 mm^2	0.40 mm^2
	Δy_4	0.00 mm^2	0.40 mm^2
	Δy_5	0.00 mm^2	0.40 mm^2
	Δy_6	0.00 mm^2	0.40 mm^2

continued on next page

Table A.2.: *continued*

Groove No.	**Input**	**Lower Limit**	**Upper Limit**
	Δy_7	0.00 mm^2	0.38 mm^2
	Δy_8	0.00 mm^2	0.80 mm^2
	Δy_9	0.00 mm^2	0.80 mm^2
	Δy_{10}	0.00 mm^2	0.80 mm^2
	Δy_{11}	0.10 mm^2	1.30 mm^2
	Δy_{12}	0.30 mm^2	1.80 mm^2
	Δy_{13}	0.50 mm^2	2.10 mm^2
	Δy_{14}	0.80 mm^2	2.40 mm^2
	Δy_{15}	0.80 mm^2	2.40 mm^2
	Δy_{16}	0.80 mm^2	2.40 mm^2

Table A.3.: Optimization Inputs for **Groove 3** for the Case Study

Groove No.	**Input**	**Lower Limit**	**Upper Limit**
Groove 3	S	-9°	6°
	R	0	1
	Δx_1	0.05°	1.50°
	Δx_2	0.05°	1.50°
	Δx_3	0.05°	1.50°
	Δx_4	0.05°	1.50°
	Δx_5	1°	3°
	Δx_6	0.05°	1.50°
	Δx_7	2°	4°
	Δx_8	2°	4°
	Δx_9	0.05°	1.50°
	Δx_{10}	0.50°	2.50°
	Δx_{11}	0.05°	1.50°
	Δx_{12}	0.05°	1.50°
	Δx_{13}	0.05°	1.50°
	Δx_{14}	0.05°	1.50°
	Δx_{15}	0.05°	1.50°
	Δx_{16}	0.05°	1.50°
	Δy_1	0.0 mm^2	0.10 mm^2
	Δy_2	0.00 mm^2	0.60 mm^2
	Δy_3	0.1 mm^2	1.10 mm^2
	Δy_4	0.00 mm^2	0.20 mm^2
	Δy_5	0.00 mm^2	0.20 mm^2
	Δy_6	0.01 mm^2	0.19 mm^2

continued on next page

Table A.3.: *continued*

Groove No.	**Input**	**Lower Limit**	**Upper Limit**
	Δy_7	0.00 mm^2	1.00 mm^2
	Δy_8	0.00 mm^2	1.00 mm^2
	Δy_9	0.01 mm^2	0.29 mm^2
	Δy_{10}	0.00 mm^2	0.70 mm^2
	Δy_{11}	0.00 mm^2	0.50 mm^2
	Δy_{12}	0.00 mm^2	0.70 mm^2
	Δy_{13}	0.00 mm^2	0.70 mm^2
	Δy_{14}	0.10 mm^2	1.10 mm^2
	Δy_{15}	0.30 mm^2	1.80 mm^2
	Δy_{16}	0.30 mm^2	1.80 mm^2

Table A.4.: Optimization Inputs for **Groove 4** for the Case Study

Groove No.	**Input**	**Lower Limit**	**Upper Limit**
Groove 4	S	-9.5°	6.5°
	R	0	1
	Δx_1	0.05°	1.50°
	Δx_2	0.05°	1.50°
	Δx_3	1°	3°
	Δx_4	4°	6°
	Δx_5	1°	3°
	Δx_6	0.1°	2°
	Δx_7	0.05°	2°
	Δx_8	0.05°	2°
	Δx_9	0.05°	2°
	Δx_{10}	0.50°	2°
	Δx_{11}	0.05°	2°
	Δx_{12}	0.05°	2°
	Δx_{13}	0.05°	2°
	Δx_{14}	0.05°	2°
	Δx_{15}	0.05°	2°
	Δx_{16}	0.05°	2°
	Δy_1	0.0 mm^2	0.70 mm^2
	Δy_2	0.00 mm^2	0.70 mm^2
	Δy_3	0.1 mm^2	0.40 mm^2
	Δy_4	0.00 mm^2	0.40 mm^2
	Δy_5	0.00 mm^2	0.40 mm^2
	Δy_6	0.00 mm^2	0.40 mm^2

continued on next page

Table A.4.: *continued*

Groove No.	**Input**	**Lower Limit**	**Upper Limit**
	Δy_7	0.00 mm^2	0.38 mm^2
	Δy_8	0.00 mm^2	0.80 mm^2
	Δy_9	0.00 mm^2	0.80 mm^2
	Δy_{10}	0.00 mm^2	0.80 mm^2
	Δy_{11}	0.10 mm^2	1.30 mm^2
	Δy_{12}	0.30 mm^2	1.80 mm^2
	Δy_{13}	0.50 mm^2	2.10 mm^2
	Δy_{14}	0.80 mm^2	2.40 mm^2
	Δy_{15}	0.80 mm^2	2.40 mm^2
	Δy_{16}	0.80 mm^2	2.40 mm^2

VITA

VITA

Abhimanyu Baruah was born in Assam, India in 1993. He completed his Bachelor of Technology from the Indian Institute of Technology, Guwahati, India with a major in Mechanical Engineering. Following this, he worked as a Junior Research Fellow at the Indian Institute of Technology, Delhi in the Department of Mechanical Engineering. He joined Purdue University as a Masters student in August, 2016. He joined Maha Fluid Power Research Center in January, 2017. The focus of his research was optimization of pump geometry for noise reduction in axial piston machines using genetic algorithms